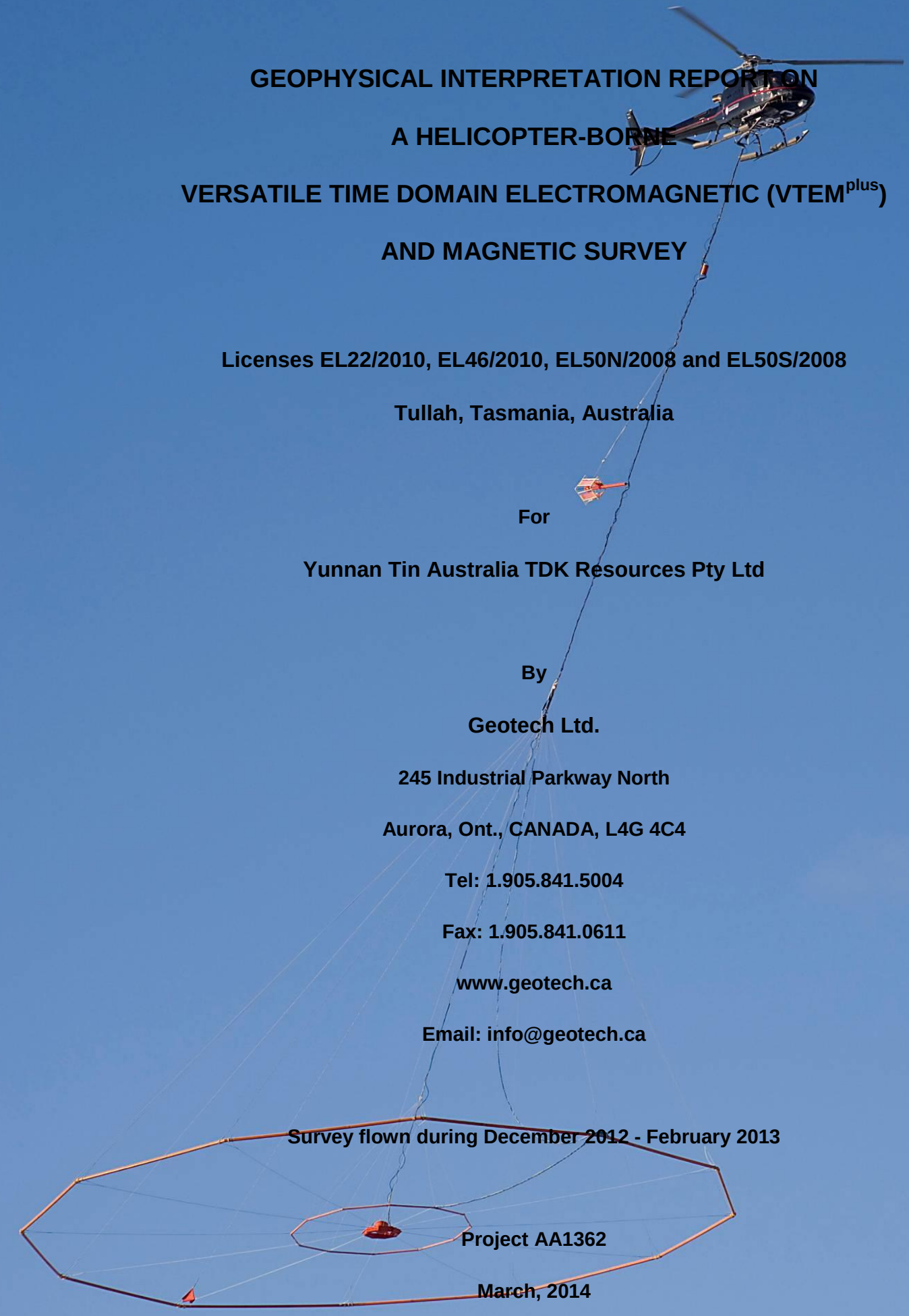

GEOPHYSICAL INTERPRETATION REPORT ON

A HELICOPTER-BORNE

VERSATILE TIME DOMAIN ELECTROMAGNETIC (VTEM^{plus})

AND MAGNETIC SURVEY

Licenses EL22/2010, EL46/2010, EL50N/2008 and EL50S/2008

Tullah, Tasmania, Australia

For

Yunnan Tin Australia TDK Resources Pty Ltd

By

Geotech Ltd.

245 Industrial Parkway North

Aurora, Ont., CANADA, L4G 4C4

Tel: 1.905.841.5004

Fax: 1.905.841.0611

www.geotech.ca

Email: info@geotech.ca

Survey flown during December 2012 - February 2013

Project AA1362

March, 2014

TABLE OF CONTENTS

LIST OF FIGURES

LIST OF TABLES

APPENDICES

GEOPHYSICAL INTERPRETATION REPORT ON A HELICOPTER-BORNE VERSATILE TIME DOMAIN ELECTROMAGNETIC (VTEM^{plus}) AND MAGNETIC SURVEY

EL22, EL46, EL50N and EL50S
Tullah, Tasmania, Australia

EXECUTIVE SUMMARY

During December 10th 2012 to February 7th, 2013 Geotech Ltd carried out a helicopter-borne geophysical survey over the licenses EL22/2010 (EL22), EL32/2010 (not requested for interpretation) EL46/2010 (EL46), EL50N/2008 (EL50N) and EL50S/2008 (EL50S) located near Tullah, Tasmania, Australia.

Principal geophysical sensors included a versatile time-domain electromagnetic (VTEM^{plus}) system, and a cesium magnetometer. Ancillary equipment included a GPS navigation system and a radar altimeter. A total of 2,291 line-kilometers of geophysical data were acquired during the survey.

Geotech Ltd has performed, on behalf of Yunnan Tin Australia TDK Resources Pty Ltd (Yunnan Tin Australia), geophysical interpretations of the magnetic and electromagnetic (EM) data for the exploration of Volcanogenic Massive Sulphide (VMS) deposits in the surveyed area.

The airborne geophysical datasets of EL22, EL46, EL50N and EL50S have been interpreted using established geophysical interpretation principles. Undifferentiated sediments and volcanic rocks have been delineated from magnetic data. Mafic dykes and faults are interpreted from the derivatives of the magnetic data. The magnetic data are also inverted to magnetic susceptibility distribution using MAG3D [1] to facilitate the geophysical data interpretation. Magnetic susceptibility 2D sections for all regular lines and selected depth slices have been created for EL46 only. The susceptibility 2D sections for EL22, EL50N and EL50S will be generated if required.

EM anomalies were picked from the electromagnetic data for EL22, EL46 and EL50N blocks. Resistivity Depth Imaging (RDI) 2D sections in Geosoft format for all regular lines have been generated for EL22, EL46, EL50N and EL50S blocks, as well as in PDF format. Conductive zones and trends are interpreted from the EM data.

Five (5) possible VMS and/or mafic or ultramafic-related PGE prospective target zones are identified for EL46 block, four possible VMS targets for EL22, one (1) possible VTEM target and two (2) possible strong Airborne Induced Polarization targets for EL50N block, and one (1) possible strong VMS targets for EL50S block. Conductors in the target zone for EL46 are modeled by Maxwell 2.5D plates. Recommended drilling parameters are provided for the Maxwell plate models.

1 MAG3D is a three-dimensional inversion program developed by University of British Columbia Geophysical Inversion Facility (UBC-GIF)

The advanced interpretation products and maps are delivered in the final DVD:

- Advanced magnetic grids;
- RDI database, 3D voxels, selected depth slices, and 2D sections for all regular lines in Geosoft Map and PDF;
- MAG3D inversions, 3D voxels, selected depth slices and 2D sections for all regular lines for EL46, and 3D voxels, selected depth slices and selected 2D sections for remaining blocks;
- Maxwell 2.5D plate modeling of selected conductors;
- Geophysical interpretation in plans and sections for selected targets;
- Final Interpretation Report.

1. SURVEY SPECIFICATIONS

1.1 General

Interpretation Report Summary	
Project	
Job	AA1362
Project	EL22, (EL32), EL46, EL50N and EL50S
Location	Tullah, Tasmania, Australia
Total Line Kilometers	2,291 kms
Survey Date	April 21st – June 24th 2013
Survey Type	VTEM / Magnetic
Manager	Alexander Prikhodko
Senior Interpreters	Zihao Han and Karl Kwan
Client	
Client	Yunnan Tin Australia TDK Resources Pty Ltd
Address	15 Gubbuteh Road, Little Bay, NSW AUS 2036
Client Representative	Dr. Joe Xie
Contact	Phone: (02) 8197 6518 Email: dr.joe.xie@gmail.com
Report	
Report Date	March 2014

1.2 Survey Location

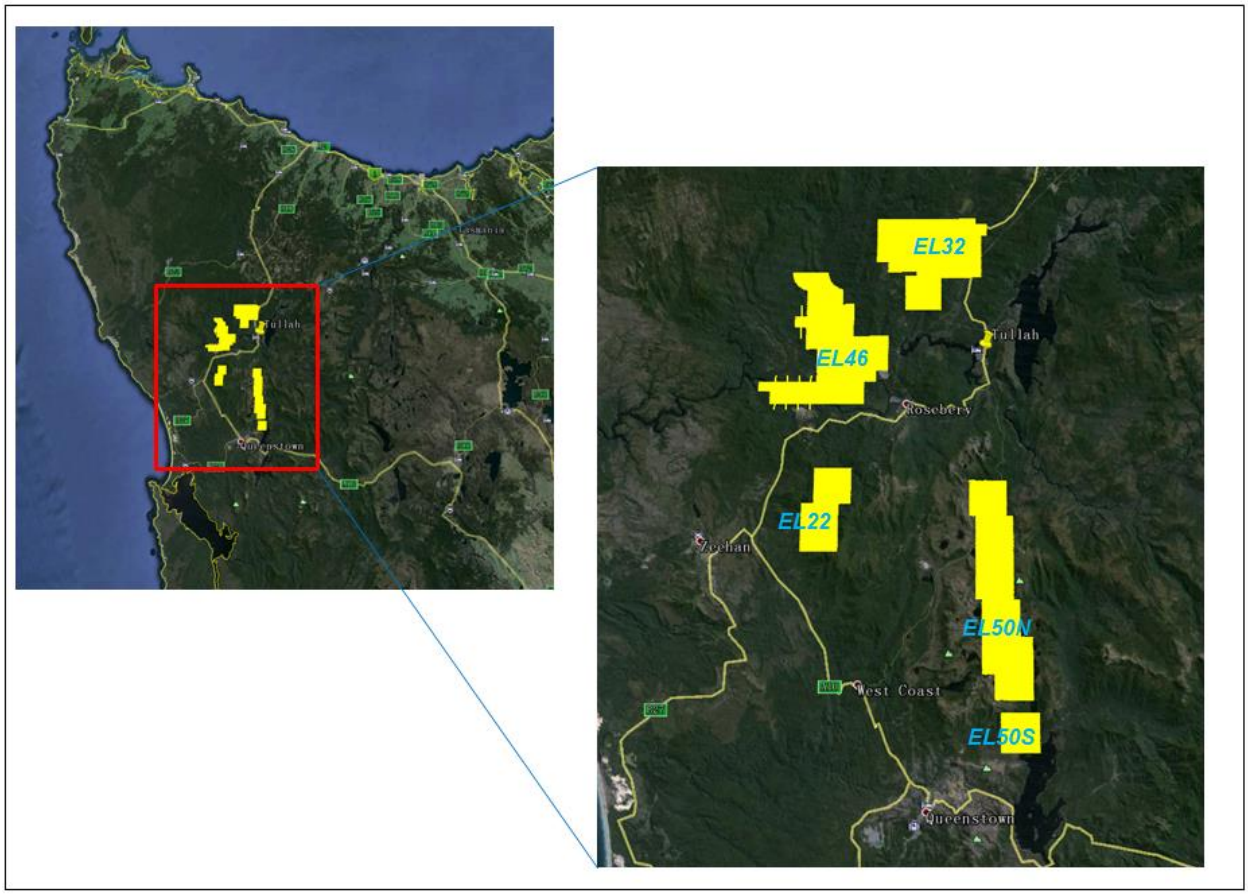

Figure 1: Surveyed Licenses locations near Tullah, Tasmania (images from Google Earth).

The survey data consists of a total of 2,291 line kilometers flown at 200 meter line spacing. The survey area is located west, southwest and south of Tullah, Tasmania, Figure 1. Geophysical data from EL22, EL46, EL50N and EL50S are selected for geophysical interpretation.

1.3 System Specifications

Survey Helicopter	
Registration	Astar 350 B3, VH-VTX
VTEM Transmitter	
Coil diameter	26 m
Number of turns	4
Pulse repetition rate	25 Hz
Peak current	187 Amp
Peak dipole moment	397,135 NIA
Pulse width	7.34 ms
Nominal terrain clearance	73 m
VTEM Receivers	
Z Coil diameter	1.2 metre
Number of turns	100
Effective area	113 m^2
X Coil diameter	0.32m
Number of turns	245
Effective area	19.69 m^2
Sampling interval	0.1 s
Nominal terrain clearance	73 m
Magnetometer	
Type	Geometrics
Model	Optically pumped Cesium vapour
Sensitivity	0.02 nT
Sampling interval	0.1 s
Nominal terrain clearance	95 m
Radar Altimeter	
Type	Terra TRA 3000/TRI 40
Position	Beneath cockpit
GPS navigation system	
Type	Novatel
Model	WAAS enabled OEM4-G2-3151W
Antenna position	Helicopter tail

2. INTERPRETATION OBJECTIVES, METHODS AND PRODUCTS

2.1 Interpretation objectives and methods

The geophysical interpretation objectives and methods are:

- To identify lithological units (volcanic, intrusive and sedimentary rocks) and structures (dykes and faults) from the magnetic data. The structures will provide guidance on the flow of potential mineralized fluids;
- To identify conductive zones using EM data, Resistivity Depth Imaging (RDI) and the modeling of selected conductors using Maxwell 2.5D plates;
- To invert the magnetic data of selected target areas using MAG3D;
- To analyze selected targets in 2D and 3D, and in detail, using all available data and interpretation products.

2.2 Advanced interpretation products and maps

The following advanced products are generated to facilitate interpretations.

Magnetics

1. Reduced-To-Pole (RTP) magnetic field;
2. First and second vertical derivative of RTP;
3. Analytical Signal of RTP;
4. Tilt-angle derivative of RTP (TDR);
5. MAG3D inversions, magnetic susceptibility 3D voxels (EL22, EL46, EL50N and EL50S), selected depth slices and 2D sections for all regular lines (EL46), Appendix F.

Electromagnetics

1. EM Anomaly Picks (EL22, EL46, EL50N and EL50S blocks);
2. Resistivity Depth Imaging (RDI), 3D voxels, selected depth slices and 2D sections (EL22, EL46, EL50N and EL50S), Appendix E;
3. Maxwell 2.5D plate modeling of selected conductors (EL46 and EL22).

3. GEOLOGY AND THE EXPLORATION MODEL

3.1 Regional Tectonic Settings and Geology of Western Tasmania

Berry and Bull 2012 described the tectonic history of Tasmania as the evolution over 900 Ma of a small fragment on the margin of Gondwana, with three episodes of passive margin sedimentation from the Mesoproterozoic to the Devonian. Tasmania rifted from the Antarctic margin during Rodinia breakup and was then involved in the so-called "West-Pacific-Style" island arc tectonics along the eastern margin of Gondwana through the Paleozoic. Arc-continent collision led to ophiolite obduction in the Cambrian.

The most important metallogenic event in Tasmania occurred in Middle Cambrian as the post collisional proximal submarine volcanism and the deposition of the Mount Read Volcanics (MRV) and associated world-class deposits (Seymour *et al*. 2007 and Green 2012), shown in Figure 2. The well-known Cambrian deposits in the Mount Read Volcanics are: Hellyer (16.5 Mt @ 13.9% Zn, 7.2% Pb, 0.38% Cu and 2.55 g/t Au, closed), Rosebery (34 Mt @ 13.8% Zn, 4.1% Pb, 0.57% Cu and 2.2g/t Au, mine), Henty-Mt Julia (2.83 Mt @ 12.5g/t Au) and Mount Lyell (311 Mt @ 0.97% Cu and 0.31 g/t Au, mine). The MRV is dominated by andesitic to basaltic volcanic rocks and intrusives deposited in a marine environment. The tectonism was mostly near east-west extensional during MRV deposition. Flanking the MRV are the marine sandstone, siltstone and conglomerate of the Late Cambrian.

The regional geology in and around the VTEM survey areas is shown in Figure 3. The Henty Fault, a prominent near NS structural feature, constitutes a fundamental metallogenic divide within the MRV (Callaghan 2001, Seymour *et al*. 2007). To the northwest, polymetallic Zn-Pb-Cu-Au volcanogenic massive sulphide (VMS) deposits are located at Hellyer, Que River, Farrell, Rosebery and Hercules, and low base metal but high Au-Ag deposits are found at South Hercules. To the southeast, Cu-Au and Au deposits such as Mount Lyell and Henty Mt Julia dominate. The most economically important is the Mount Lyell field disseminated chalcopyrite-pyrite ore bodies in alteration assemblages of mainly quartz-sericite or quartz-chlorite-sericite.

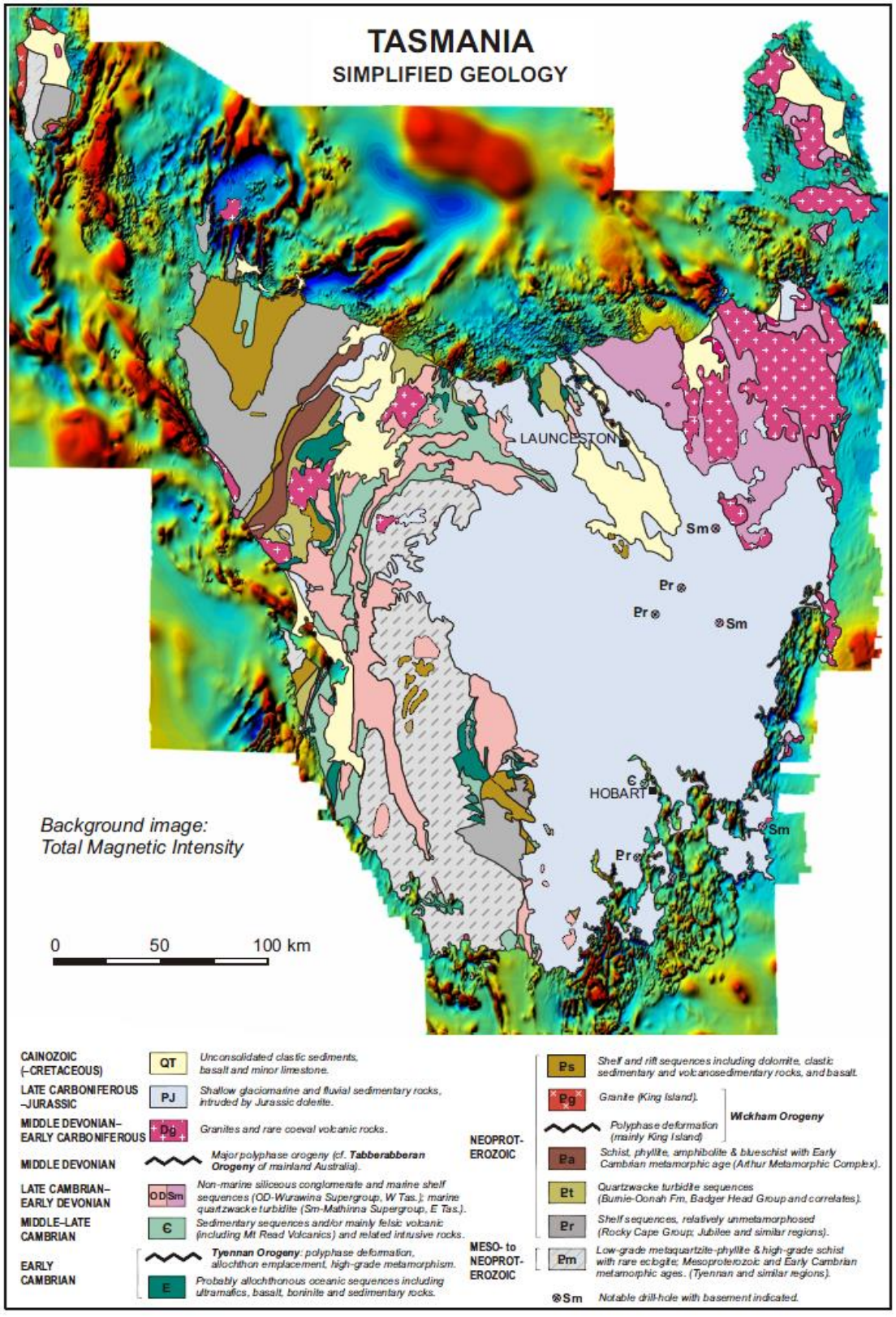

Figure 2: Simplified geology of Tasmania (from Seymour *et al.* 2007).

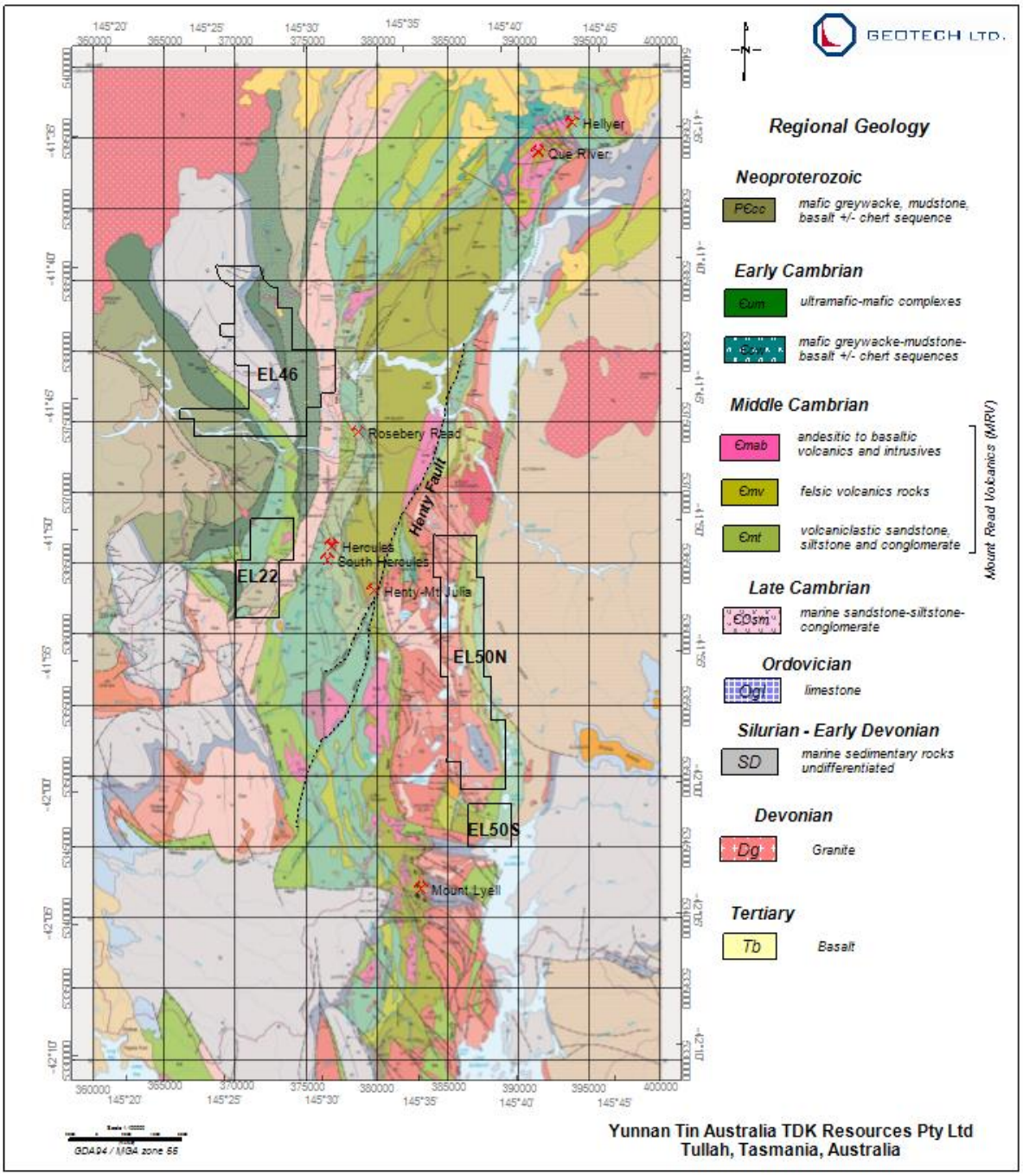

Figure 3: Regional geology over the survey areas (sourced from Department of Resources[2], Tasmania).

3.2 Property Geology

The 1:25,000 scale digital geology map series over the Mount Read Volcanics belt are

2 Department of Infrastructure, Energy and Resources

provided by Yunnan Tin Australia, and were originally created by Western Tasmanian Regional Minerals Program, Mount Read Volcanics Compilation, Department of Infrastructure, Energy and Mines in 2005.

The descriptions of the relevant property geology over EL46, EL22, EL50N and EL50S blocks are extracted mainly from Corbett, 2002, "Updating the geology of the Mount Read Volcanics belt".

3.2.1 EL46 block

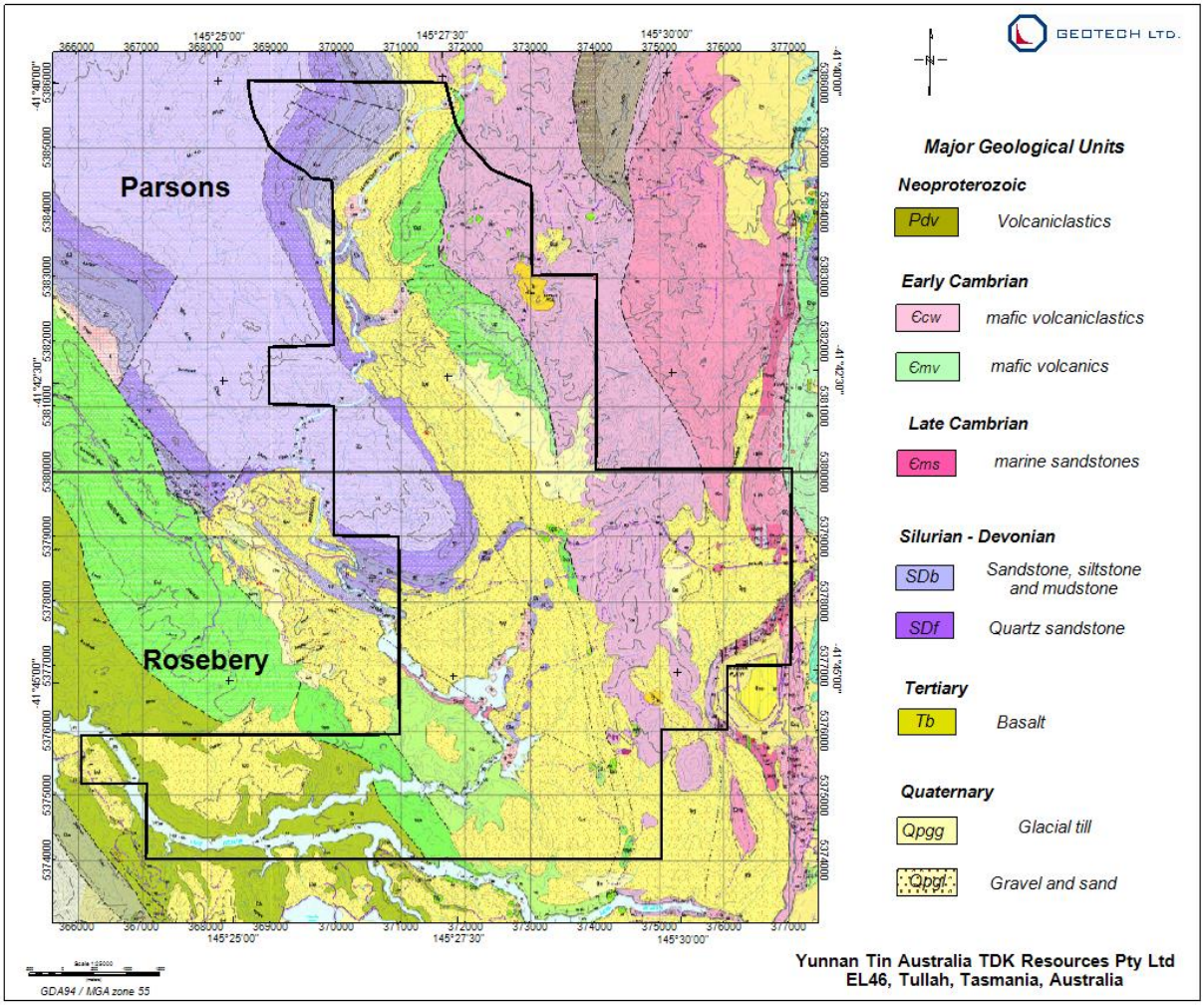

Figure 4: Local geology (1:25,000), EL46 (sourced from Department of Resources, Tasmania).

EL46 block covers 1:25,000 Parsons and Rosebery sheets, Figure 4. In the north of EL46, two ultramafic bodies (Ꞓmv) flanking the Huskisson Syncline filled with Silurian to Devonian sediments coincides with strong linear magnetic anomalies. Most of the areas within EL46 are covered by glacial till or gravel and sand of the Quaternary age. Neoproterozoic to early Cambrian volcaniclastics fill the rest of the block. Along the NE boundary of EL46, there is an isolated basalt body of Tertiary age (Tb) having strong magnetic responses.

3.2.2 EL22 block

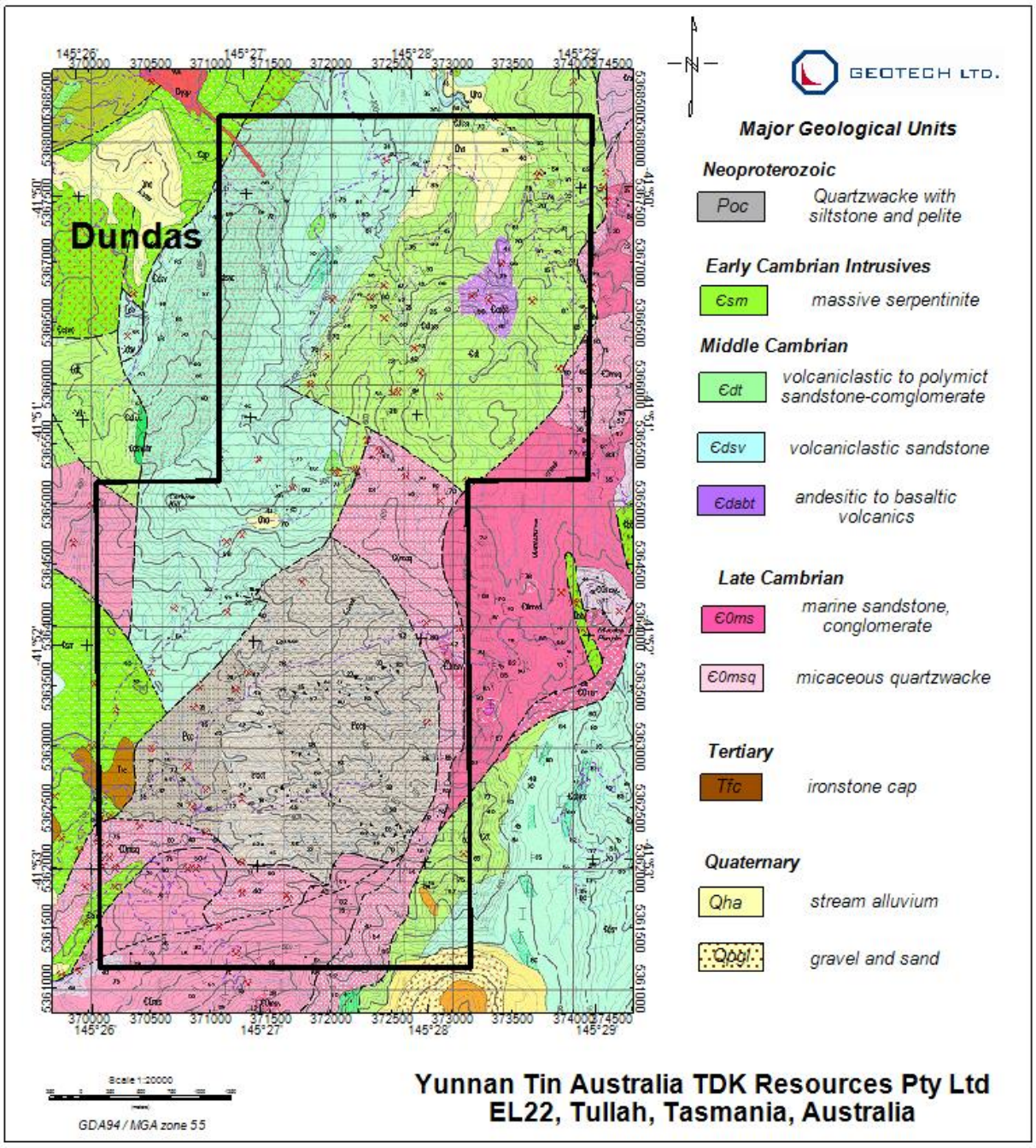

Figure 5: Local geology (1:25,000), EL22 (sourced from Department of Resources, Tasmania).

EL22 block is located in Dundas sheet, Figure 5. In the north of the block, the geology is dominated by Early to Middle Cambrian volcaniclastics. There is an outcrop of andesitic to basaltic volcanic rocks in the north too. In the south, the centre is covered by

Neoproterozoic sediments surrounded by Late Cambrian marine sandstone, conglomerate and micaceous quartzwacke. Along the south-western edge of the block, there are some massive serpentinite intrusives coinciding with strong magnetic anomalies.

3.2.3 EL50N block

EL50N block spans three sheets, from north to south, Selina, Tyndall and Gormanston, Figure 6. The western half of the block is covered by Late Cambrian quartz sandstone (Є0su), Ordovician limestone (Ol) and Quaternary alluvium and marine sediments. The eastern half is dominated by the Middle Cambrian volcanics with strong magnetic responses. To the east of the block, there is Neoproterozoic quartzwacke with siltstone and pelite.

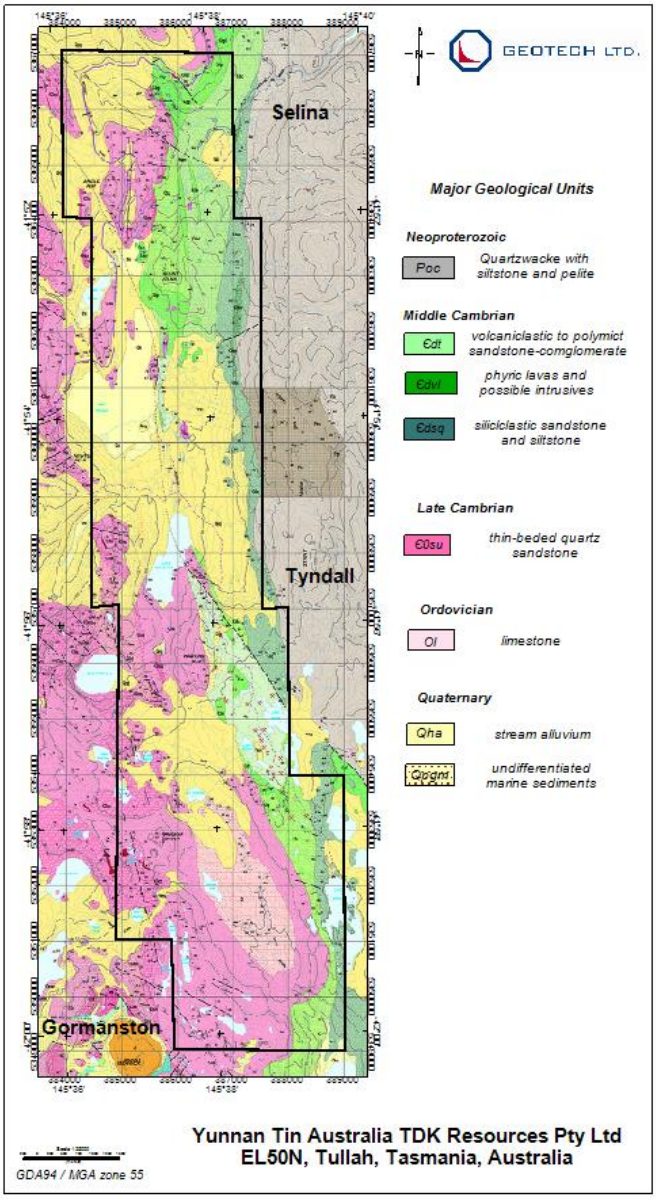

Figure 6: Local geology (1:25,000), EL50N (sourced from Department of Resources, Tasmania).

3.2.4 EL50S block

EL50S block is located entirely within Gormanston sheet, Figure 7. The NW quadrant of the block is dominated by Middle Cambrian volcanics (possibly intrusives) and volcaniclastics. The rest of EL50S is covered by sediments of the Middle to Late Cambrian, and Quaternary ages.

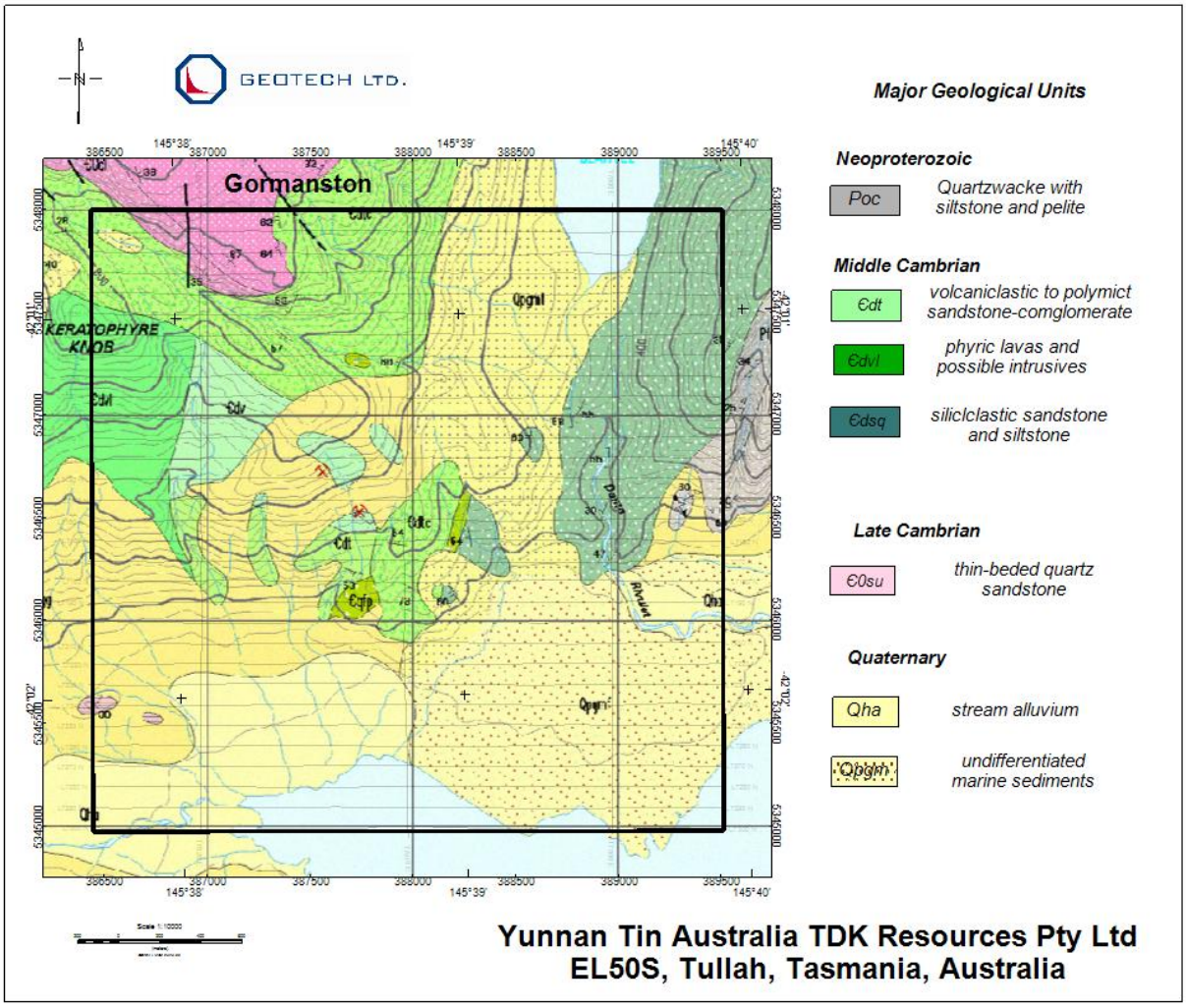

Figure 7: Local geology (1:25,000), EL50S (sourced from Department of Resources, Tasmania).

3.3 Mineralization Model

Mineral deposits of significant economic interest in Western Tasmania include Cambrian Volcanic-Hosted Massive Sulphide (VHMS), as known as Volcanogenic Massive Sulphide (VMS), base metal (Pb-Zn-Cu) and gold (Au) and ultramafic-related Platinum Group Elements (PGE) and chromite deposits (Seymour *et al*. 2007 and Green 2012).

VMS deposits are major sources of Pb, Zn, Cu, Ag and Au, and they typically occur as lenses of polymetallic massive sulphide that form at or near the sea floor in submarine volcanic environment (Galley *et al*., 2007). They form from metal-enriched fluids associated with seafloor hydrothermal convection, and are hosted in either volcanic or sedimentary rocks. VMS deposits are discovered in submarine volcanic terranes ranging in age from the Archean to modern. The most common feature in VMS deposits is that they are formed in extensional tectonic settings, including oceanic and continental nascent-arc, rifted-arc, and back-arc environments. Significant VMS mining districts, such as Mount Read, Tasmania and Bathurst, New Brunswick, Canada, are defined by deposit clusters formed within rifts or calderas. Their clustering is further attributed to a common heat source that triggers large-scale sub-seafloor fluid convection systems. These sub-volcanic intrusions may also supply metals to the VMS hydrothermal systems through magmatism. A genetic VMS deposit model is illustrated in Figure 8.

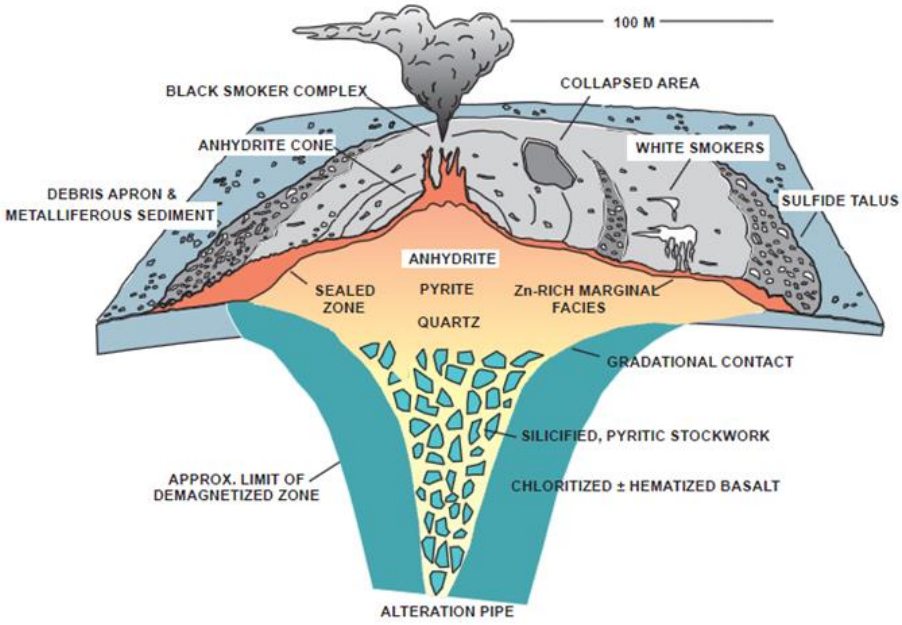

Schematic diagram of the modern Trans-Atlantic Geothermal (TAG) sulphide deposit on the Mid-Atlantic Ridge, depicting a cross-section of a VMS deposit with concordant semi-massive to massive sulphide lens underlain By a discordant stockwork vein system and associated alteration halo (from Galley et al., 2007).

Figure 8: A cross-section of a genetic VMS model (from Galley *et al*., 2007).

Most VMS deposits have two components. There is a mound-shaped to tabular, stratabound body composed mainly of massive sulphide, quartz, and iron oxide minerals and altered silicate wall-rock. The stratabound bodies are typically underlain by discordant to semi-concordant stockwork veins and disseminated sulphides. These stockwork veins, or “pipes”, are surrounded by distinctive alteration halos, which may extend into the hanging-wall strata above the VMS deposit.

Most VMS deposits have strong electromagnetic and magnetic responses. Pb, Zn and Cu often occur in highly conductive lenses of massive sulphides, and therefore are ideal targets for electromagnetic (EM) surveys (Ford *et al*., 2007).

Most VMS deposits in MRV have strong EM responses. Cu-rich ores have best EM response, while Zn-rich, Cu-poor ores have very weak to non-existent EM responses (Gemmell *et al*., 1998). Ores in MRV have no magnetic signature. However, the magnetic data can define major geological structures and volcanic units. EM method was responsible for the discovery of Que River and Hellyer deposits.

The cross-section of a typical mound-style VMS deposits in MRV is shown in Figure 9. The important mineralization features include the stratiform Pb-Zn massive sulphide, cross-cutting Cu-rich footwall stringers and the vertical (up-stratigraphy) zonation of Cu and Pb+Zn (Gemmell *et al*., 1998).

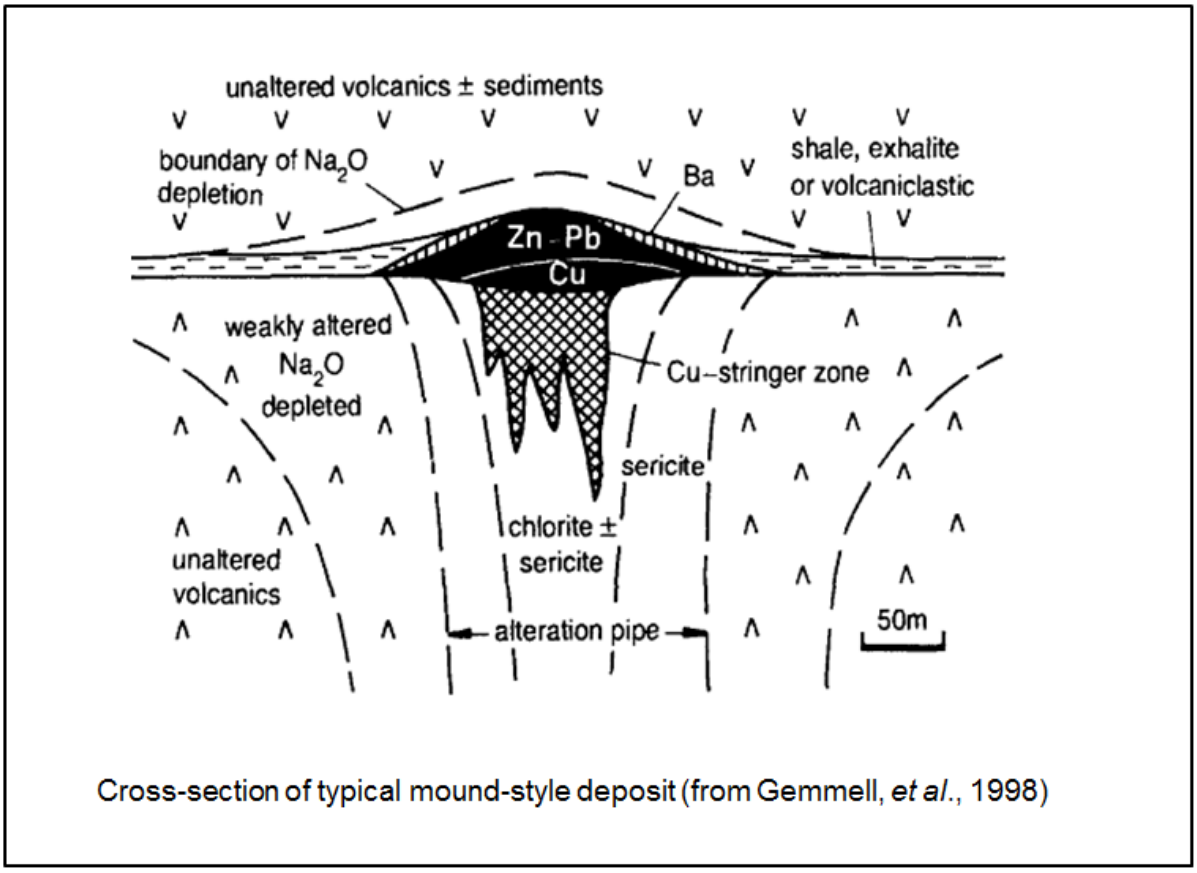

Figure 9: Mineralization features of mound-style VMS deposits in MRV (from Gemmell, *et al*., 1998).

Magmatic deposits containing economic quantities of Ni, Cu and Platinum Group Elements (PGE) are associated with variable amounts of localized sulphide concentrations in mafic and ultramafic rocks (Eckstrand *et al*., 2007). Ni-Cu deposits are associated with high concentration of sulphides, and the host bodies can be mafic to ultramafic rocks or dykes. Gabbro dykes of probable Neoproterozoic age host minor, but

locally high grade, Ni-Cu-Pt-Pd-Au mineralization in the Cu-Ni district, near Zeehan (Green 2012).

Ultramafic-related Platinum Group Elements (PGE) deposits are highly conductive and magnetic, and therefore are ideal targets for EM and magnetic methods.

3.4 Known Pb-Zn and Cu mineralization

Major Cambrian deposits in the Mount Read Volcanics (MRV), their tonnage and ore grades are listed in Table 1 (Seymour *et al*., 2007) and shown in Figure 10. Other known mineral occurrences in and around the survey blocks are also displayed.

Deposit	Tonnage and ore grades
Hellyer	16.5 Mt @13.9% Zn, 7.2% Pb, 0.38% Cu, 169 g/t Ag, 2.55 g/t Au
Que River	3.3 Mt @ 13.3% Zn, 7.4% Pb, 0.7% Cu, 195 g/t Ag, 3.3 g/t Au
Rosebery Read	34.04 Mt @ 13.8% Zn, 4.1% Pb, 0.57% Cu, 143 g/t Ag, 2.2 g/t Au
Hercules	3.33 Mt @ 17.3% Zn, 5.5% Pb, 0.4% Cu, 171 g/t Ag, 2.8 g/t Au
South Hercules	0.56 Mt @ 3.7% Zn, 1.9% Pb, 0.1% Cu, 157 g/t Ag, 3.0 g/t Au
Henty Mt Julia	2.83 Mt @ 12.5 g/t Au
Mount Lyell	311 Mt @ 0.97% Cu, 0.31 g/t Au

Table 1: Major Cambrian deposits in the MRV located near the survey blocks (Seymour *et al*., 2007).

Most of the known mineral occurrences, originally sourced from the Government of Tasmania and provided by Yunnan Tin Australia, are distributed near the major deposits, along the Henty Fault Zone, along a MRV corridor in EL50N and areas west of Hercules. The mineral occurrences were discovered either by geochemistry surveys or prospecting. There are a large number of known occurrences in EL22, but very few in EL46 and EL50S.

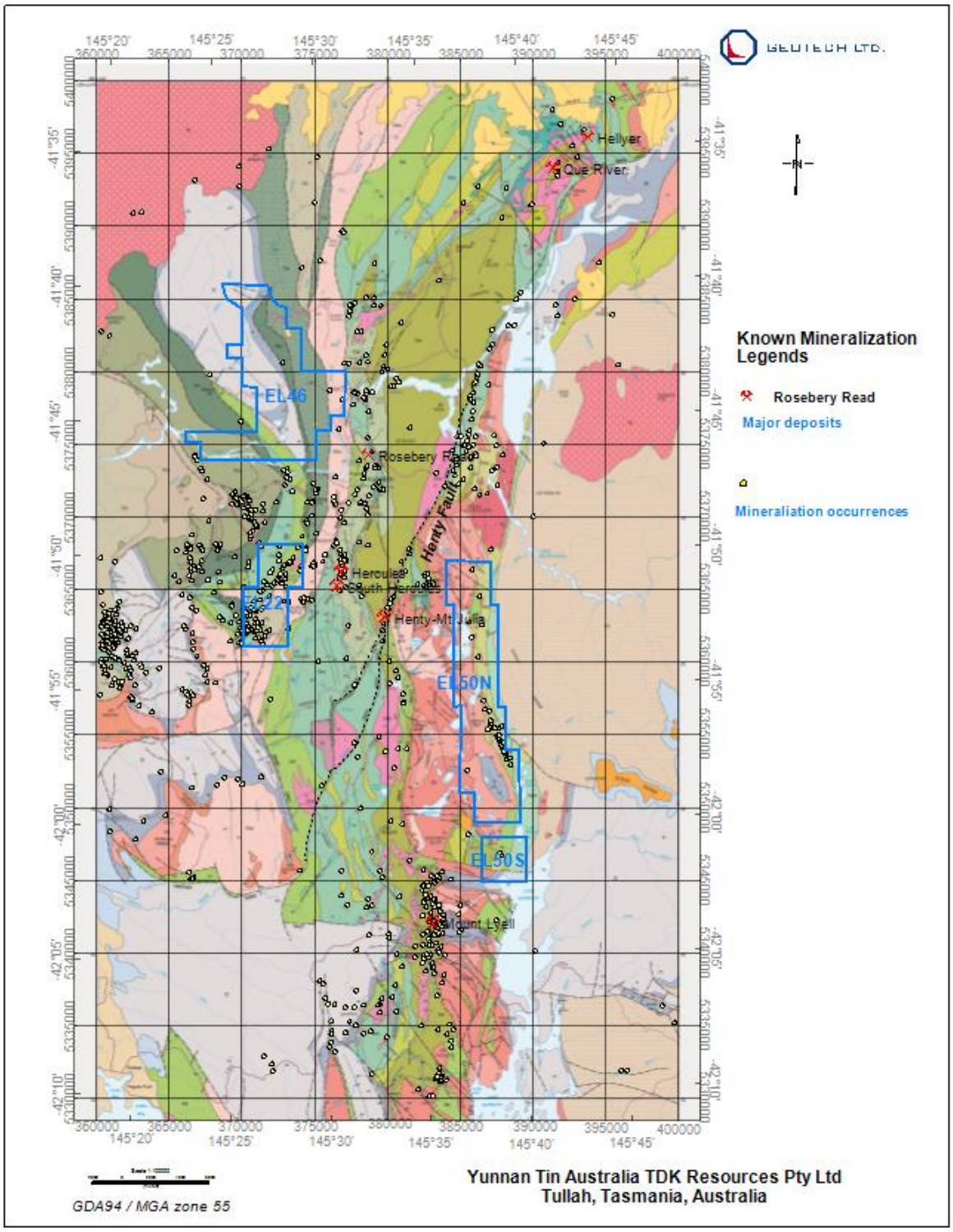

Figure 10: Known deposits and mineralization occurrences located close to the survey blocks.

3.5 Previous exploration work

Results of historical drilling in EL22 block (only one drillhole) and EL50N block (several

drillholes) are provided by Yunnan Tin Australia. The locations of these drillholes are displayed in Figure 11. The drilling results will be discussed during the detailed interpretation of targets for these two blocks.

Soil sampling data within EL22 block are provided by Yunnan Tin Australia to help interpretation. The data will be discussed in the context of target analysis for EL22.

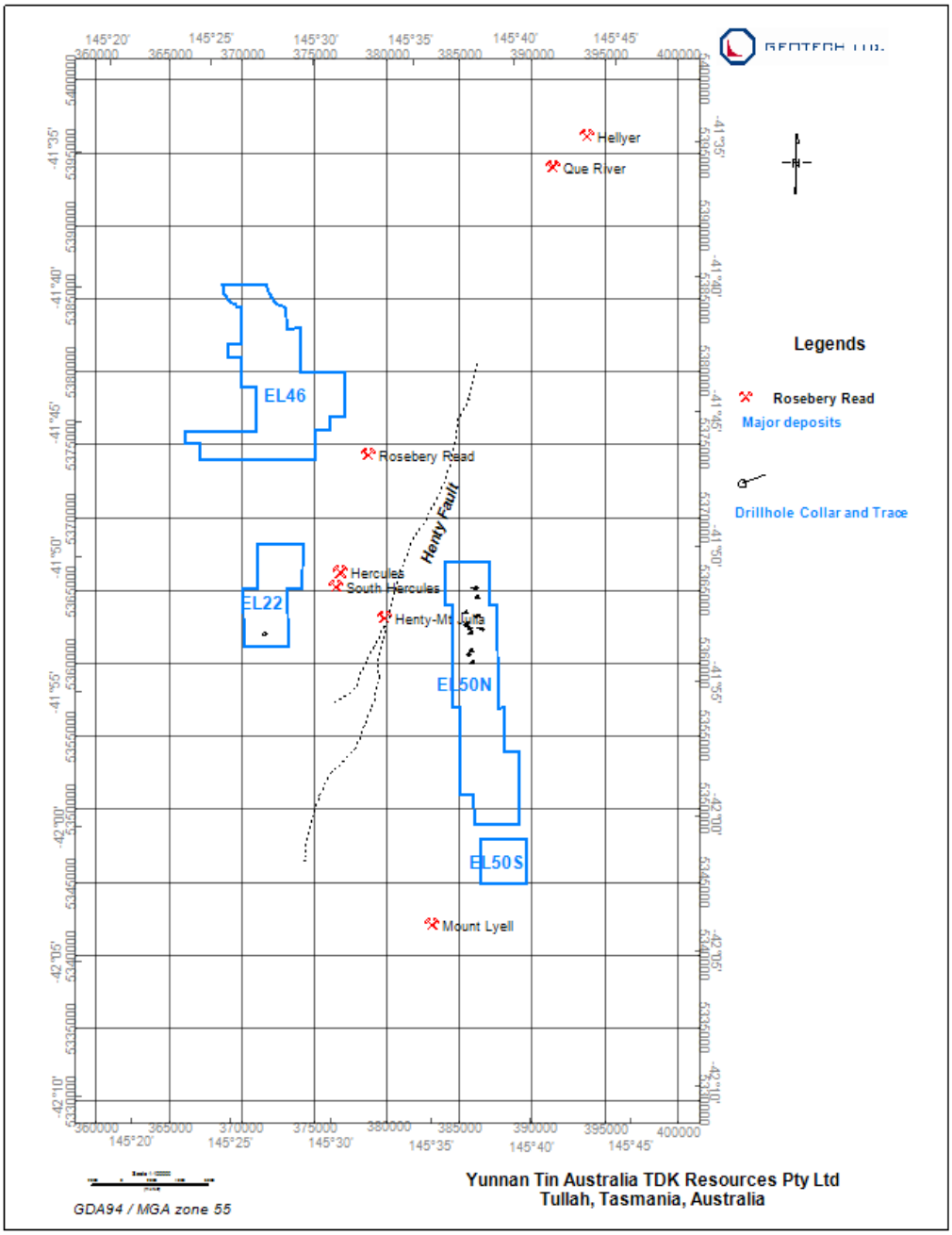

Figure 11: Locations of drillholes in EL22 and EL50N (supplied by Yunnan Tin Australia).

4. RESULTS OF INTERPRETATION

4.1 Description of Interpretation Methods

4.1.1 Magnetic interpretation methods

To simplify the interpretation, the magnetic data are reduced to the magnetic pole (RTP), assuming that the rocks in the survey area are magnetized parallel to the earth's magnetic field, i.e., induced magnetization.

Advanced derivatives are derived from the RTP, and they are:

- First and second vertical derivatives, which can increase spatial resolution and amplify the high frequency data;
- Analytic Signal, which is independent of the orientation of the magnetizations, including remanent magnetization, of the magnetic sources and can help to determine the locations of the magnetic sources, Nabighian 1972 and 1984;
- Tilt-Angle Derivatives, which can estimate both the horizontal locations and the depth of the magnetic bodies, Salem *et al*, 2008.

MAG3D, a magnetic 3D inversion program developed by the Geophysical Inversion Facility, University of British Columbia (UBC-GIF), is used to invert magnetic field into three-dimensional distribution of magnetic susceptibility. MAG3D is fully described in Li and Oldenburg 1996. To better understand MAG3D, a number of synthetic forward models and the magnetic responses from them were generated. The magnetic data were then inverted to test MAG3D. The results are presented in Appendix A.

MAG3D inversions for the survey areas are carried out. The mesh sizes in X and Y and in Z are listed in Table 2.

Block	Mesh size in X and Y (m)	Mesh size in Z (m)
EL22	75	50
EL46	100	50
EL50N	100	50
EL50S	50	50

Table 2: The mesh sizes used in MAG3D inversions;

Depth slices are extracted from the 3D magnetic susceptibility. 2D sections for all traverse lines are generated for EL46 block. Selected 2D magnetic susceptibility sections relevant in the analysis of targets have been created for other blocks. All MAG3D depth slices and 2D sections are delivered in the final DVD in Geosoft and raster formats. For details, please refer to Appendix F.

One of the main objectives of interpretation is to derive structural and lithological information for the survey area from the magnetic data. The interpretation will identify lithological units (volcanics, sediments and dykes) and structures, such as faults and magnetic “ridges”. The lithologies have been interpreted from the analytic signal, the second vertical derivative of the RTP and MAG3D depth slices. The faults and “ridges” have been interpreted from the second vertical and tilt-angle derivatives.

4.1.2 Electromagnetic interpretation methods

All regular survey lines are processed for Resistivity Depth Imaging (RDI) and 2D sections in Geosoft map format of the lines are generated. The RDI 2D sections for all regular lines are presented in PDF format as well. RDI Depth slices at various depths are extracted from RDI 3D voxel. The Geosoft maps of these RDI depth slices are generated. All the RDI products will be delivered in the final DVD. For details, please refer to Appendix E. The theory of RDI and some examples using synthetic VTEM data are presented in Appendix B.

EM anomalies will be picked from the VTEM data. Conductive zones will also be identified. Selected potential targets will be analyzed in detail, and some of the targets will be modeled by Maxwell © 2.5D plates[3] and the results are presented in separate PDF documents and they are:

AA1362_EL46_Maxwell_Modeling.pdf, and

AA1362_EL22_Maxwell_Modeling_R.pdf.

4.2 Results of 3D inversion of magnetic data

Magnetic data of EL22, EL46, EL50N and EL50S blocks are inverted to magnetic susceptibility distribution in 3D. Different rock types have different magnetic susceptibilities. The volcanic rocks are normally associated with high magnetic susceptibility while sediments usually have low magnetic susceptibility. Typical magnetic susceptibilities for some common rocks and minerals are shown in Figure 12.

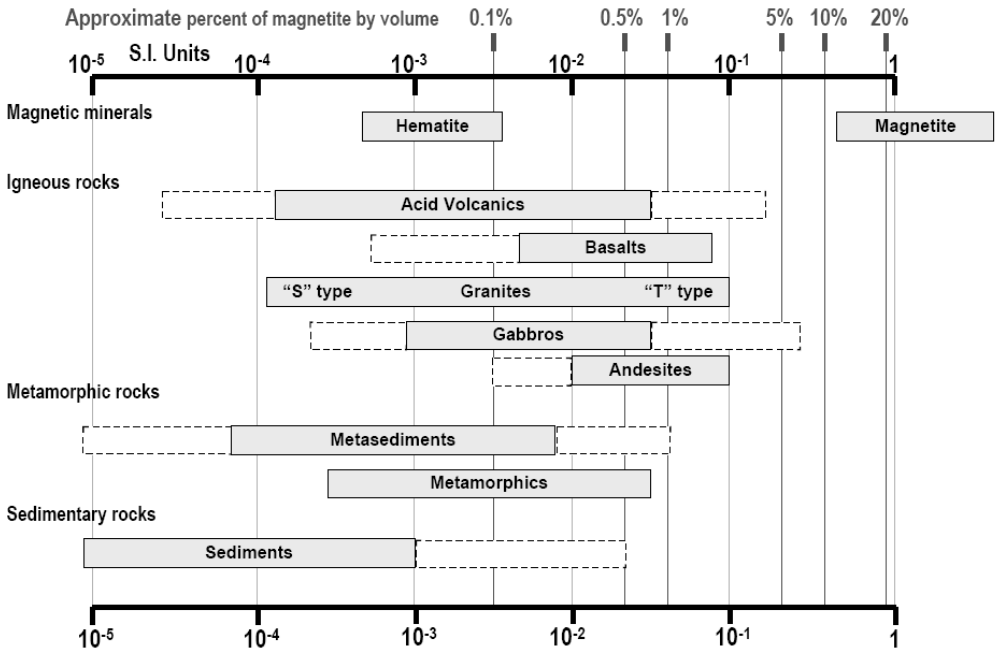

3 Maxwell 2.5D plate software is developed by ElectroMagnetic Imaging Technology (EMIT).

Figure 12: Typical magnetic susceptibilities for some common minerals and rocks (modified from Clark and Emerson, 1991).

A 3D view of the MAG3D susceptibility depth slices at depths from 50m to 350m at 50m interval, and from 500m to 3500m at 500m interval below ground, looking in the NW direction, EL46, is displayed in Figure 13.

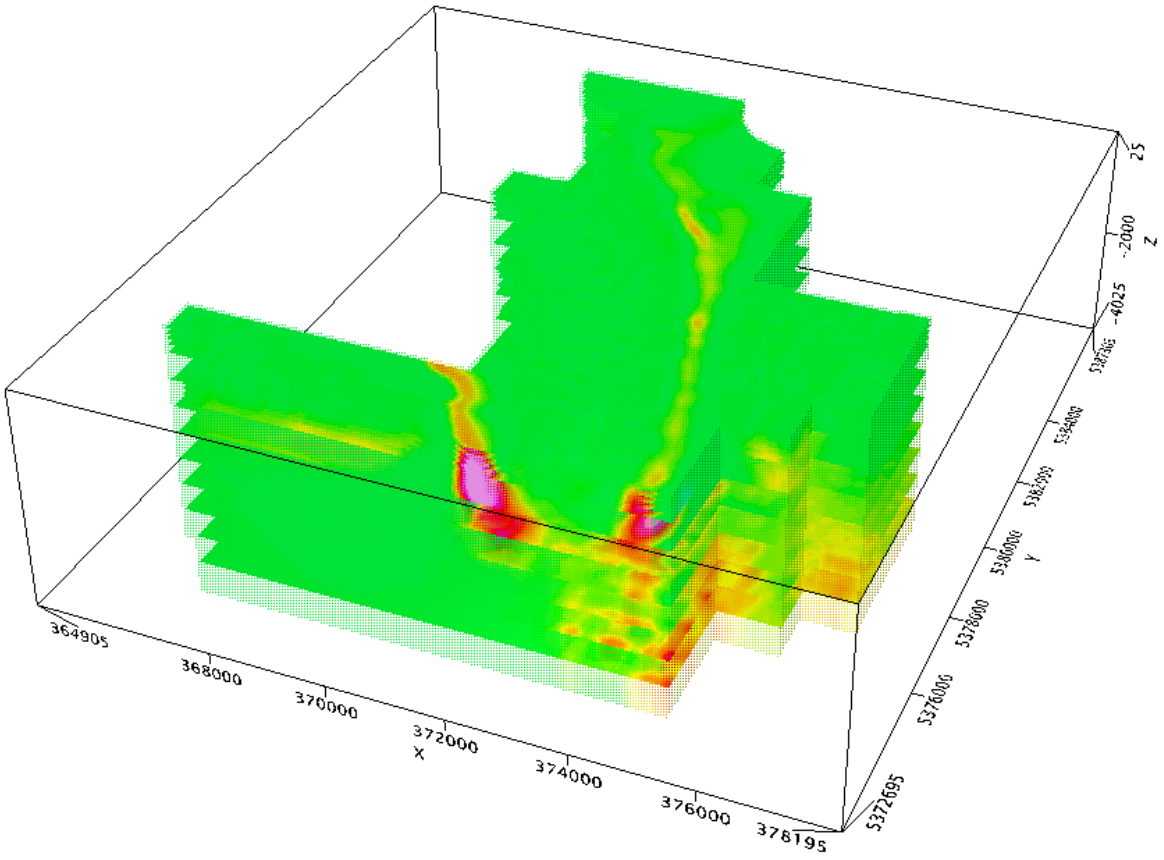

Figure 13: 3D view of MAG3D depth slices, looking NW, EL46.

Depth slices from 50m to 400m at 50m interval, and from 500m to 2500m at 500m intervals below ground are extracted for EL22 and shown in Figure 14.

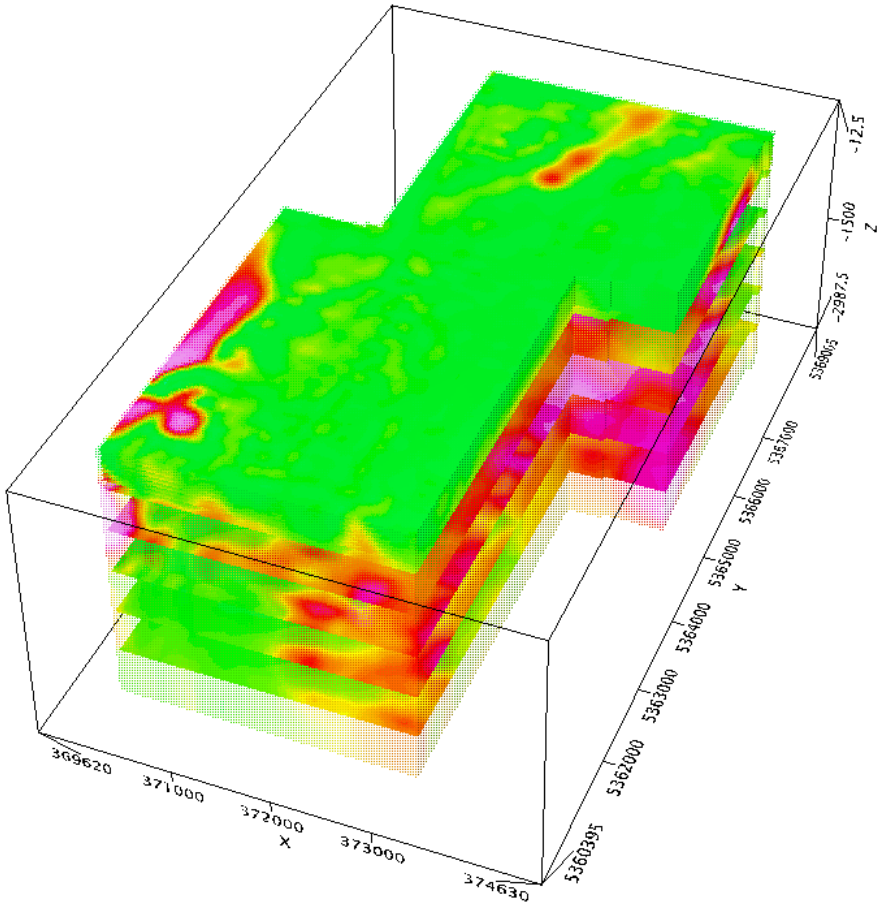

Figure 14: 3D view of MAG3D depth slices, looking nearly north, EL22.

For EL50N, depth slices from 50m to 350m at 50m interval, and from 500m to 3500m at 500m intervals below ground are extracted and are shown in Figure 15.

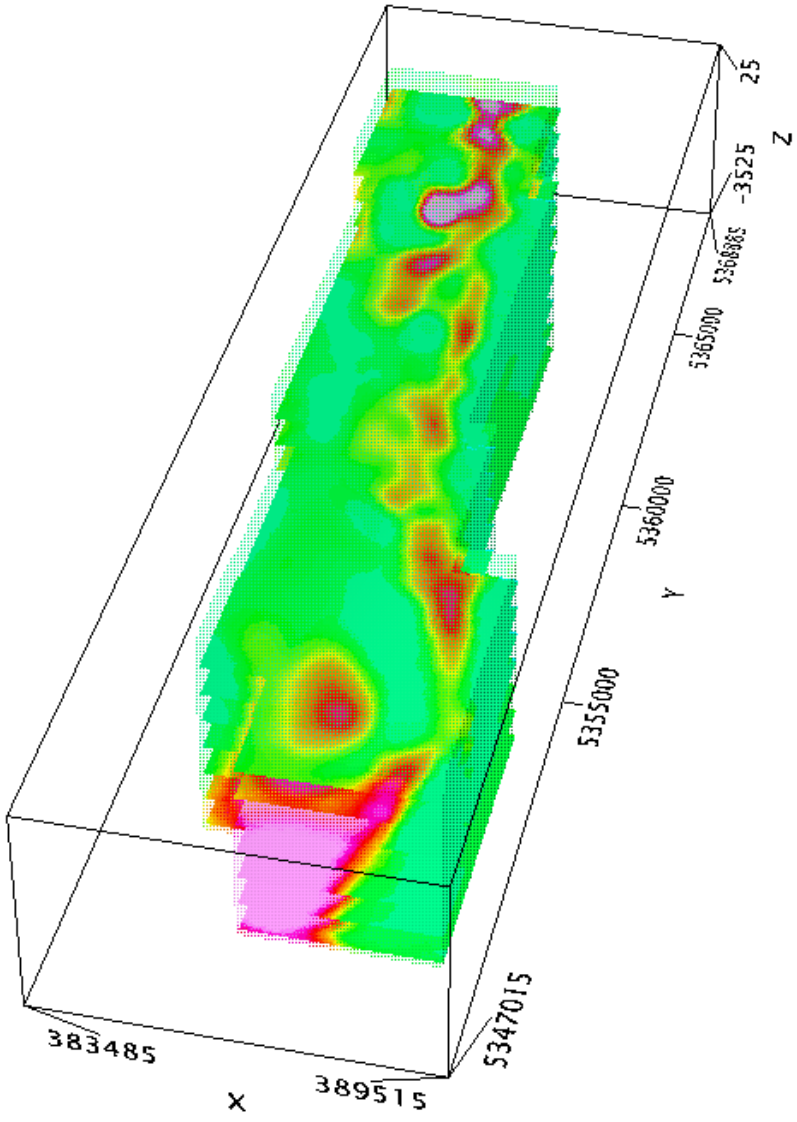

Figure 15: 3D view of MAG3D depth slices, starting at -500m level, looking nearly north, EL50N.

Finally, for EL50S, depth slices from 50m to 350m at 50m interval, and from 500m to 2000m at 500m intervals below ground are extracted and are shown in Figure 16.

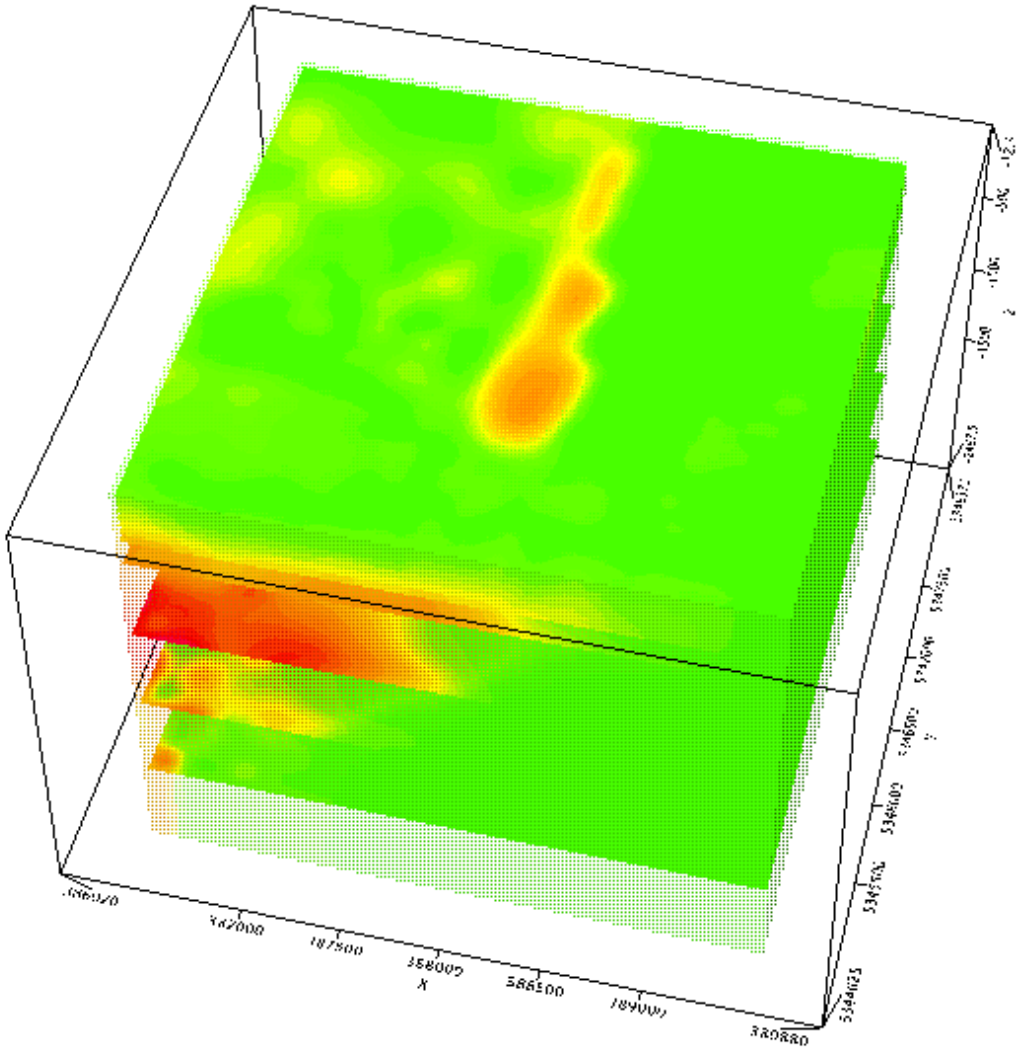

Figure 16: 3D view of MAG3D depth slices, looking north, EL50S.

One of the main advantages of the magnetic data is that they don't have the severe limit on the depth of the sources than the electromagnetic data. Normally, the magnetic data can detect large sources up to kilometers deep, while the depth of investigations of the time-domain EM data is in the order of hundreds of meters. Therefore, magnetic data and 3D inversions of the data are useful for locating geological structures favorable for VMS mineralization, i.e., faults, dykes or intrusives at depths much deeper.

There is a distinct possibility that some deep conductors lying over the magnetic sources are not detectable, or another possibility that some mineralization zones are not very conductive at all. In either scenario, the magnetic sources and their apical zones can be considered as potential targets for further exploration, even including test drilling. However, it is also reported that the Cambrian VMS ores don't have magnetic signatures at all (Gemmell, *et al*., 1998).

4.3 Structural and lithological interpretation of magnetic data

The interpreted structures and lithologies from the magnetic data of EL46, EL22, EL50N and EL50S blocks are presented in the following sections. Zones of very high magnetic responses correspond to mafic to ultramafic volcanics. Zones of moderate to high magnetic amplitudes are interpreted as volcaniclastics. Zones with low to moderate magnetic responses are interpreted as undifferentiated sediments, including sandstones, conglomerates, and limestones etc. The magnetic "ridges", which connect the magnetic highs, and structural lineaments, such as faults and dykes, are interpreted from the derivatives of the RTP, such as the second vertical derivative (2VD) and the tilt-angle derivative.

4.3.1 EL46 block

The prominent structural features in the survey area are the NNW-SSE trending mafic dykes, Figure 17. The directions of the interpreted faults are mainly in NE-SW and NW-SE directions.

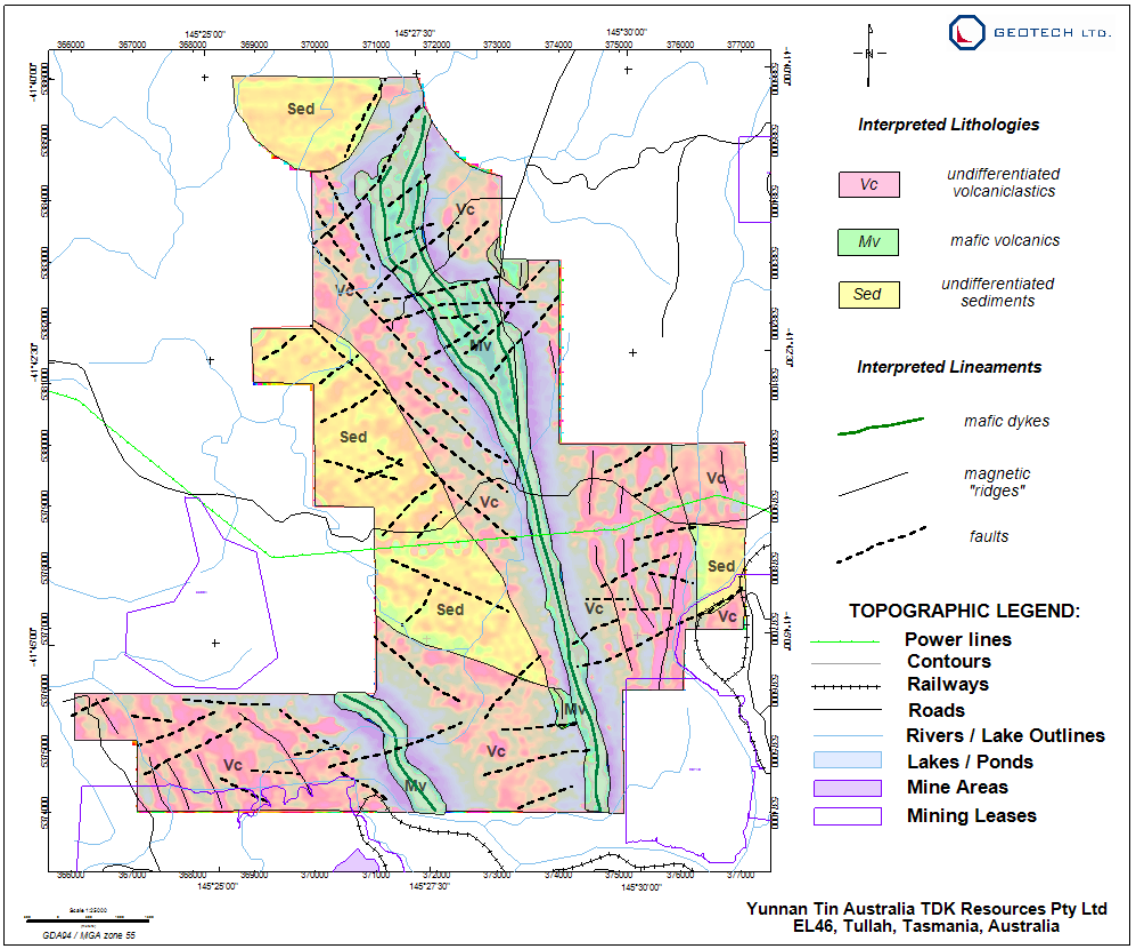

Figure 17: Interpretations of magnetic data, EL46, over 2VD.

The mafic dykes and volcanics (*Mv*) are flanked by undifferentiated volcaniclastics (*Vc*), and further away by undifferentiated sediments (*Sed*).

4.3.2 EL22 block

The dominant interpreted lithology in EL22 block is the Early Cambrian intrusive rock, the massive serpentinite (*Mvi*), Figure 18. The rest of the block is interpreted as volcaniclastics and undifferentiated sediments (*Vc-Sed*). Possible dykes, trending mainly NS, are also interpreted. The dykes in the sediments appear to be older, perhaps of Proterozoic age. The interpreted faults are trending mainly in the SW-NE direction.

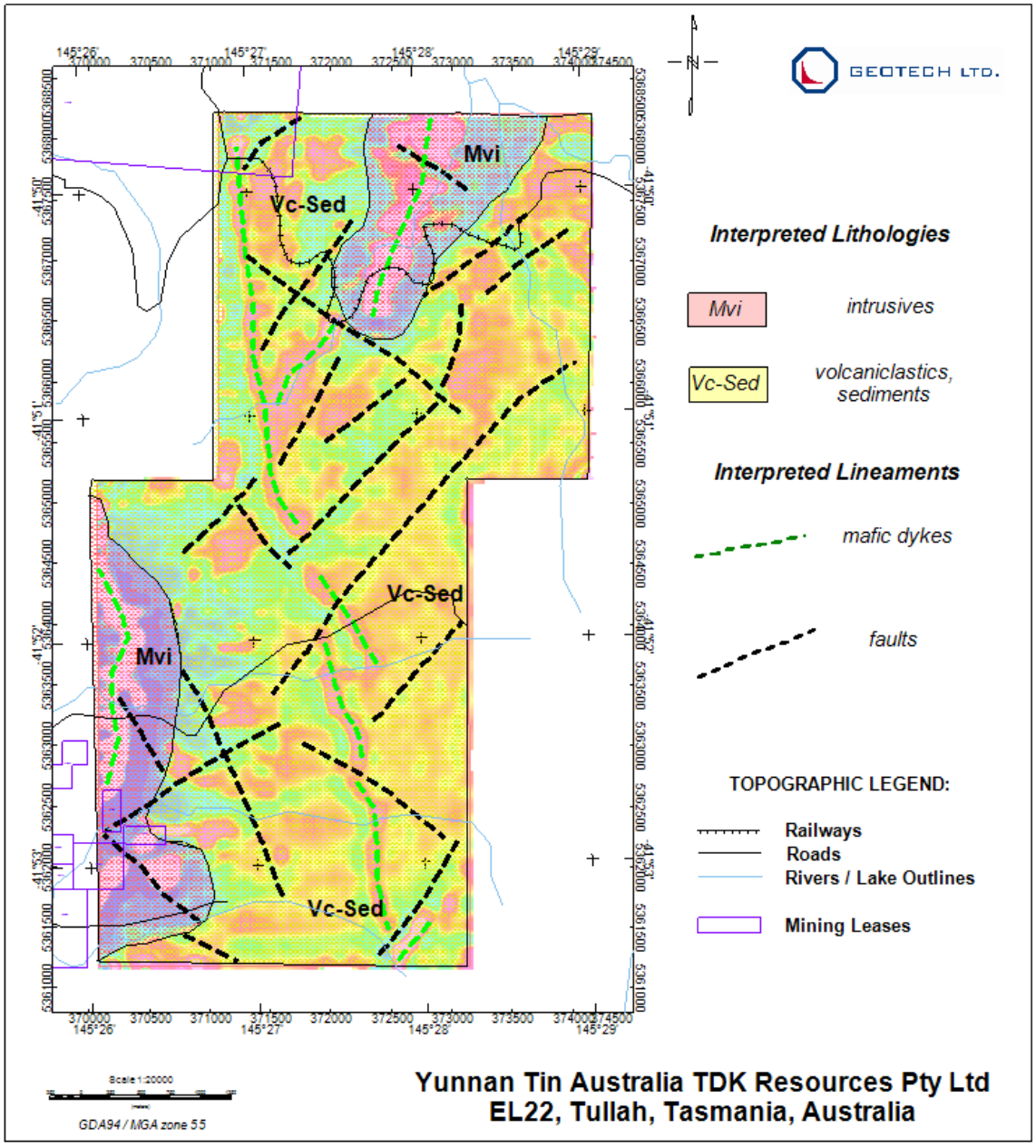

Figure 18: Interpretations of magnetic data, EL22, over 2VD.

4.3.3 EL50N block

The interpreted lithologies of EL50N block are almost equally divided into volcanics (*Mv),* including intrusives and volcaniclastics and undifferentiated sediments (*Sed*), Figure 19. A number of NS trending dykes are clearly seen in the volcanics. Faults are generally trending in WSW-ENE and NW-SE directions.

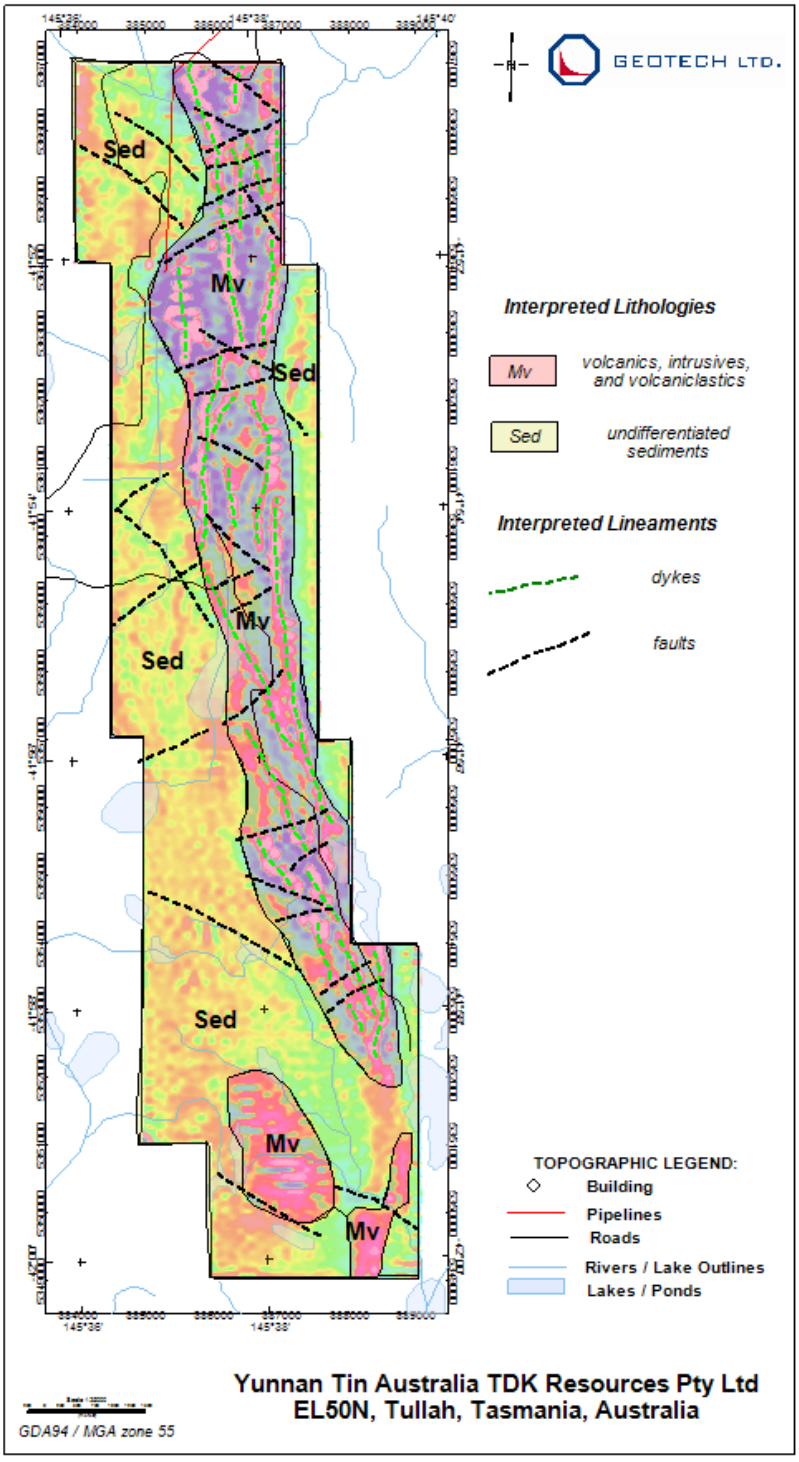

Figure 19: Interpretations of magnetic data, EL50N, over 2VD.

4.3.4 EL50S block

The high magnetic responses cover most of the NW region of EL50S block are interpreted as volcanics, intrusives and volcaniclastics (*Mv*), Figure 20. The rest are interpreted as

undifferentiated sediments (*Sed*). A couple of NS dykes are seen in the volcanic zone. Faults are generally trending in WSW-ENE and NW-SE directions.

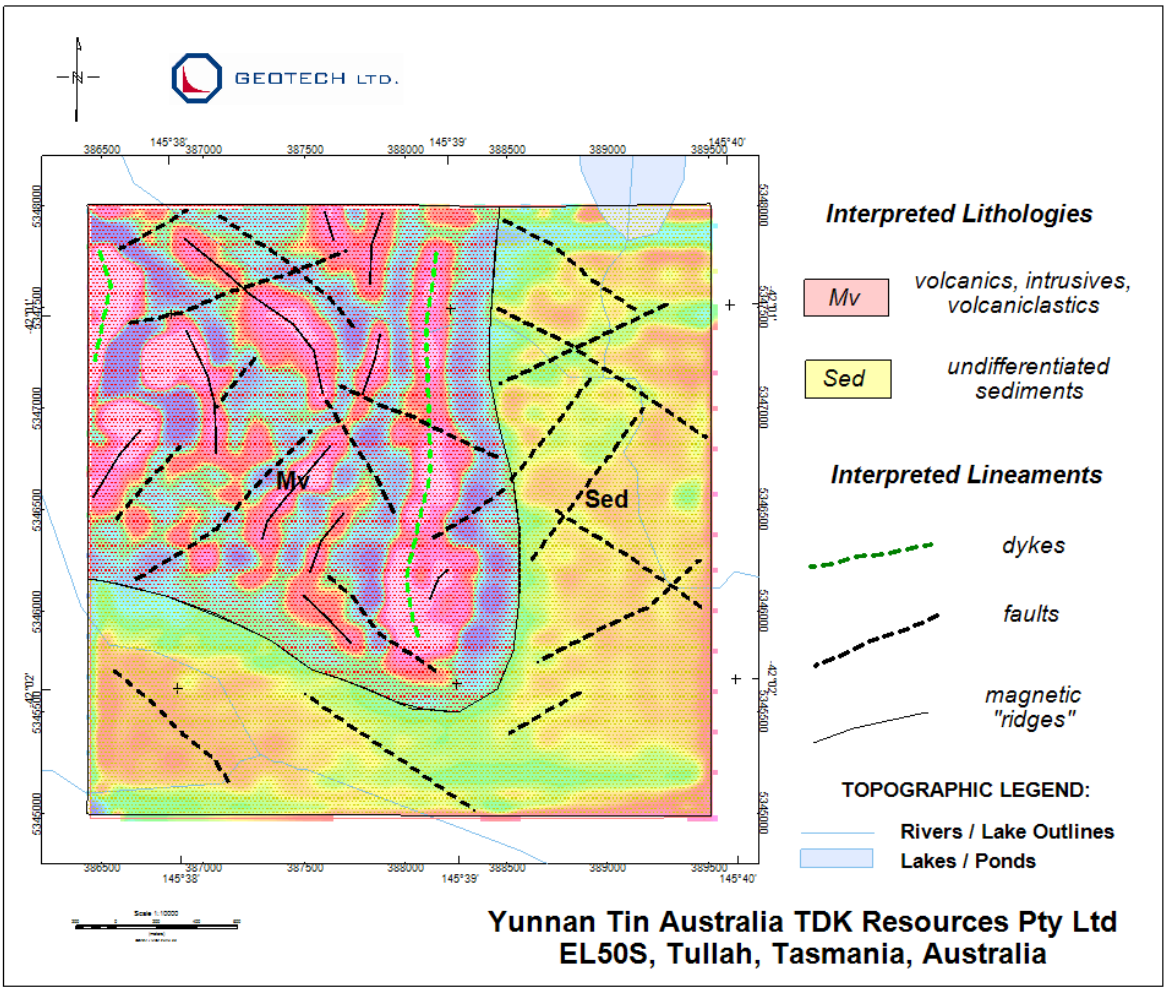

Figure 20: Interpretations of magnetic data, EL50S, over 2VD.

4.4 Results of EM Data Interpretation

The interpretation of EM data is accomplished by the picking of the EM anomalies, the analysis of EM data by Resistivity Depth Imaging (RDI) method explained in Appendix B, and the modelling of conductive targets by Maxwell 2.5D plates. Some synthetic Maxwell 2.5D plate models for VTEM are presented in Appendix D.

The objectives of EM interpretation are to identify conductive zones and trends and to model suitable conductors using Maxwell plates.

The EM data were screened by an anomaly recognition process that uses all time domain channels of the B-Field and dB/dt profiles, Tau and Power Line Monitor (PLM) profiles. The locations of the picks correspond approximately to the target's centre projected onto the surface. Each individual anomaly pick is represented by an anomaly symbol classified

according to calculated conductance[4]. Identified anomalies were classified into one of six categories, according to their conductance values. An anomaly symbol is accompanied by the calculated dB/dt and B-field conductances, thin conductor symbol, and anomaly ID, an identification letter unique to each anomaly along a flight line. The anomalous EM responses have been picked, reviewed and edited on a line by line basis. Power lines were not picked, but marked by special symbols for cultural anomalies. The anomaly picks are provided as a Geosoft GDB binary database and a Geosoft XYZ ASCII file.

4.4.1 EL46 block

The EM anomaly picks for EL46 are presented as overlays on time-constant TAU, Figure 21. Most of the thin conductors coincide with the NS mafic dyke in the south and follow a conductive axis east of the dyke in the north.

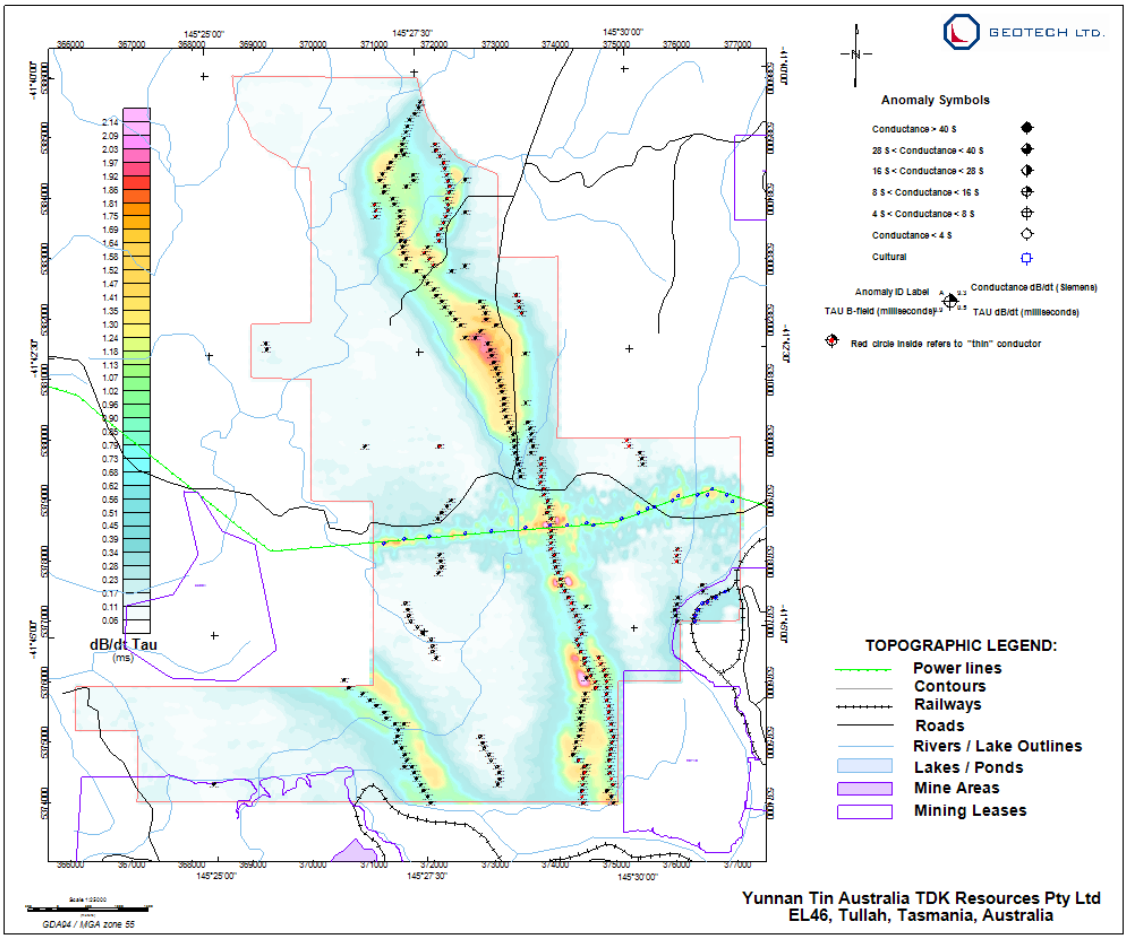

Figure 21: EM anomaly picks, EL46, over time-constant TAU.

The conductance and TAU ranges for the picked anomalies are listed in Table 3.

4 Conductance values were obtained from the dB/dt and B-Field EM time constants (Tau) whose relationships to Tau were calculated using the oblate spheroid model of McNeill, 1980.

Number of picked anomalies	Conductance, S dB/dT (min-max)	Conductance, S B-field (min-max)	TAU dB/dT (msec) (min-max)	TAU B-field (msec) (min-max)
275	1.14-58.7	0.01-112.8	0.06-3.16	0.01-6.06

Table 3: Conductance and TAU ranges for EM anomaly picks, EL46.

Conductive zones and axes are interpreted from the time-constant TAU and RDI depth slices, Figure 22. The mafic dykes coincide with strong linear conductors. However, the linear conductor in the north, to the east of the main mafic dyke, is associated with moderate magnetic responses.

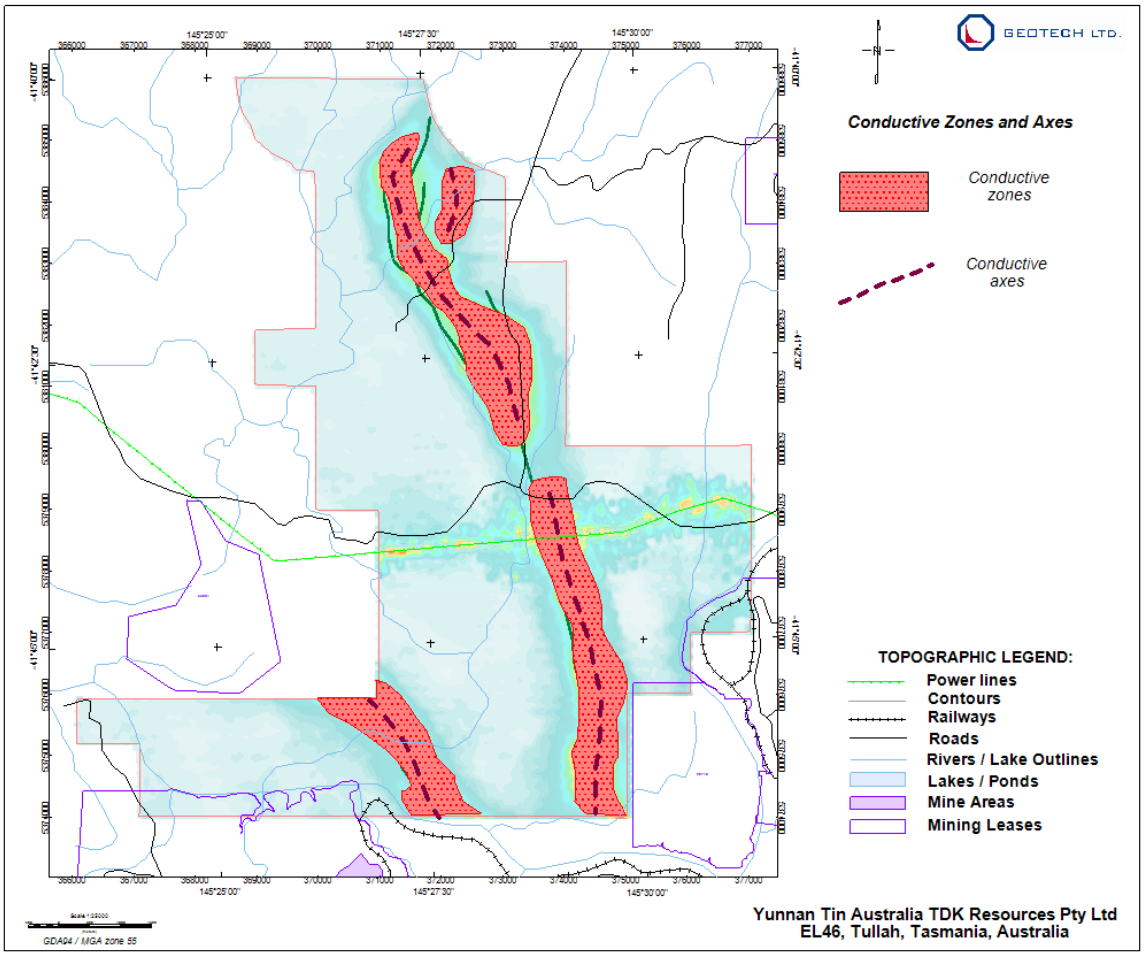

Figure 22: EM conductive zones and axes, EL46, over TAU.

4.4.2 EL22 block

The EM anomaly picks for EL22 are shown as overlays on time-constant TAU in Figure 23. Most of the quality and thin conductors are located in the north of EL22, along the serpentinite intrusives.

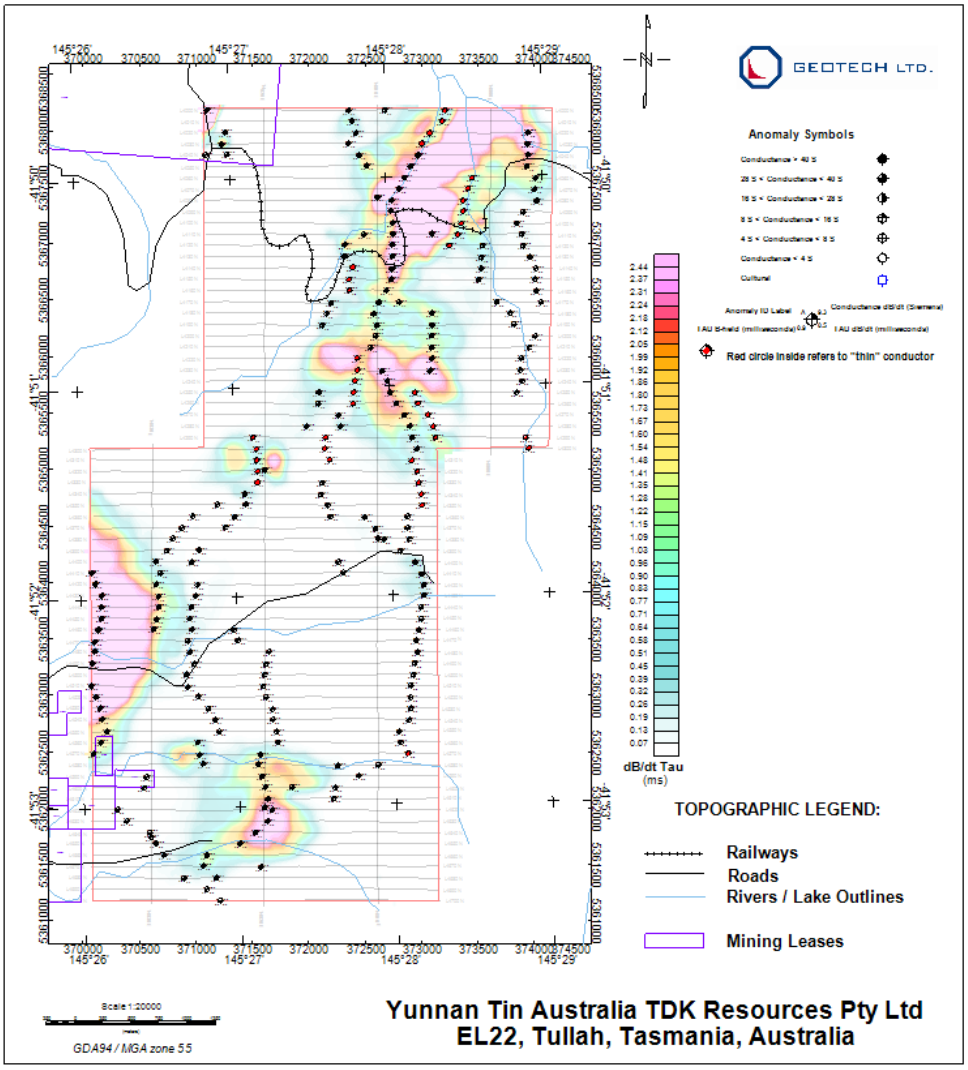

Figure 23: EM anomaly picks, EL22, over time-constant TAU.

The conductance and TAU ranges for the picked anomalies are listed in Table 4.

Number of picked anomalies	Conductance, S dB/dT (min-max)	Conductance, S B-field (min-max)	TAU dB/dT (msec) (min-max)	TAU B-field (msec) (min-max)
252	5.31-62.3	0.01-123.6	0.29-3.35	0.01-6.64

Table 4: Conductance and TAU ranges for EM anomaly picks, EL22.

Conductive zones and axes are interpreted from the time-constant TAU and RDI depth slices, shown in Figure 24. The main conductive zones coincide with the magnetic intrusive rocks in the south and along western edge of the block. However, three conductive zones in the center and south don't possess significant magnetic responses.

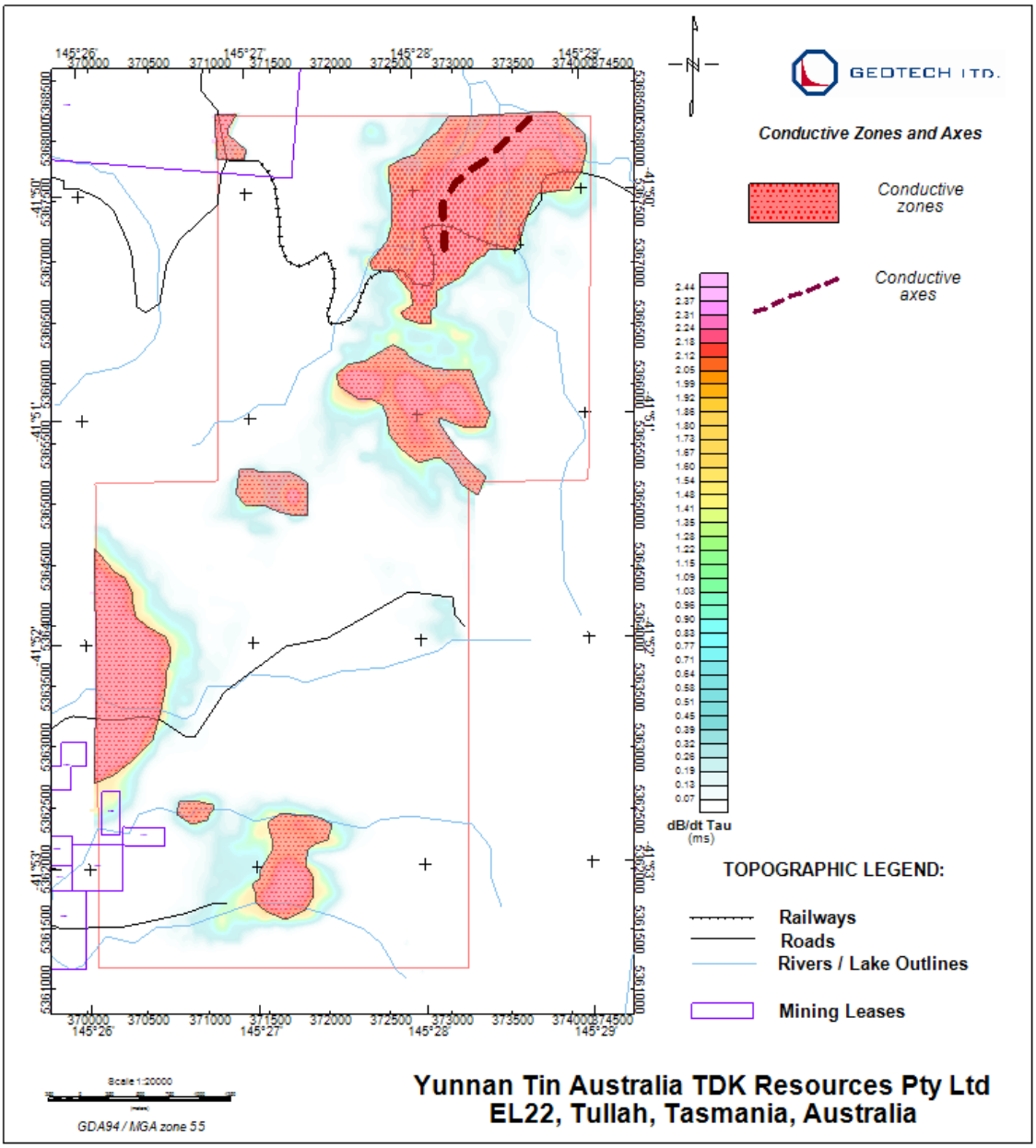

Figure 24: EM conductive zones and axes, EL22, over TAU.

Geochemistry (soil sampling) data

Yunnan Tin Australia has provided to Geotech some soil sampling data, some of which are from EL22, shown in Figure 25. The high assay counts of Cu, Pb and Zn are from locations either within or close to the conductive zones.

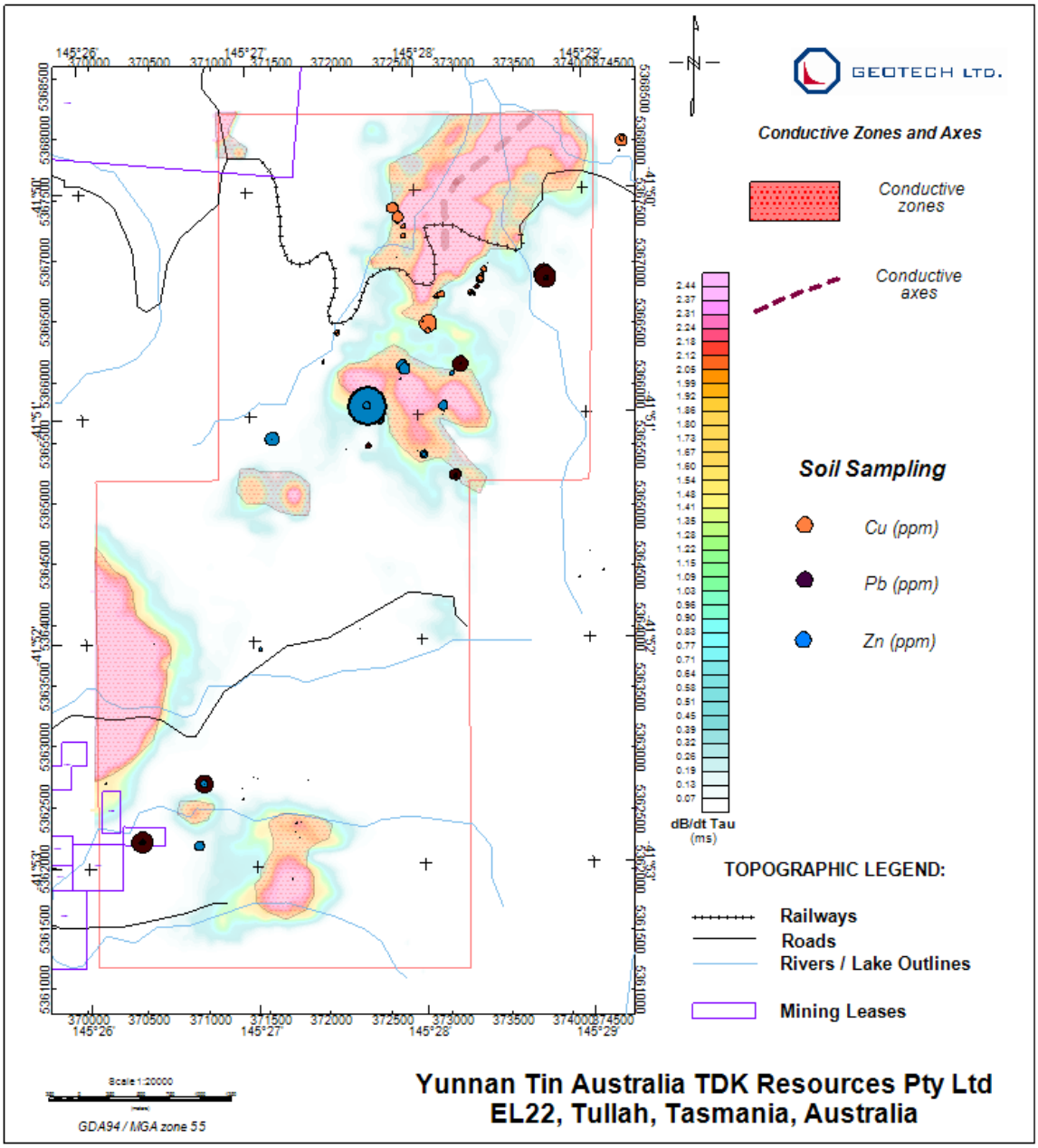

Figure 25: Geochemistry (soil sampling) data in EL22 (provided by Yunnan Tin Australia).

4.4.3 EL50N block

The EM anomaly picks for EL50N block are shown in Figure 26. Most of the quality and thin conductors are located along the eastern boundary of the block in the north, to the east of the volcanic rocks and the intrusives. Anomalous EM responses in the NW corner of the block belong to the man-made structures.

A number of notable negative EM anomalies, due to possible Airborne Induced Polarization (AIP) effect (Kratzer and Macnae 2012 and Weidelt 2002), are picked in the south of EL50N.

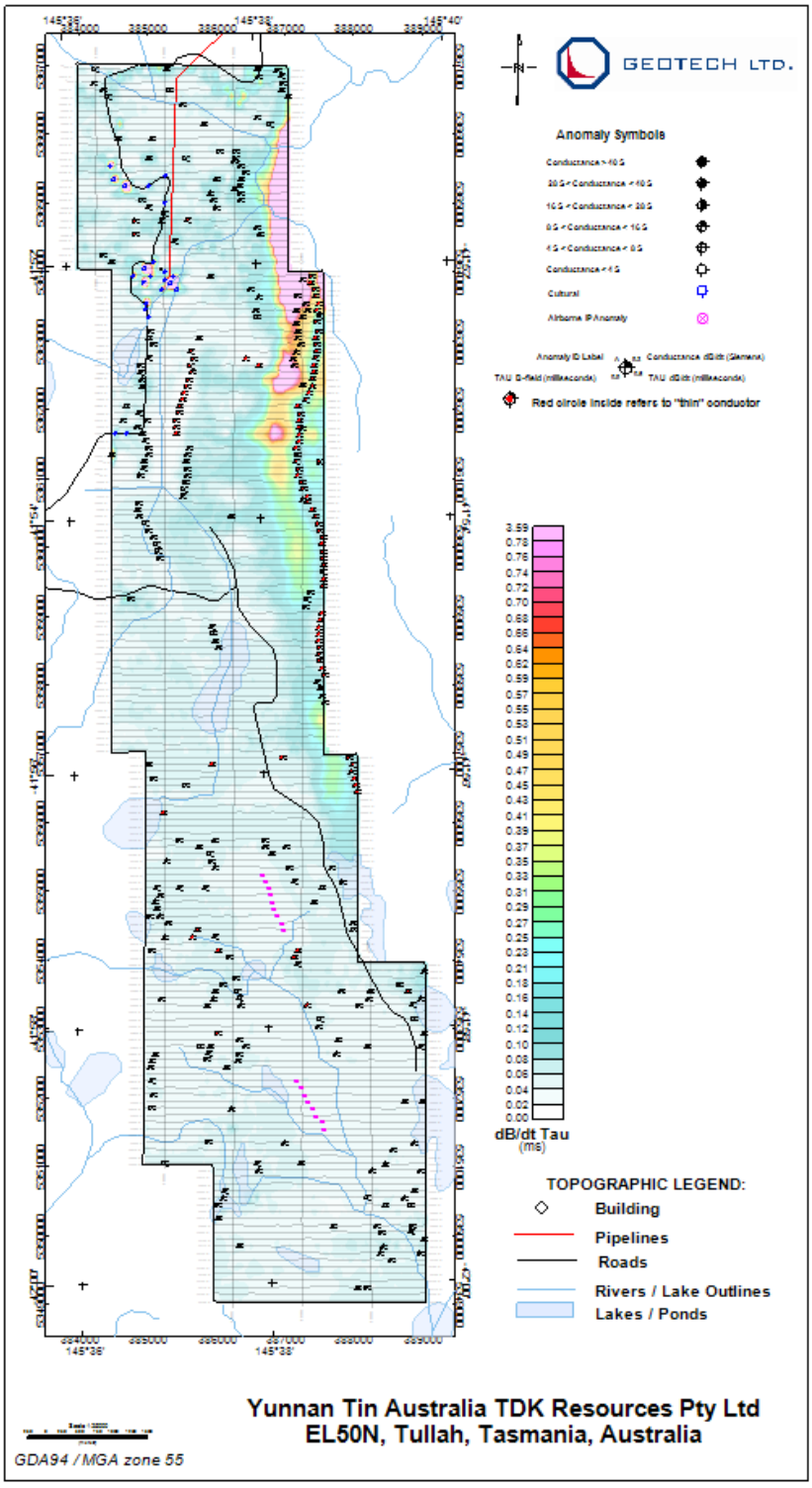

Figure 26: EM anomaly picks, EL50N, over time-constant TAU.

The conductance and TAU ranges for the picked anomalies are listed in Table 5.

Number of picked	Conductance, S	Conductance, S	TAU dB/dT	TAU B-field

anomalies	dB/dT (min-max)	B-field (min-max)	(msec) (min-max)	(msec) (min-max)
322	0.28-30.3	0.01-96.03	0.01-1.63	0.01-5.16

Table 5: Conductance and TAU ranges for EM anomaly picks, EL50N.

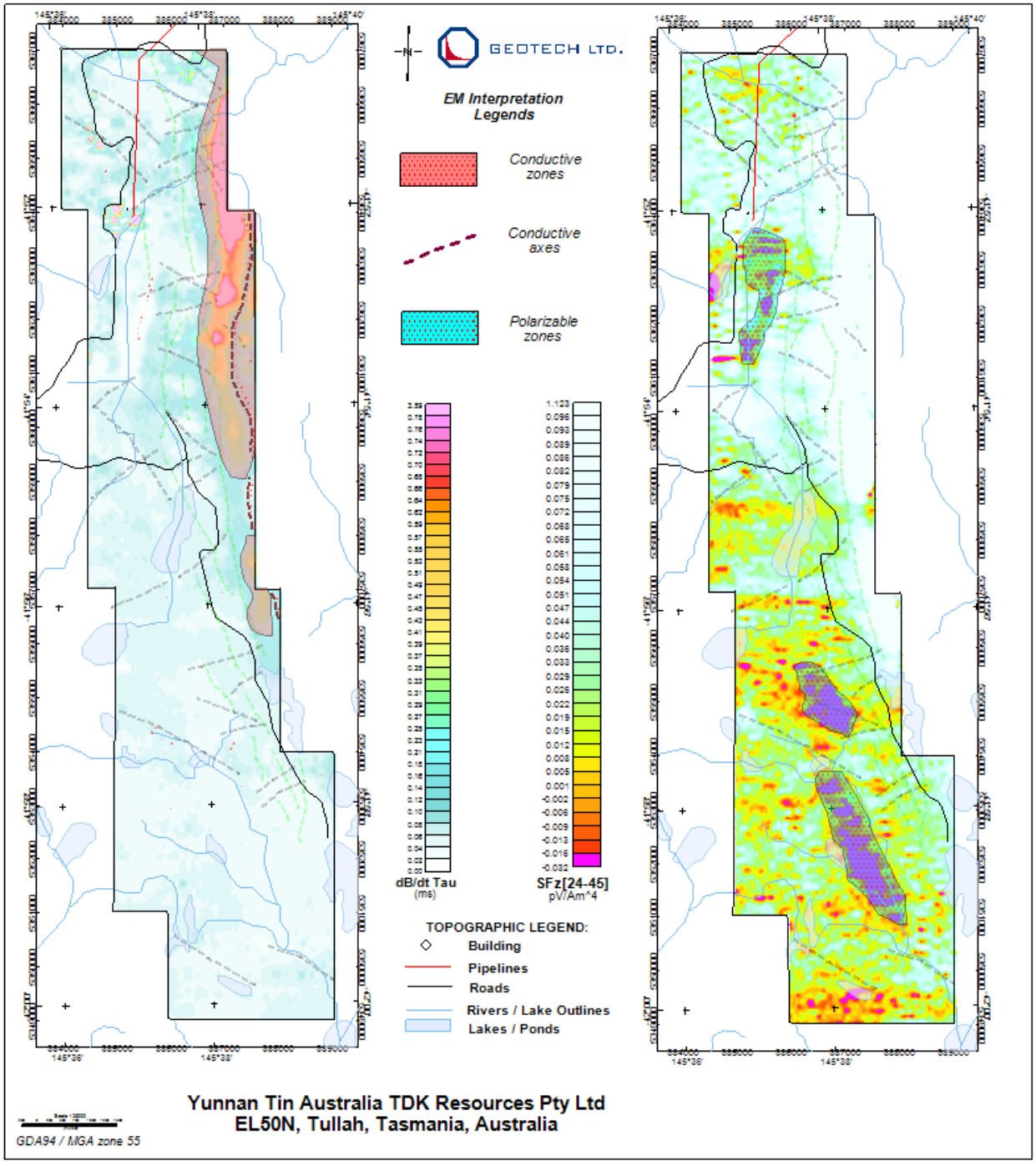

Figure 27: EM conductive (left) and polarizable (right) zones, EL50N, over TAU and SFz channels 24 to 45.

The conductive zones and axes interpreted from time-constant TAU and RDI depth slices.

They are located along the eastern edge of the block in the north. Three possible zones of AIP are identified, one in the north and two in the south, shown in Figure 27. The grids in the background are TAU for conductive zones (left) and dB/dt Z component off-time channels 24 to 45, or 0.358ms to 7.56ms, showing the negative transients for possible inductive polarization zones (right).

4.4.4 EL50S block

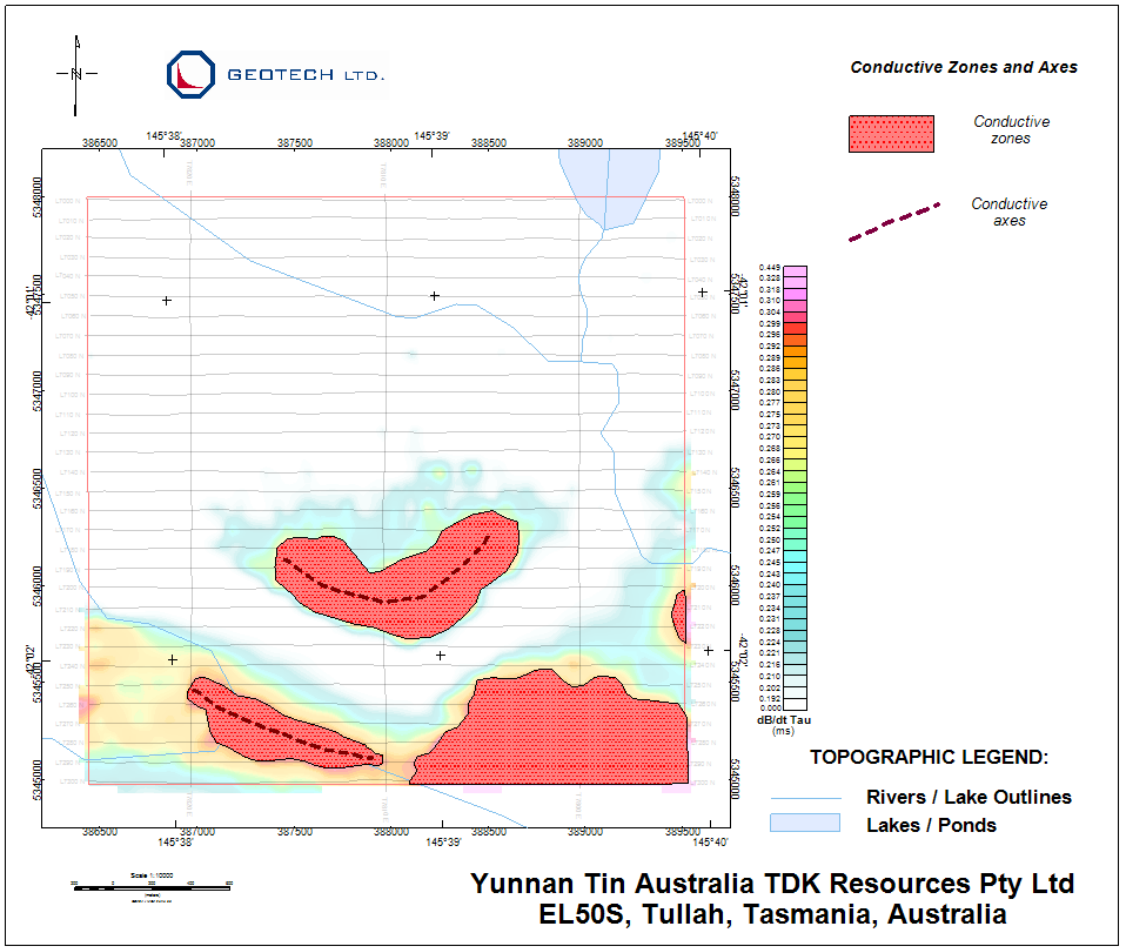

Figure 28: EM conductive zones and axes, EL50S, over TAU.

Conductive zones and axes for EL50S are interpreted from the time-constant TAU and RDI depth slices, shown in Figure 28. They are located in the south of the block.

4.5 Detailed Analysis of Conductive Targets

Based on the geophysical interpretation of the magnetic and EM (VTEM) data from the project areas, prospective targets have been selected for further follow-ups. Suitable targets are modelled with Maxwell 2.5D plate approximation.

The detailed analyses of each target zone are presented as a composite map of a

selected line within the zone. In the composite map, a plan view showing the location of the target zone and the selected line, a RDI 3D voxel view showing the RDI 2D section of the selected line and the Maxwell plate (if available), 2D RDI section with Calculated Vertical Gradient (CVG) profile, and MAG3D 2D section.

4.5.1 EL46 block

MAXWELL 2.5D PLATE MODELING

Five (5) targets, MX1 to MX5, are selected, and a number of Maxwell 2.5D plates are used to model the targets, Figure 29. For each Maxwell plate, recommended drillhole parameters are provided. The results are presented in a separate document, AA1362_EL46_Maxwell_Modeling.pdf.

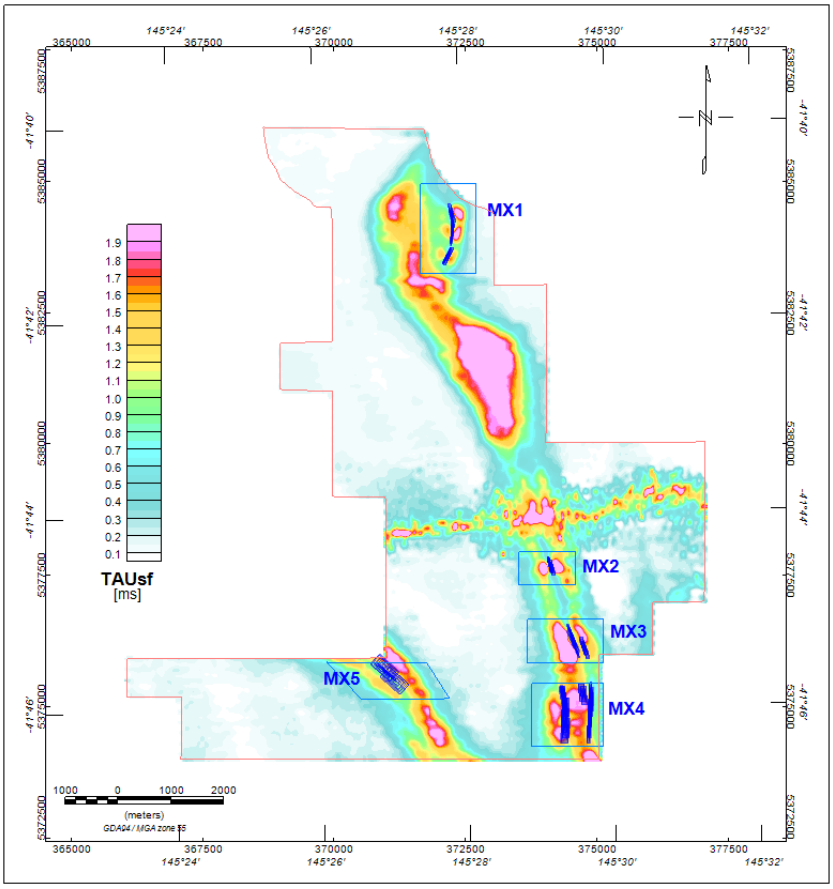

Figure 29: Prospective targets and Maxwell 2.5D plates, EL46.

MX1, L2200

Target MX1 is located in the northeast part of EL46. Shown in Figure 30 are detailed views of MX1 under L2200. The conductive target modelled by Maxwell 2.5D plate, MX1-L2200, has no or very little magnetic signature, but is next of a vertical mafic to ultramafic dyke. It seems to fit the description of Cu-rich (good EM responses) mineralization with no magnetic signature (Gemmell *et al*., 1998). The conductor is sub-vertical.

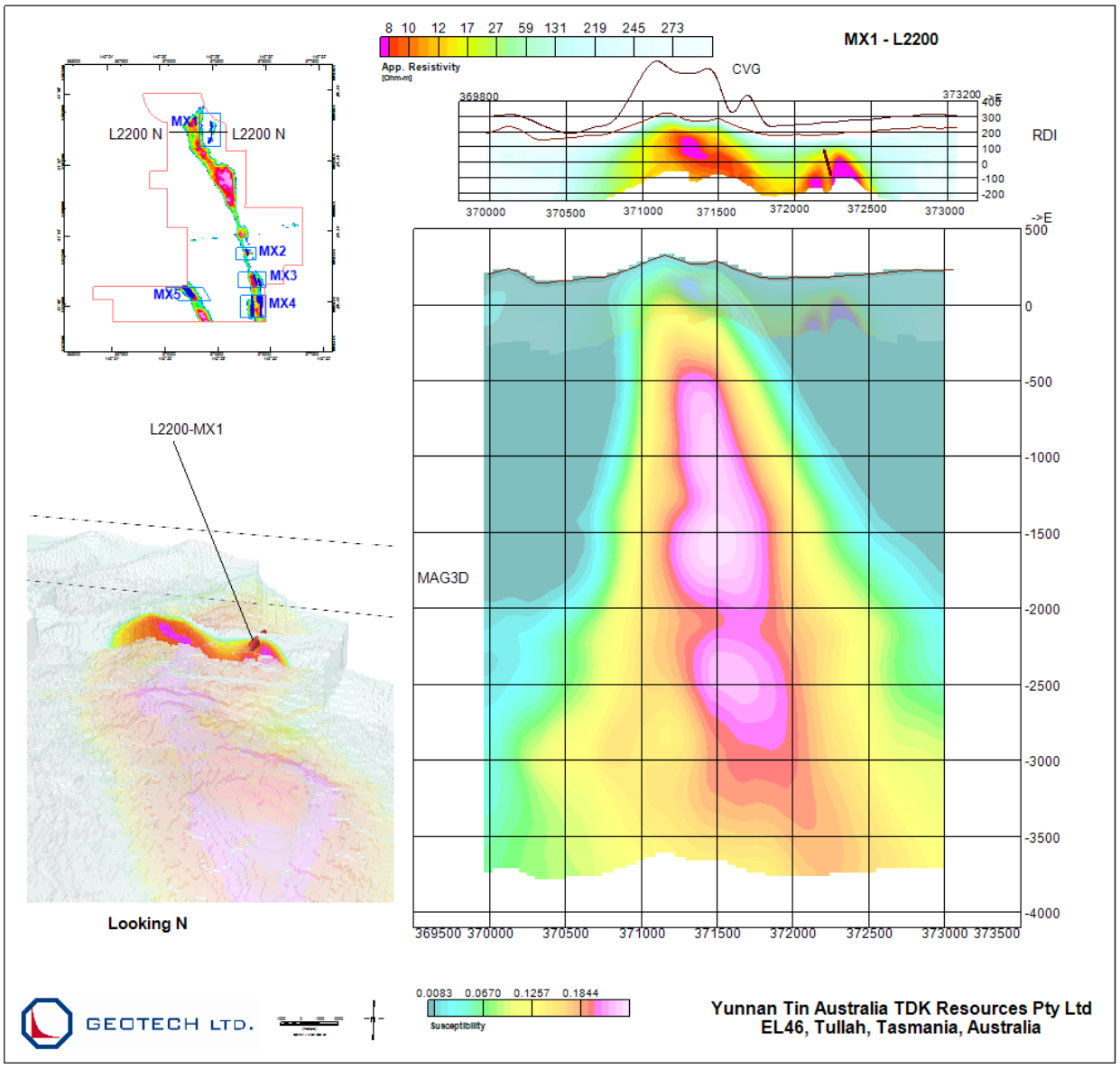

Figure 30: Detailed views of MX1, L2200 of EL46.

MX2, L2820

MX2 is located in the south of EL46 block, along the interpreted mafic to ultramafic dyke. Maxwell plate modeling of the conductor on L2820 indicates that it is sub-vertical, and is located on the eastern side of the mafic dyke, Figure 31. It has both the VMS and the ultramafic-related PGE potential.

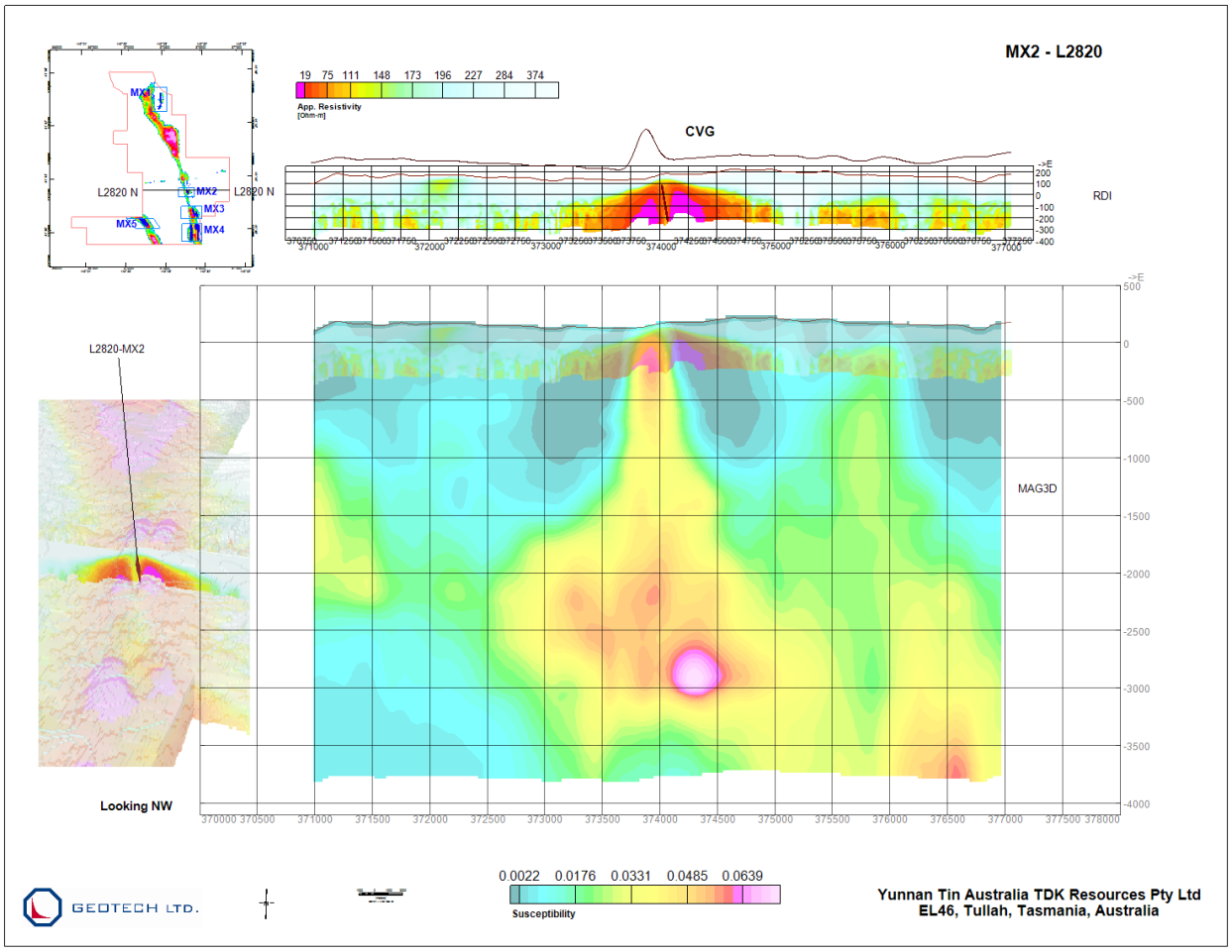

Figure 31: Detailed views of MX2, L2820 of EL46.

MX3, L2960

Further south of MX2 along the interpreted mafic dyke lies MX3. The conductor on L2960 modelled by Maxwell 2.5D plate is sub-vertical, located just east of the dyke, as shown in Figure 32. MX3 has the potential for VMS as well as ultramafic-related PGE mineralization.

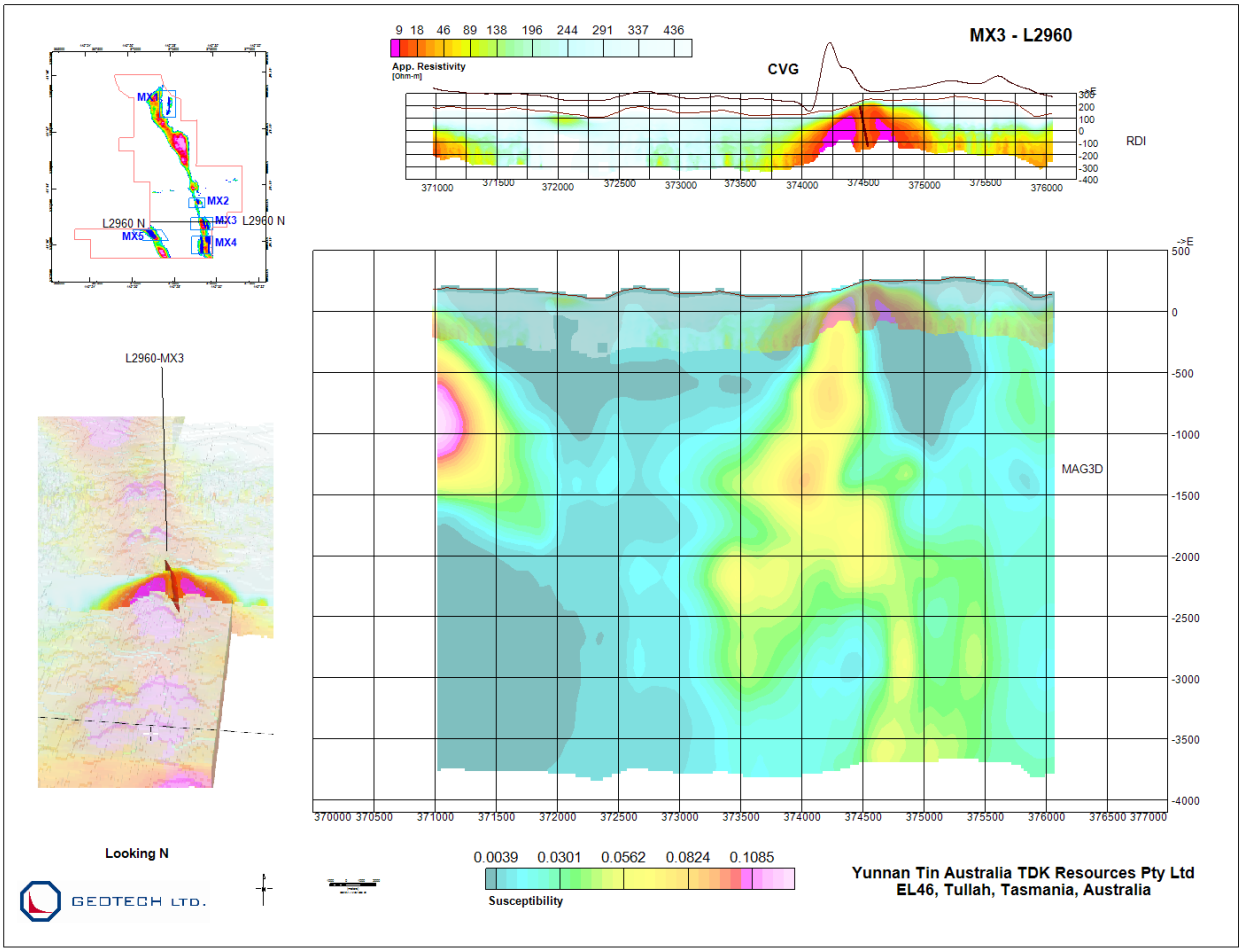

Figure 32: Detailed views of MX3, L2960 of EL46.

MX4, L3110

Target MX4 is located near the southern edge of EL46 block. The EM anomaly at the eastern end of L3110 is modelled by two sub-vertical Maxwell plates, on the sides of the mafic to ultramafic dyke, Figure 33. MX4 has both VMS and PGE mineralization potential.

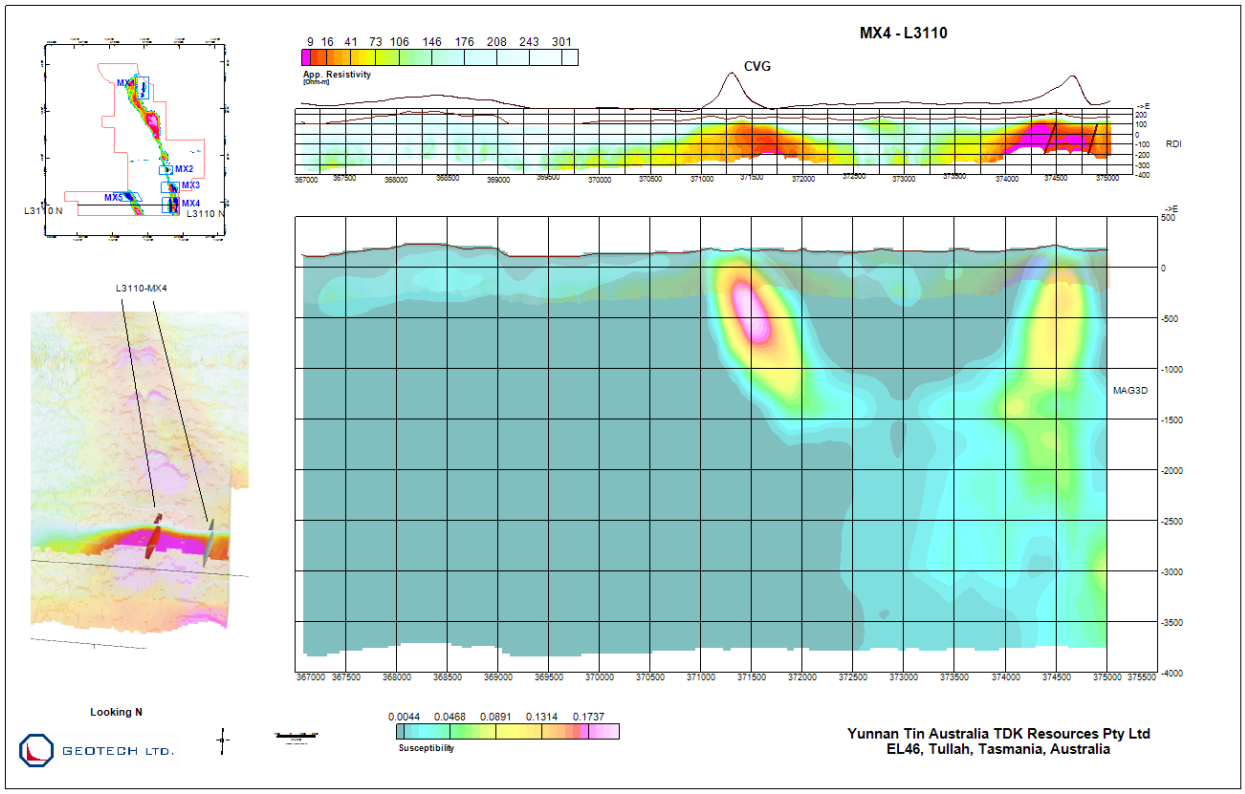

Figure 33: Detailed views of MX4, L3110 of EL46.

MX5, L3050

West of the main conductive trend is another linear conductor, and part of it is marked as target MX5, Figure 34. The conductor on L3050 is modelled by two sub-vertical Maxwell plate, striking along the conductor trend. The conductor seems to coincide with the interpreted mafic dyke. So it may have mafic-related PGE potential.

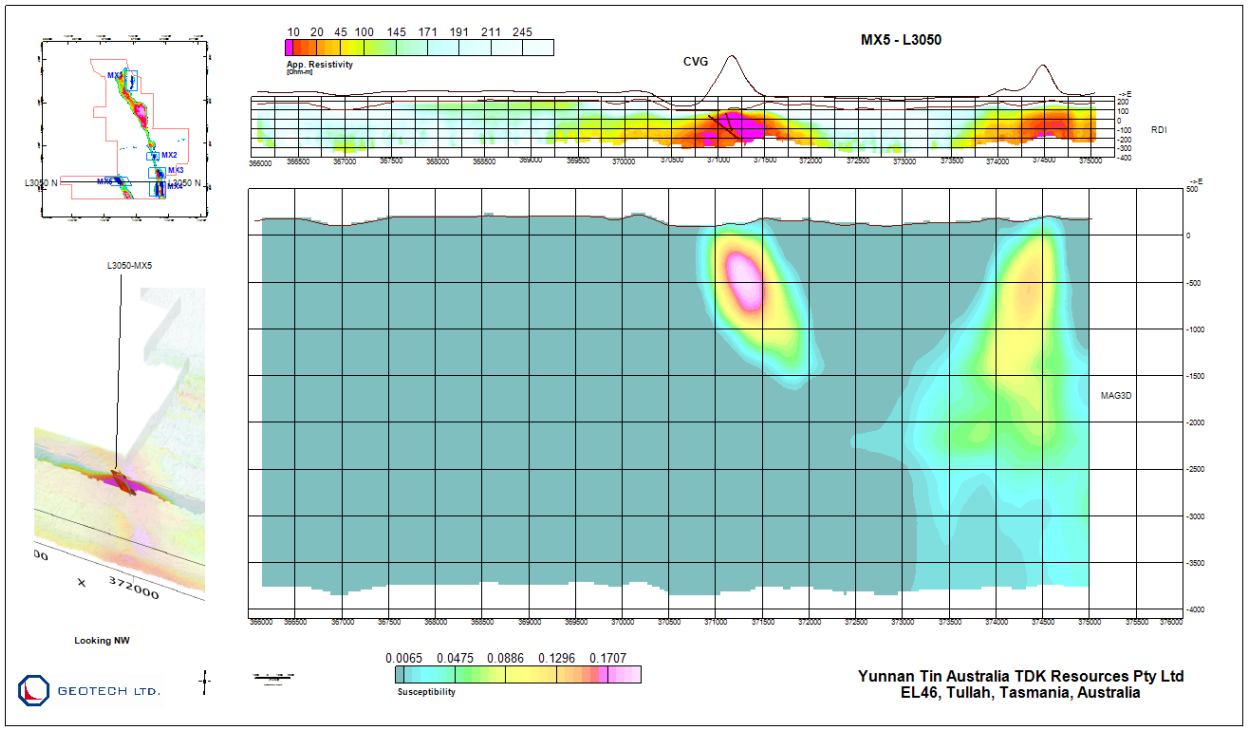

Figure 34: Detailed views of MX5, L3050 of EL46.

4.5.2 EL22 block

MAXWELL 2.5D PLATE MODELING

Four target zones are selected for Maxwell plate modelling in EL22. The locations of the plate models are shown in Figure 35. The descriptions of the Maxwell modelling results, along with recommended test drilling parameters, are presented in a separate document named as AA1362_EL22_Maxwell_Modeling_R.pdf.

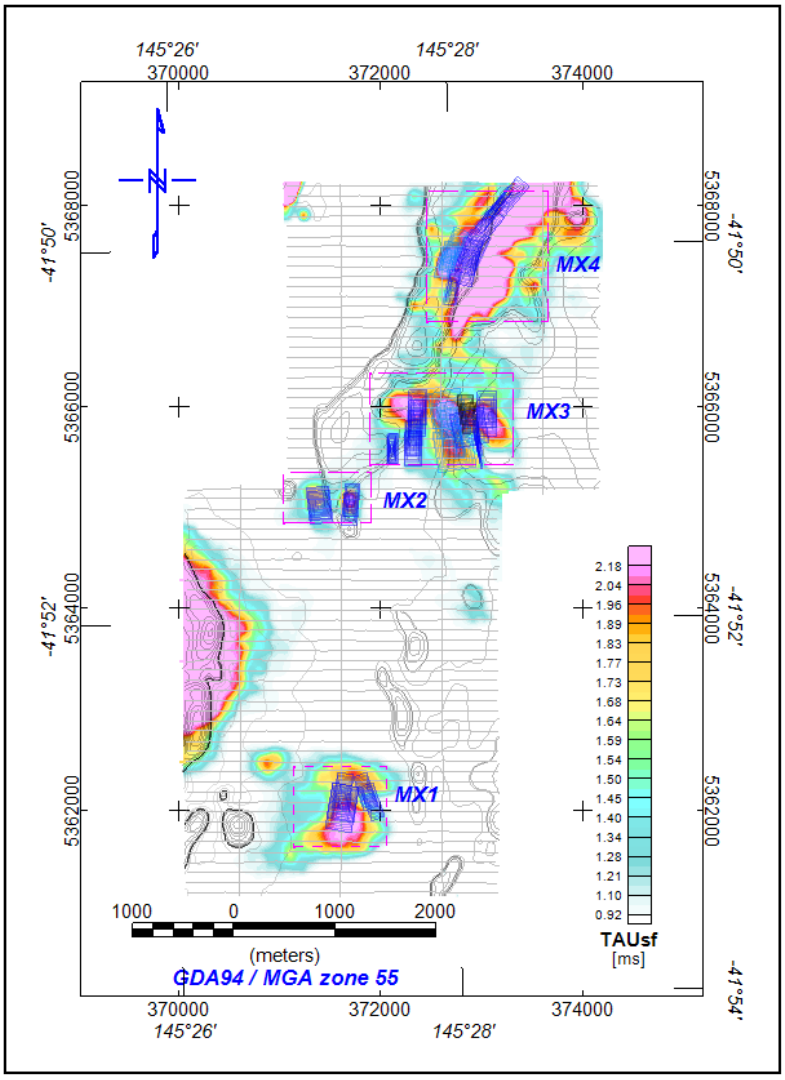

Figure 35: Target and Maxwell 2.5D plate locations, EL22.

MX1, L4610

MX1 is located in the south of EL22. Line L4610 is selected for detailed analysis of the target, Figure 36. There is a drillhole, DDH CC0_5, near the centre of L4610. The conductor test drilled by CC0_5 is modelled by a sub-horizontal plate, which appears to coincide with the Pb/Zn assay highs. Approximately 300m below the plate, there is a Cu high. At nearly 400m below ground, the Cu mineralization appears to be beyond the depth of investigation (DOI) of the VTEM system in that particular geological environment. The drillhole trace and assay results are also projected onto the RDI and MAG3D 2D sections. The vertical zonation of Pb/Zn and Cu mineralization appears to support that this target could be a typical mound-style VMS model described in Gemmell *et al*. 1998. From the MAG3D section, it appears the target is located close to a major contact or fault zone.

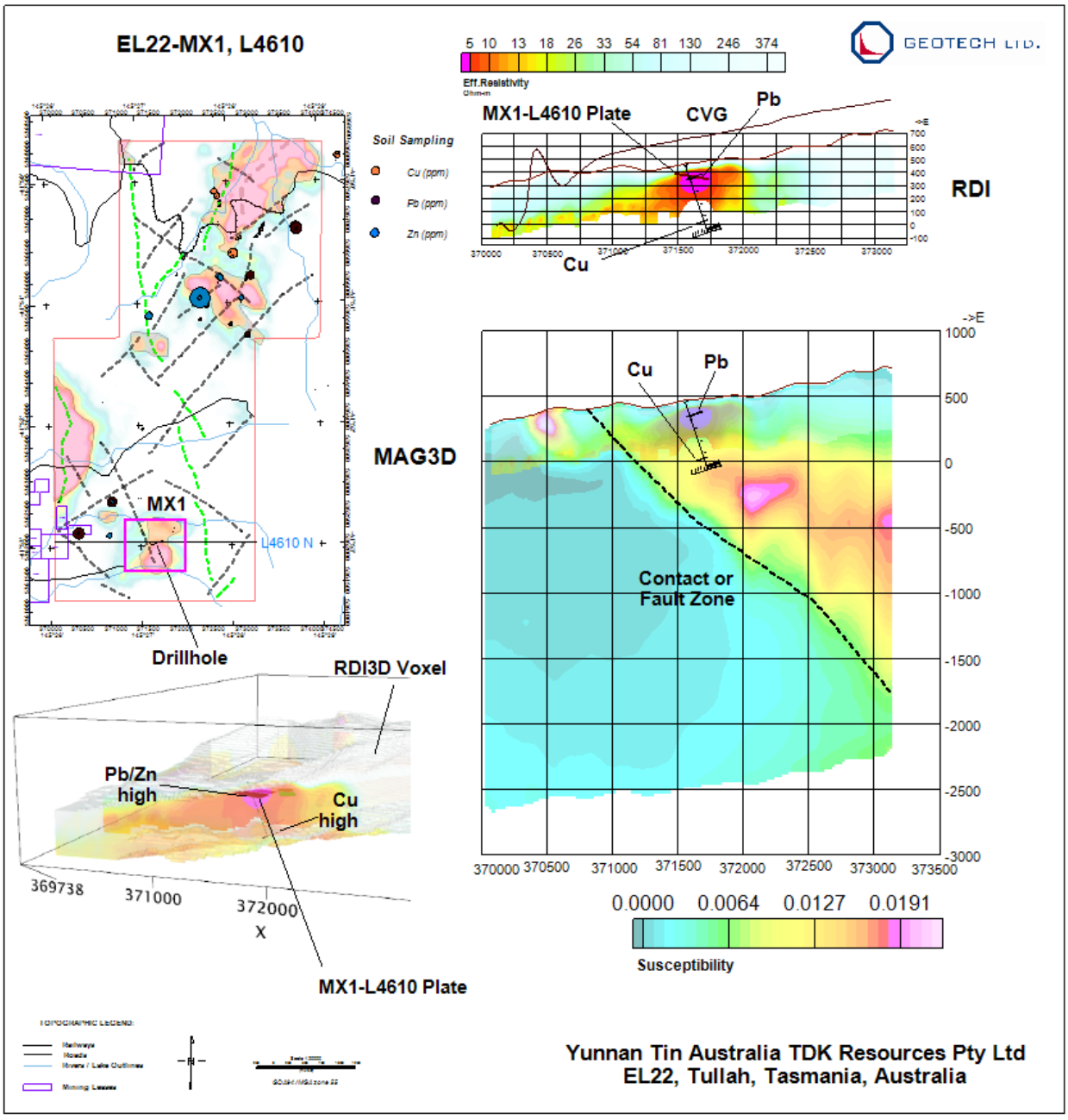

Figure 36: Detailed views of MX1, L4610 of EL22.

MX2, L4310

Target MX2 is located in the west central of EL22. Line L4310 is selected for the detailed analysis, Figure 37. The conductors underneath L4310 are modelled by two sub-horizontal Maxwell plates. Below the conductors, there is a thick layer of volcaniclastics, shown clearly in the MAG3D section.

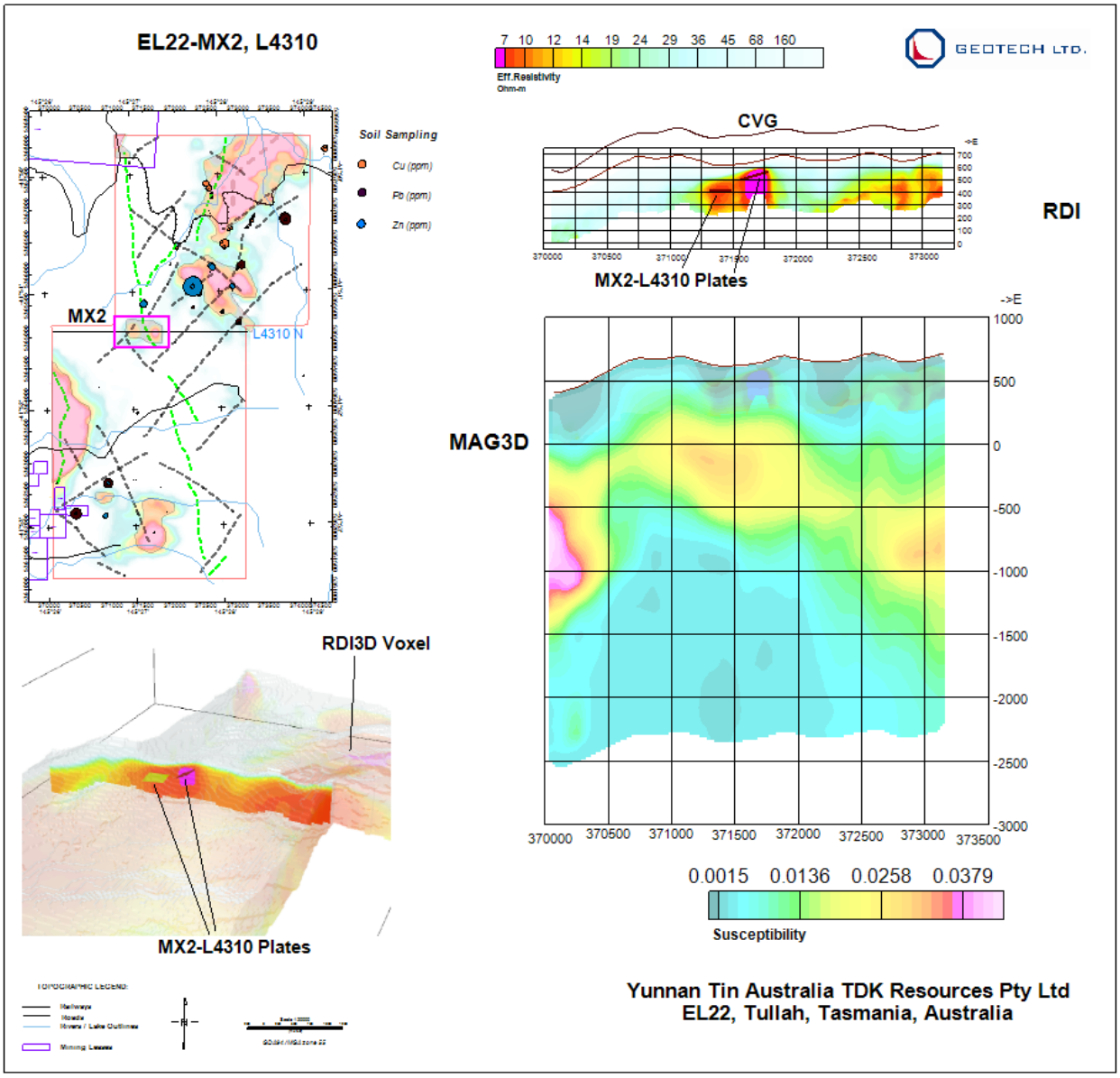

Figure 37: Detailed views of MX2, L4310 of EL22.

MX3, L4230

One cannot fail to see that there are geochemical (Zn) anomalies within target zone MX3, located in the northeast of EL22, Figure 38. Line L4230 is selected for detailed analysis of the target. The conductors beneath the line are modelled by four sub-vertical plates. Below the conductors, there is substantial amount of volcaniclastics. A major fault is clearly visible in the MAG3D section, and dividing the conductors into two groups.

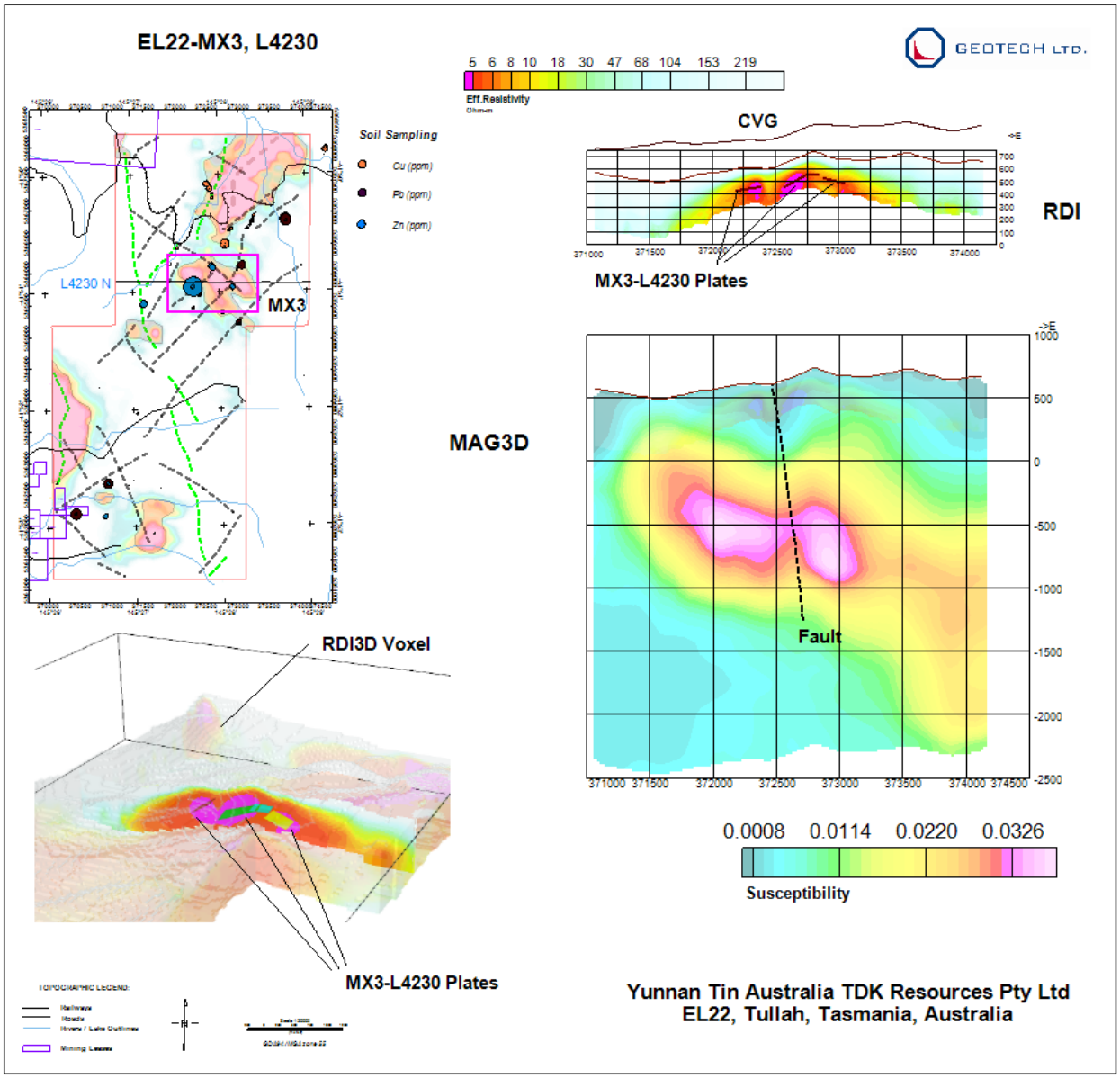

Figure 38: Detailed views of MX3, L4230 of EL22.

MX4, L4030

Target MX4 is located in the north of EL22. Two lines, L4030 and L4100, are selected for detailed analysis of the target. The conductor underneath L4030 is modelled by a sub-vertical Maxwell 2.5D plate, Figure 39. The conductor appears to be located next to an intrusive with strong magnetic responses.

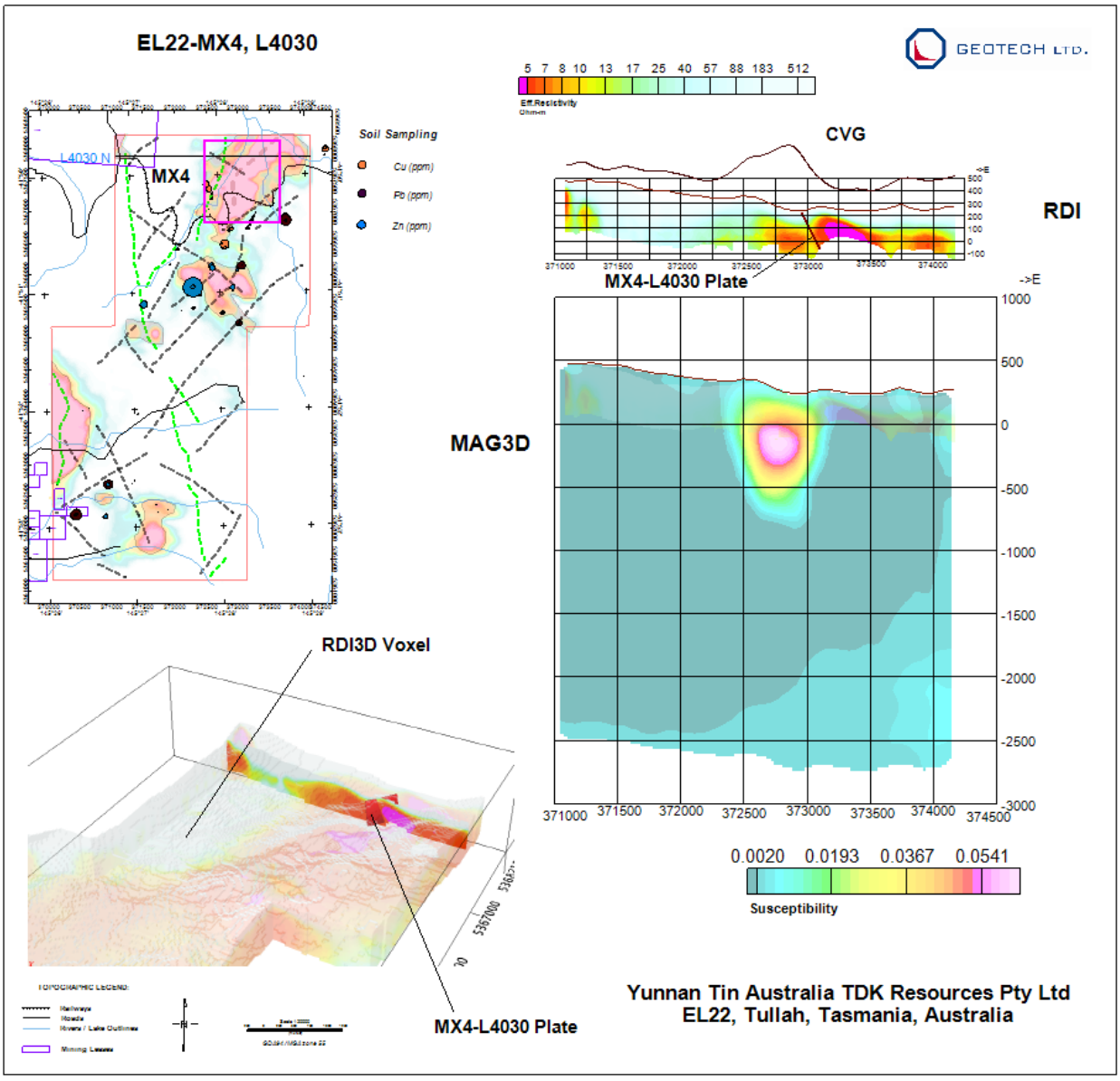

Figure 39: Detailed views of MX4, L4030 of EL22.

MX4, L4100

Line L4100 is located south of L4030 and still covers the strong intrusive in the magnetics, Figure 40. A sub-vertical plate is used to model the strongest part of the conductor under L4100. It appears that the plate is located on the east side of the intrusive.

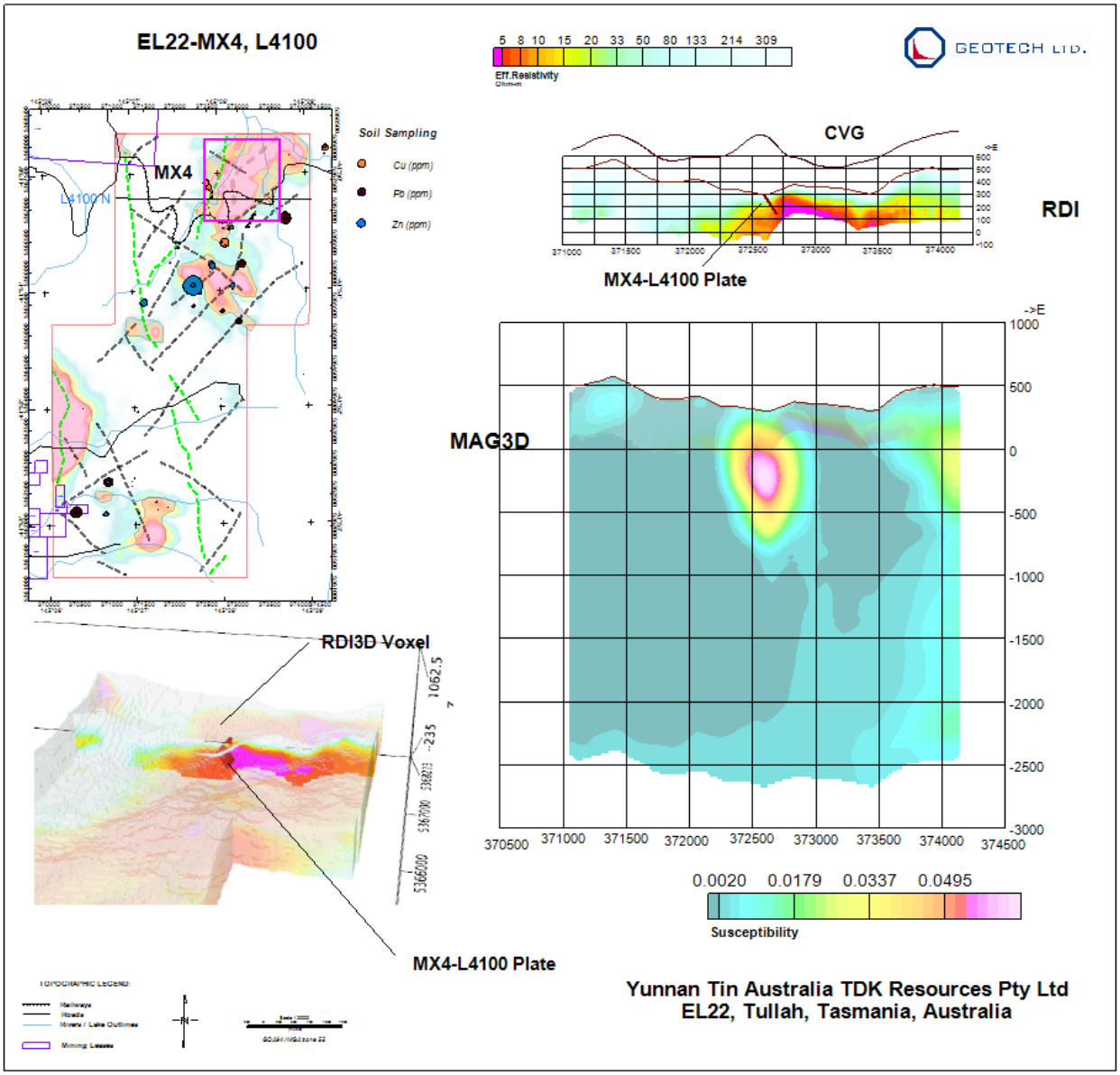

Figure 40: Detailed views of MX4, L4100 of EL22.

4.5.3 EL50N block

A potential VMS target, EL50N-T1, is selected for EL50N. The target covers the conductive zone of the block, along the eastern boundary in the north. Possible Airborne Induced Polarization (AIP) anomalous zones, EL50N-AIP-T1 to EL50N-AIP-T3, are also identified in the south of the block. The targets are displayed in Figure 41.

The targets will be analysed in detail, using 2D RDI and MAG3D sections of elected lines over the targets, to be presented in the following sections.

The coordinates of the targets are listed in Table 6.

EL50N-T1					
Corner	GDA95 / MGA zone 55		Corner	GDA95 / MGA zone 55	
	X	Y		X	Y
1	387007	5366227	10	387420	5357352
2	386869	5366044	11	387512	5356205
3	386755	5364920	12	387718	5356113
4	386892	5363498	13	388016	5356113
5	387007	5363200	14	388016	5357008
6	386801	5362351	15	387535	5357008
7	386755	5361549	16	387557	5364026
8	386847	5360769	17	387053	5364048
9	387053	5359255			
EL50N-AIP-T1					
Corner	X	Y	Corner	X	Y
1	385322	5361167	5	385226	5363710
2	385082	5361263	6	385994	5363662
3	385082	5361839	7	385610	5362151
4	385370	5362607	8	385322	5361551
EL50N-AIP-T2					
Corner	X	Y	Corner	X	Y
1	387026	5354304	4	386498	5355600
2	386282	5354808	5	386906	5355192
3	386210	5355432	6	387242	5354784
EL50N-AIP-T3					
Corner	X	Y	Corner	X	Y
1	386426	5353488	5	387649	5350921
2	387002	5353728	6	387026	5351785
3	388129	5351449	7	386762	5353008
4	388153	5350873			

Table 6: Coordinates of potential VMS and AIP targets, EL50N.

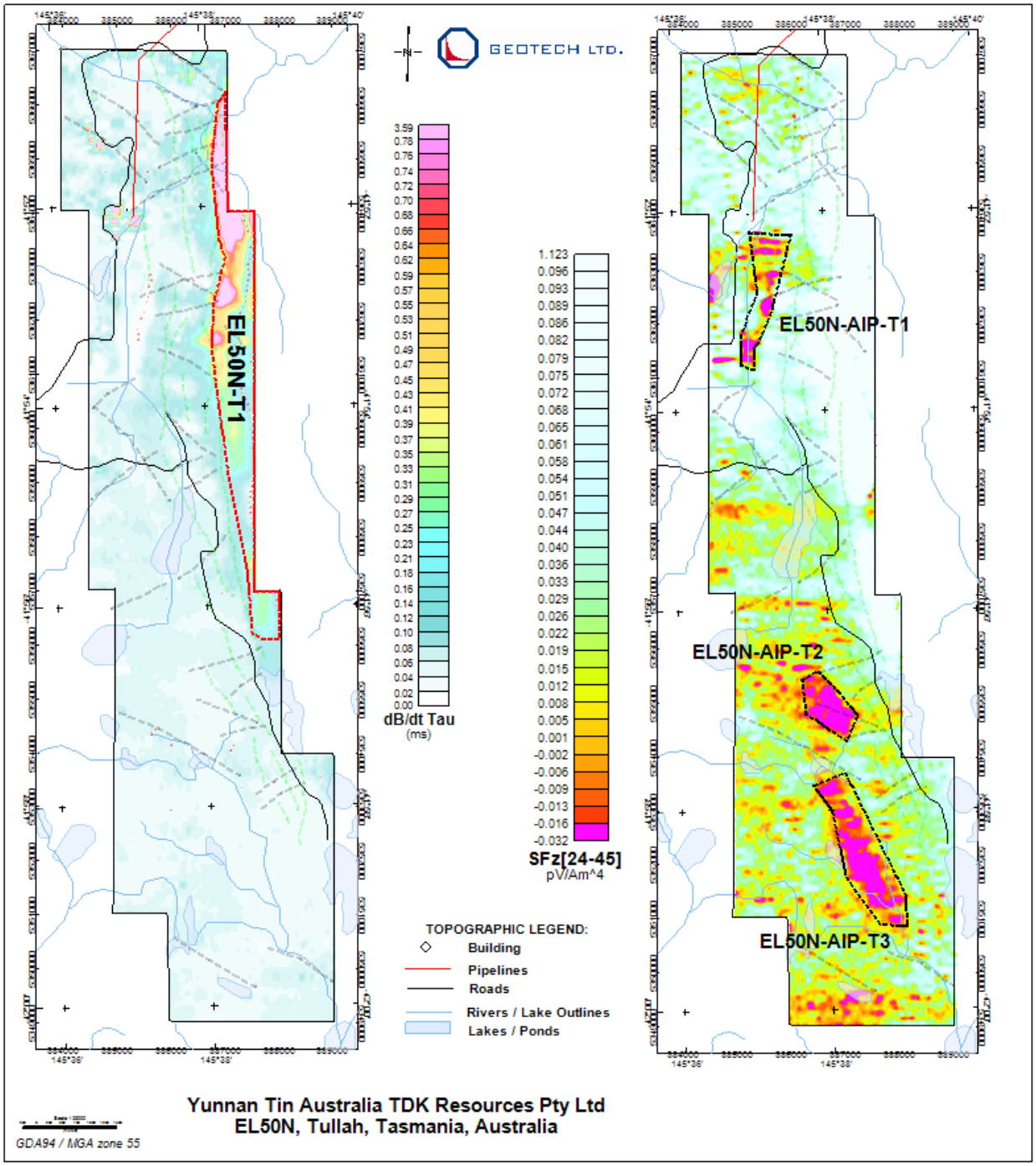

Figure 41: Potential VMS target, EL50N-T1, and AIP targets, EL50N-AIP-T1 to EL50N-AIP-T3, in EL50N.

Three lines, L5310, L5530, L6010, are selected for the analysis of target EL50N-T1.

EL50N-T1, L5310

L5310 is located in the north of the block. The RDI section shows a sizable, sub-vertical and deep conductor (double-peak in late times) at the eastern end, Figure 42. The two

conductors in the west are cultural. The target conductor lies on the eastern side of a belt of volcanic rocks, trending NS. To the west of the conductor, some drilling was carried out, seen in the RDI 3D insert. Some of the drillholes intersected Cu mineralization, at approximately 200m depths and beyond.

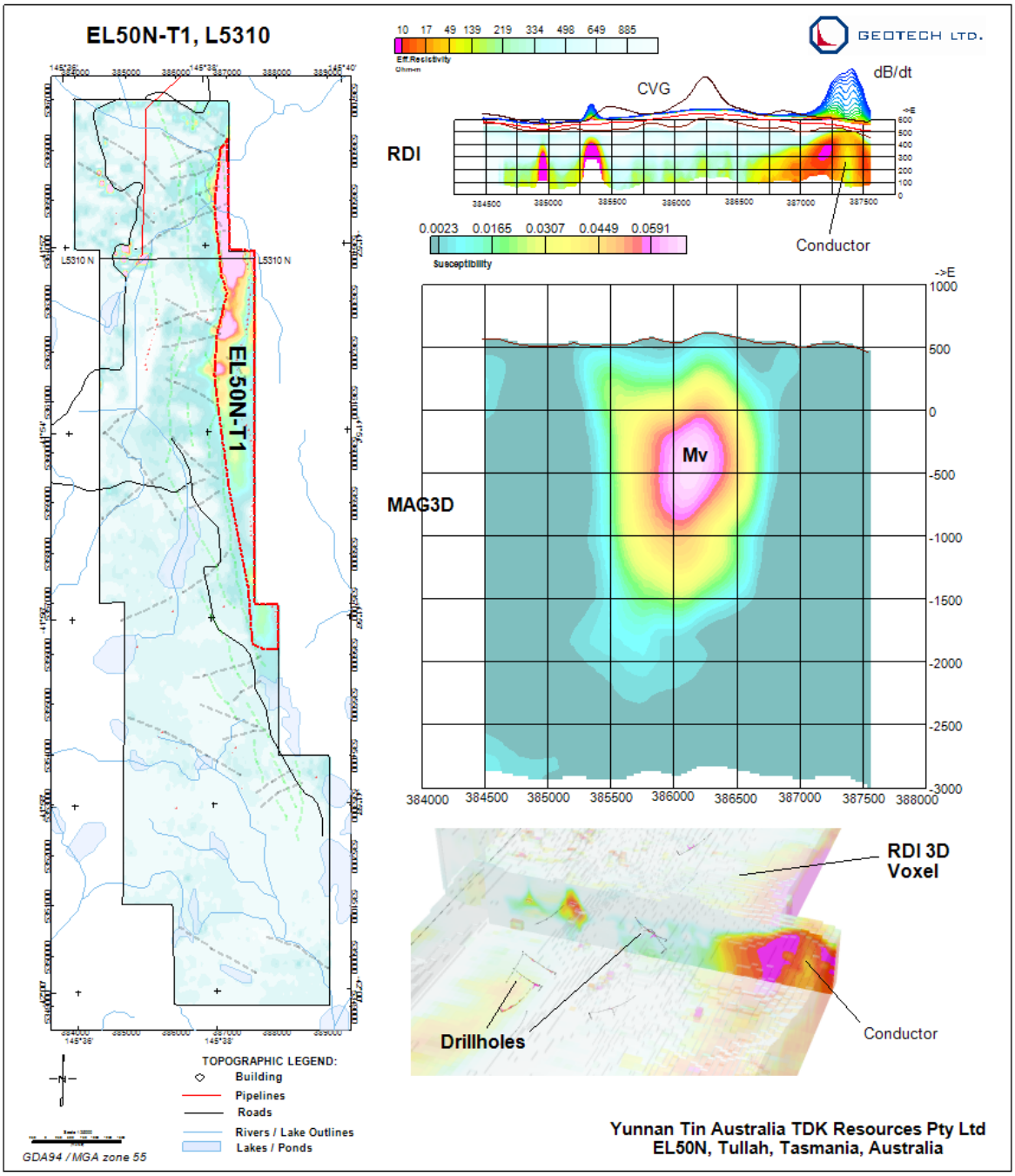

Figure 42: Detailed 2D/3D views of target EL50N-T1, L5310, EL50N.

EL50N-T1, L5530

Further to the south lies L5530. The RDI section depicts a strong, sub-vertical conductor about 200m below quickly rising topography, Figure 43. The conductor, located on the eastern side of a volcanic belt, is modelled by two Maxwell 2.5D plates, one sub-horizontal closest to the volcanics and the other sub-vertical further east.

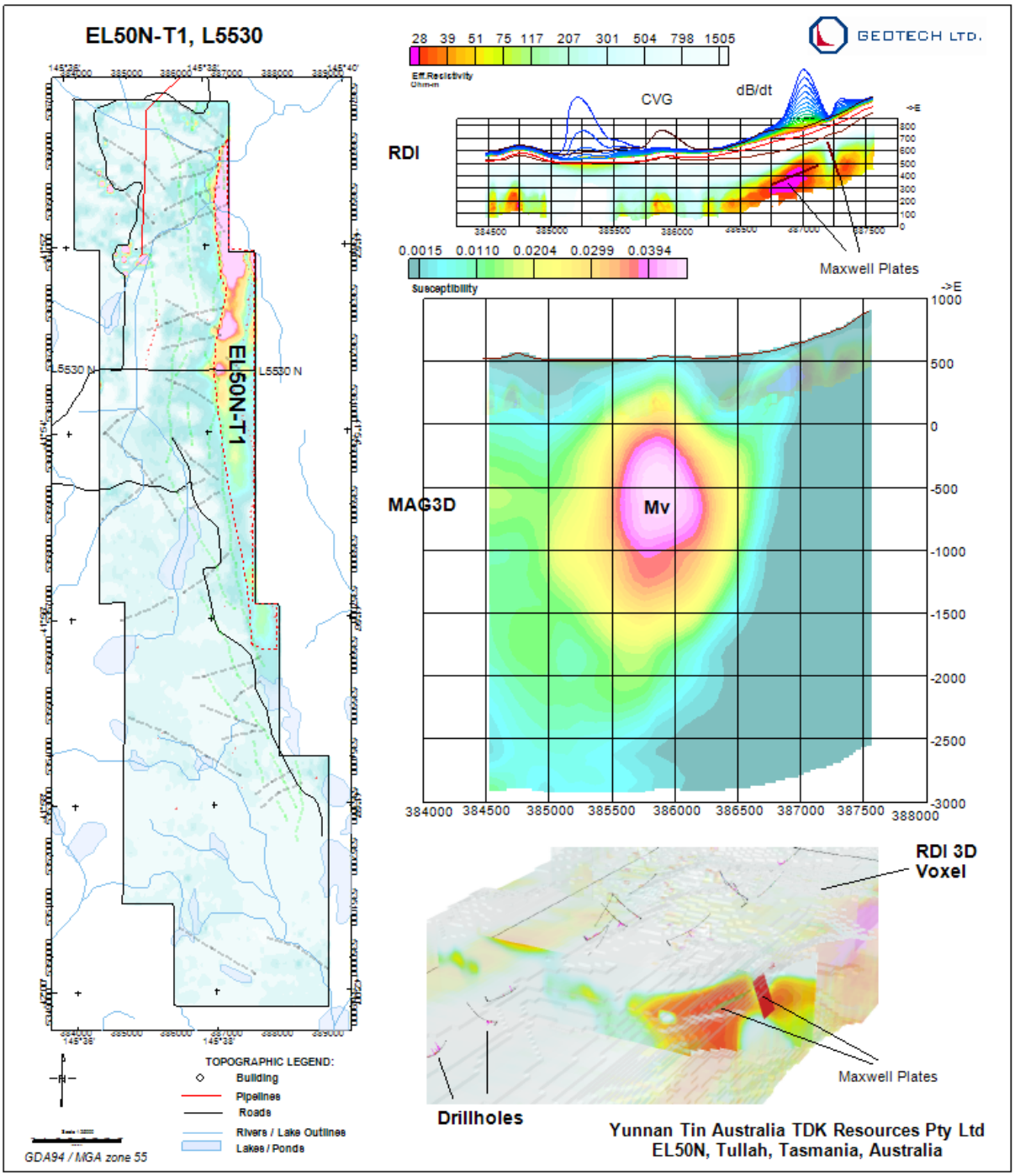

Figure 43: Detailed 2D/3D views of target EL50N-T1, L5530, EL50N.

Drillholes to the west of the target conductor intersected some minor amount of Cu mineralization.

EL50N-T1, L6010

L6010 is situated at the southern end of the target zone, Figure 44. The RDI section shows a part of the EM responses of a sub-vertical conductor, located on the eastern side of the volcanic belt.

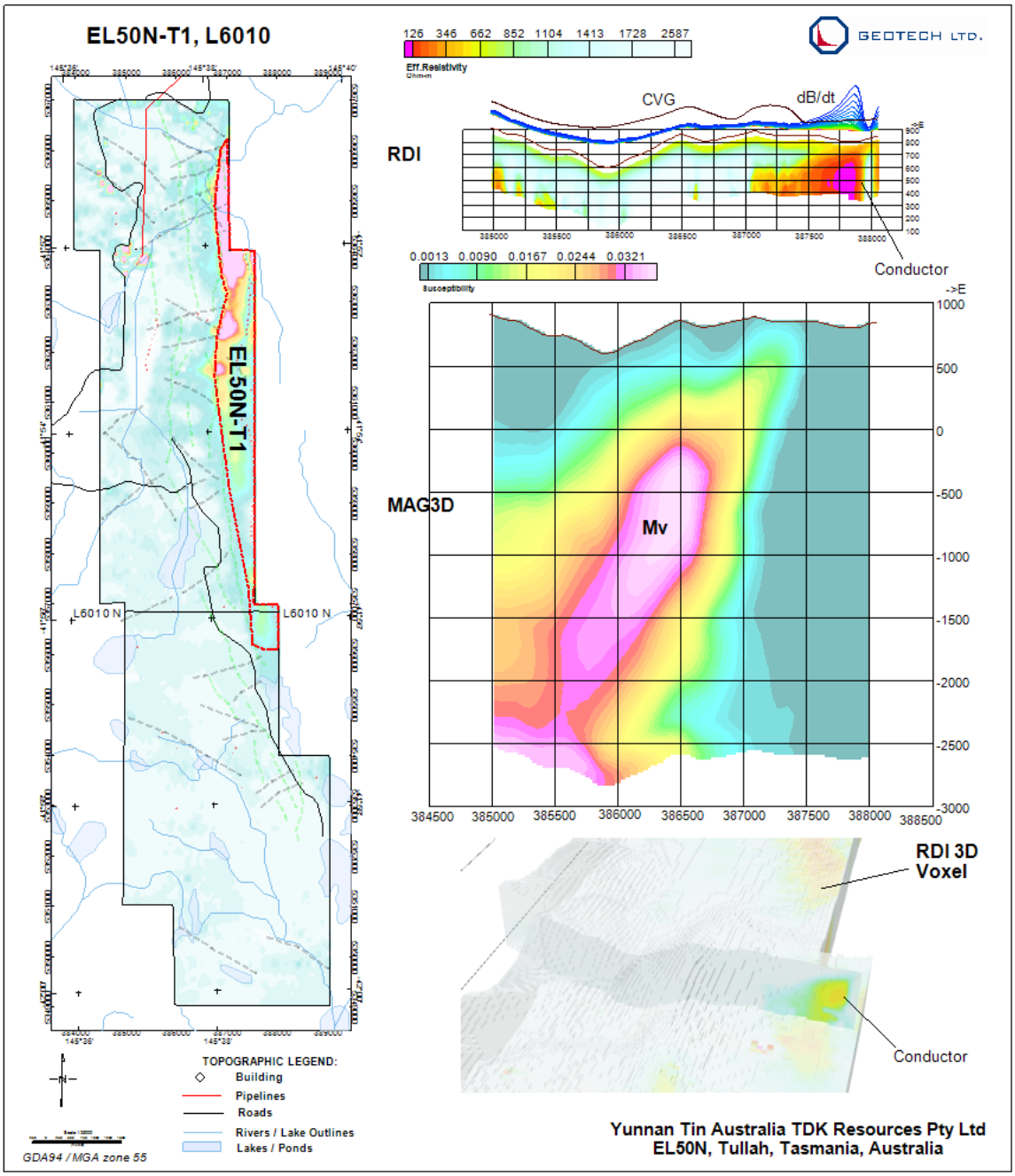

Figure 44: Detailed 2D/3D views of target EL50N-T1, L6010, EL50N.

Airborne Induced Polarization (AIP)

Numerous negative transients have been reported for coincident ground TEM systems (Smith and West, 1988) and in-loop airborne TEM systems (Kratzer and Macnae 2012) over a variety of geological situations, such as kimberlite pipes (Boyko, Paterson and Kwan, 2001), in the Arctic (Smith and Klein, 1996, GEOTEM®) and even over massive sulphide bodies in a specific configuration in Russia (Alexander Prikhodko, Pers. Comm. and Walker and Rudd, 2007). The negative transients are attributed to possible Inductive IP (IIP) effect. This effect can be exploited for the search of potential polarizable or chargeable targets, such as disseminated sulphides or clay minerals.

A commonly used empirical formulation to describe the IP effects is the Cole-Cole relaxation model for impedance $\rho(\omega)$ in the frequency domain (Cole and Cole, 1941, and Pelton *et al*., 1978).

$$\rho(\omega) = \rho_0 \left[1 - m\left(1 - \frac{1}{1+(i\omega\tau)^c}\right)\right],$$

Where ρ_0 is the low-frequency asymptotic resistivity, m is the chargeability, τ is the time constant, and c is the frequency dependence factor.

The AIP modelling of layered earth and thin plates embedded in a uniform half-space for VTEM data can be done by LeroiAir (CSIRO[5]/AMIRA) program. A couple of AIP models, one for chargeable half-space and a chargeable thin plate in half-space, are shown in Figure 45. All are able to generate negative transients in mid to late off-times.

5 Commonwealth Scientific and Industrial Research Organization (CSIRO).

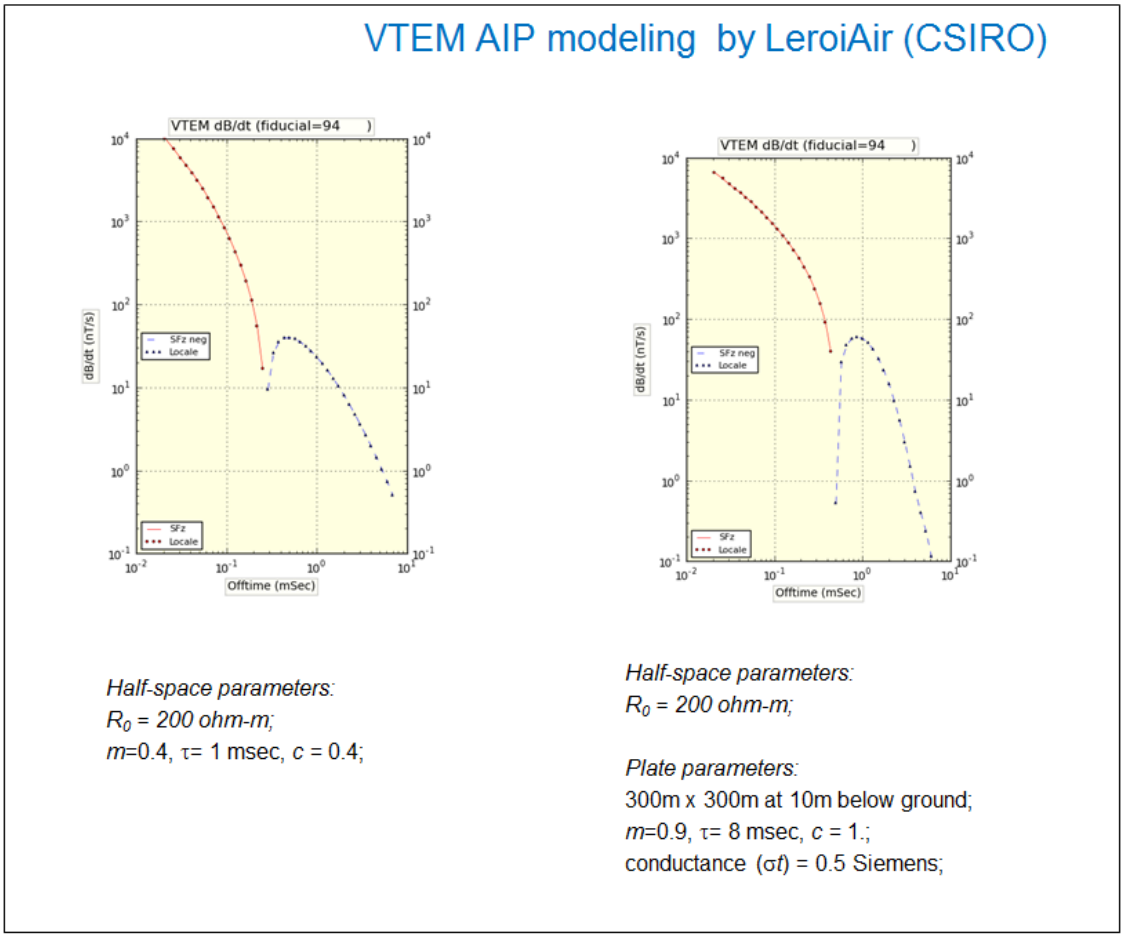

Figure 45: AIP modeling results for VTEM.

In the VTEM data over EL50N, negative transients are observed of throughout the block. Three potential AIP targets are identified and will be analysed in detail in the following sections.

EL50N-AIP-T1, L5460

AIP target EL50N-AIP-T1 is located in the north of the block, to the west of the main NS trending conductive trend along the eastern boundary, Figure 46. Line L5460 is selected for detailed analysis of the AIP anomaly, identified by the negative transients in the mid to late off-time channels, shown in the top profile panel. There is only weak magnetic response associated with the anomaly. There is a drillhole, LS4, close to the line. The drillhole trace and Cu and Pb assays are projected to the MAG3D 2D section. Elevated Cu counts are encountered in the drillhole from 310m to 312m section. No abnormal high Pb or Zn counts are intersected in the drillhole. Sulphide contents are variable but not high.

It appears that the negative transients in L5460 are localized and strong. This elongated target zone is trending NS and confined in extent as seen in the profiles.

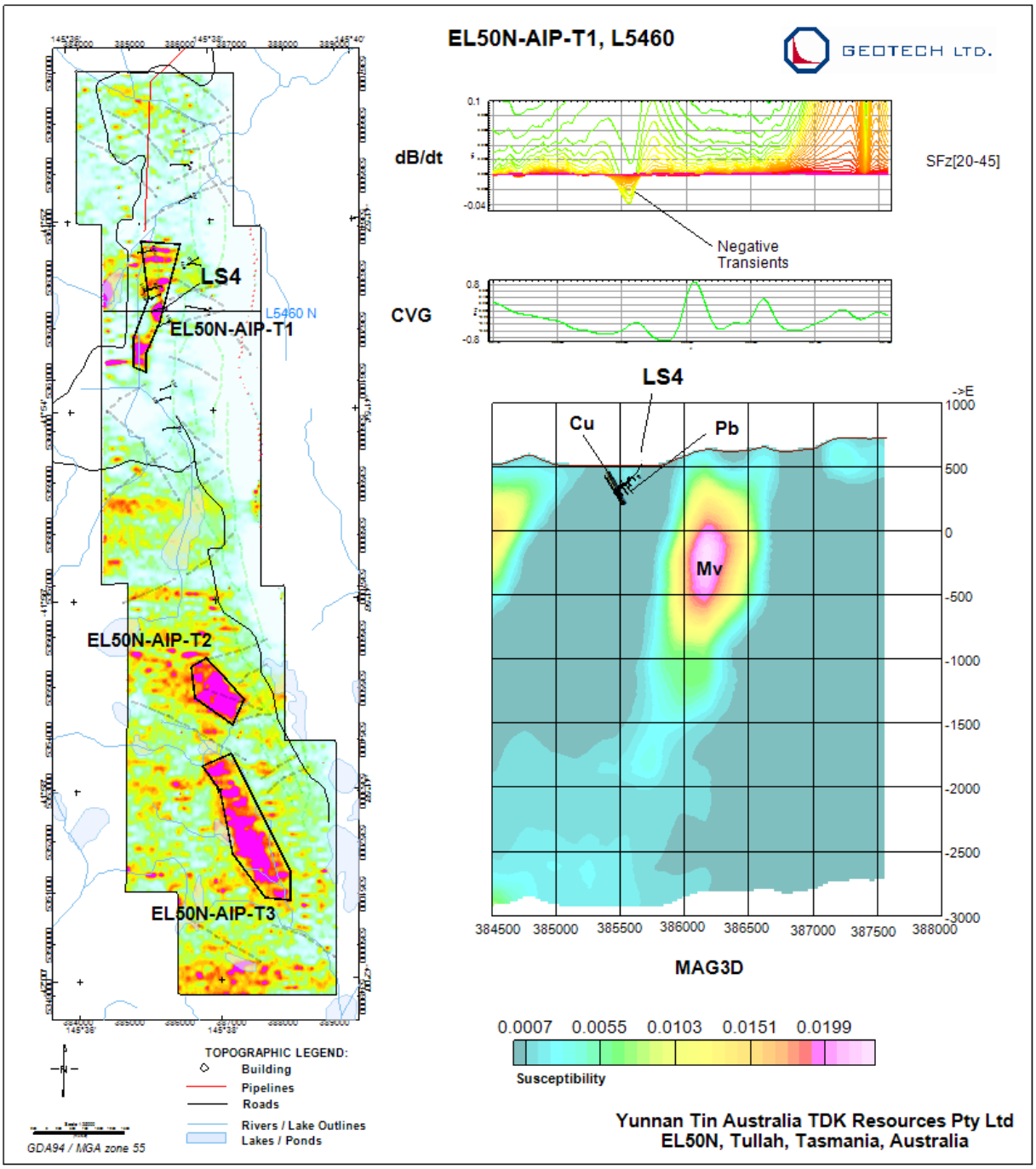

Figure 46: Detailed 2D/3D views of target EL50N-AIP-T1, L5460, EL50N.

EL50N-AIP-T2, L6200

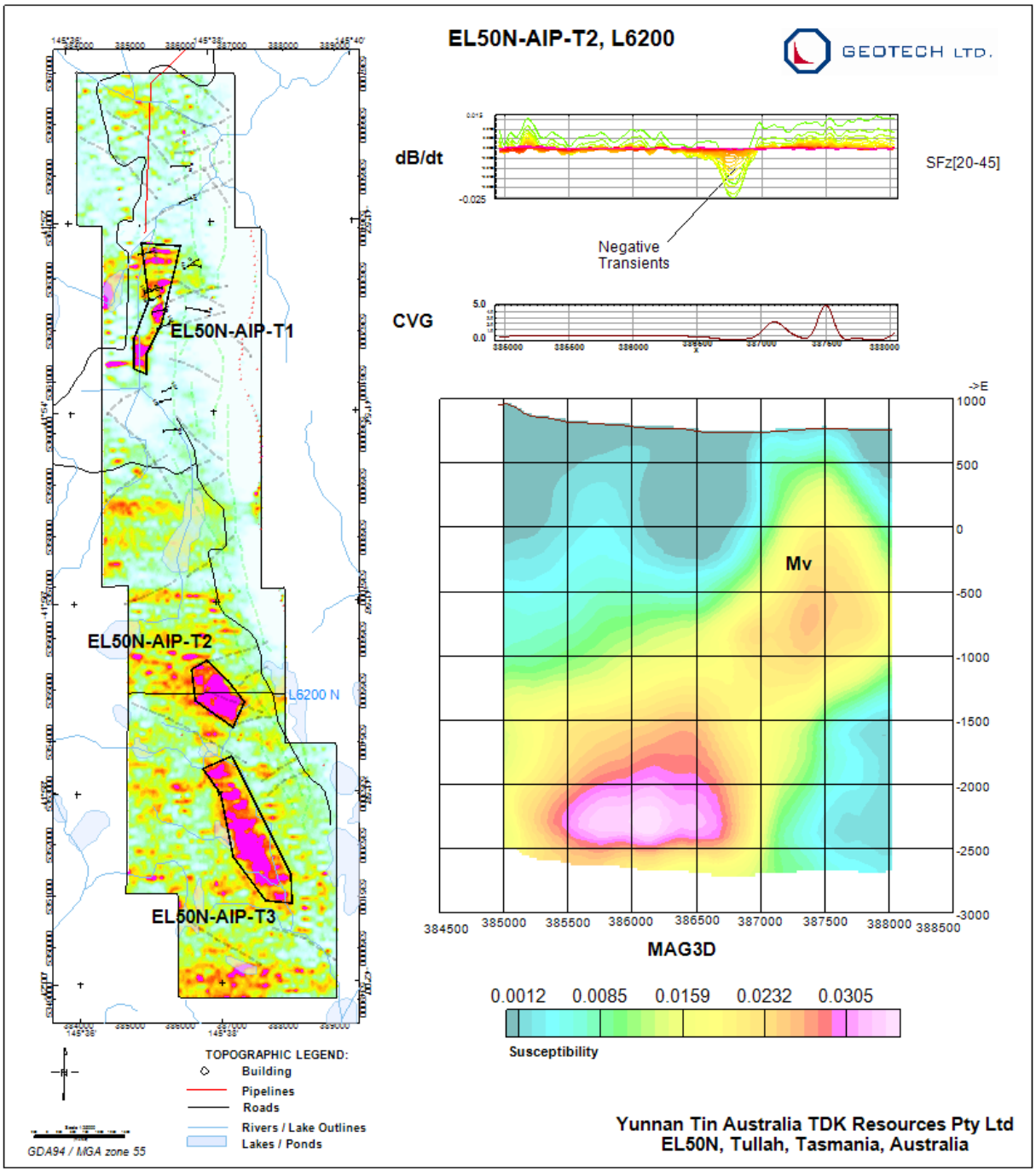

Figure 47: Detailed 2D/3D views of target EL50N-AIP-T2, L6200, EL50N.

L6200 is chosen for the analysis of AIP target EL50N-AIP-T2. The still strong negative transients and MAG3D section are shown in Figure 47. The target is located on the western side of the volcanic belt. The short but still elongated target zone is trending SSE, and confined as seen in the EM profiles. It has no magnetic signature.

EL50N-AIP-T3, L6200

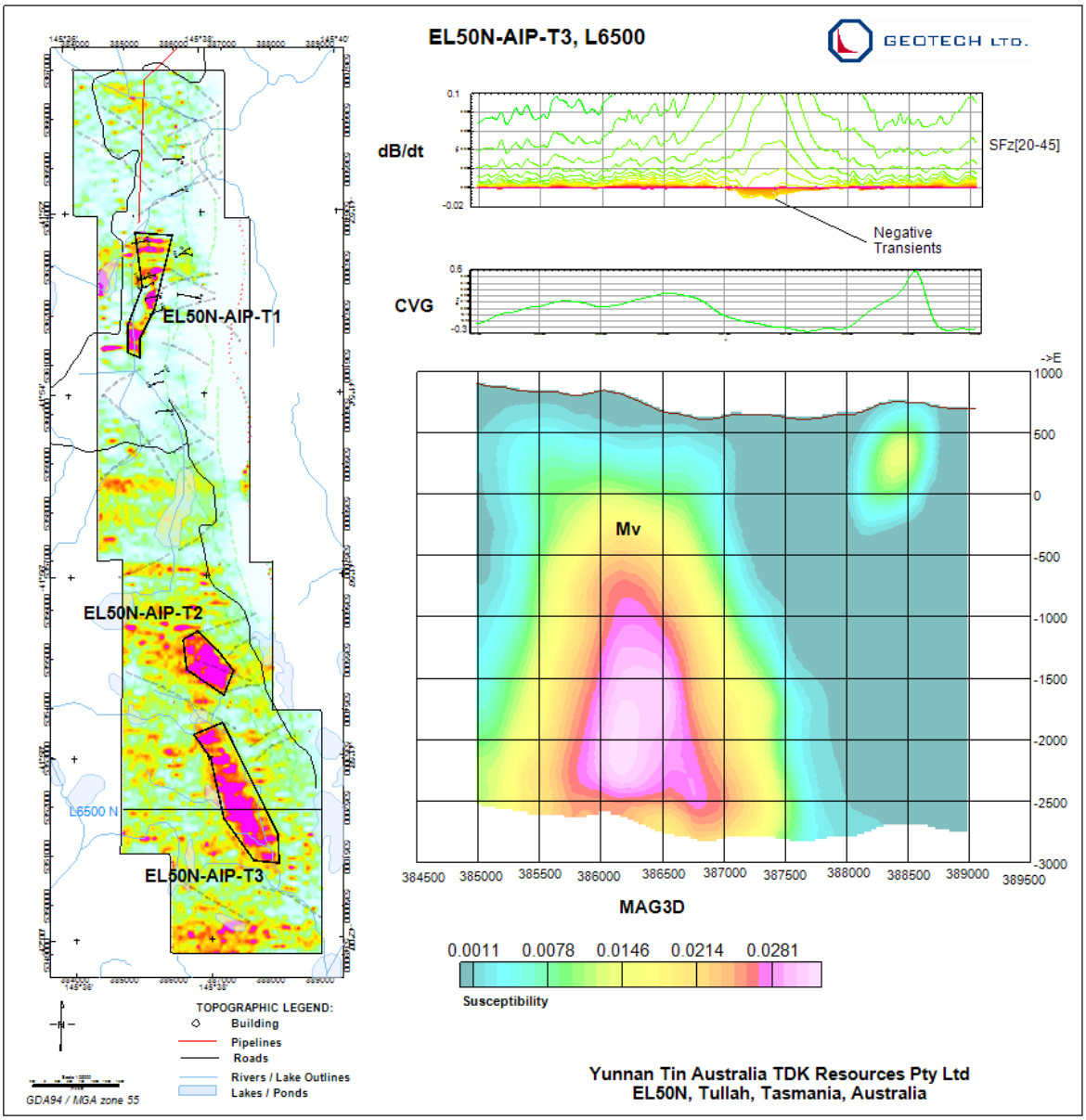

Figure 48: Detailed 2D/3D views of target EL50N-AIP-T3, L6500, EL50N.

AIP target EL50N-AIP-T3 is located in the south of the block and elongated. Line L6500 is selected for the analysis of the target, Figure 48. The strength of the negative transients in this target is notably weaker than those in the other two target zones to the north. The negative transient seen in the profiles appear to be spreading over a distance approximately 500m or so. Again, no noticeable magnetic signature can be associated

with this target.

It will be very interesting to know what in the target zones actually causes the negative transients the VTEM data. Targets EL50N-AIP-T1 and EL50N-AIP-T2 are recommended for further ground follow-ups, including ground IP or even test drilling. Before test drilling, the AIP anomaly should be modelled first, maybe with the 3D AIP inversion algorithm by Oldenburg *et al*., 2013 or other AIP 3D inversion software.

4.5.4 EL50S block

Potential VMS targets within EL50S block, EL50S-T1 and EL50S-T2, are selected, Figure 49. EL50S-T1 is situated at the southern end of the NS trending dyke. North of the target, the topography rises sharply. EL50S-T2 is located at the SE corner of the block. The targets are selected based on the interpretation of the magnetic and EM data, and the RDI depth slices and 2D sections.

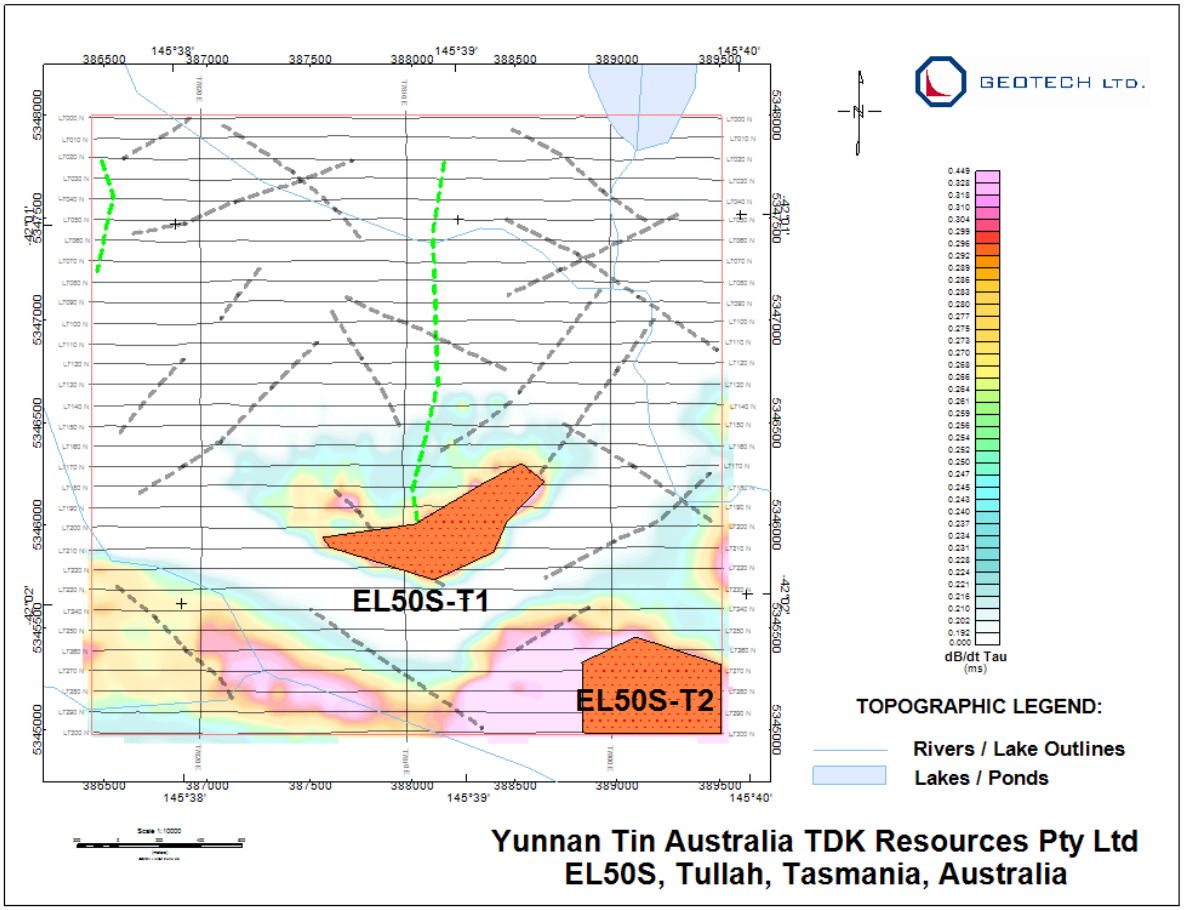

Figure 49: Potential VMS target, EL50S-T1, in EL50S.

The coordinates of the targets are listed in Table 7.

EL50S-T1			
Corner	**GDA95 / MGA zone 55**	Corner	**GDA95 / MGA zone 55**

	X	Y		X	Y
1	387561	5345943	6	388457	5346019
2	388009	5346007	7	388393	5345867
3	388347	5346205	8	388102	5345733
4	388533	5346304	9	387596	5345897
5	388644	5346211			
EL50S-T2					
Corner	X	Y	Corner	X	Y
1	389504	5345319	4	388834	5344987
2	389085	5345459	5	389510	5344981
3	388829	5345331			

Table 7: Coordinates of potential VMS targets, EL50S.

The following presents the detailed 2D/3D analyses of the targets.

EL50S-T1, L7180

L7180 is located in the NE part of the target area, Figure 50. The most conductive zone underneath L7180 lies on the eastern side of the dyke, which is clearly seen in the MAG3D 2D section. The depth of the conductor is about 200m below ground.

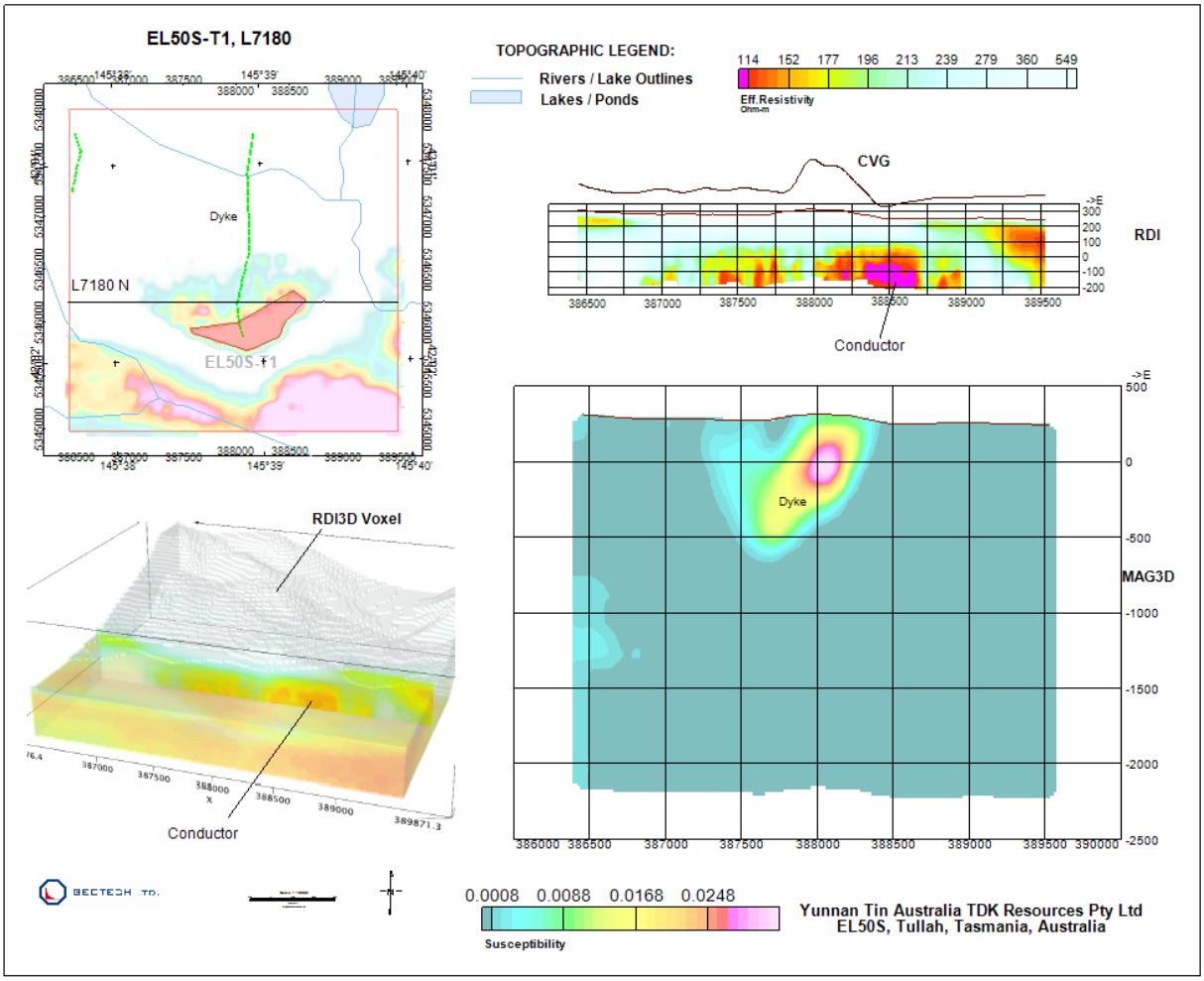

Figure 50: Detailed 2D/3D views of target EL50S-T1, L7180, EL50S.

EL50S-T1, L7200

L7200 runs through the centre of the target, Figure 51. The most conductive zone appears to be just off the main axis of the dyke, located about 200m below ground.

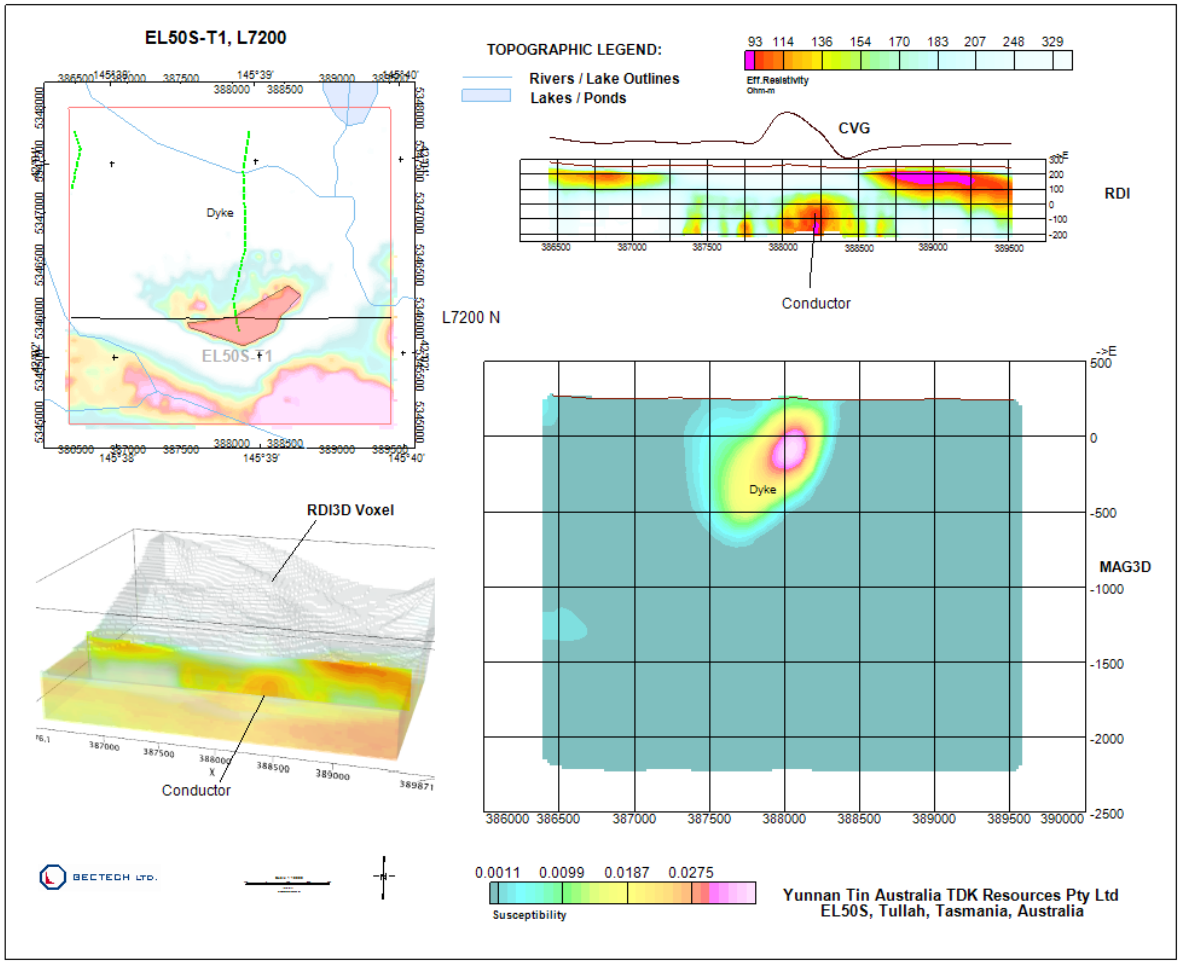

Figure 51: Detailed 2D/3D views of target EL50S-T1, L7200, EL50S.

EL50S-T1, L7220

Along the southern edge of the target lies L7220, Figure 52. The conductive zone lies about 250m below ground, and appears to be on the top of the magnetic dyke.

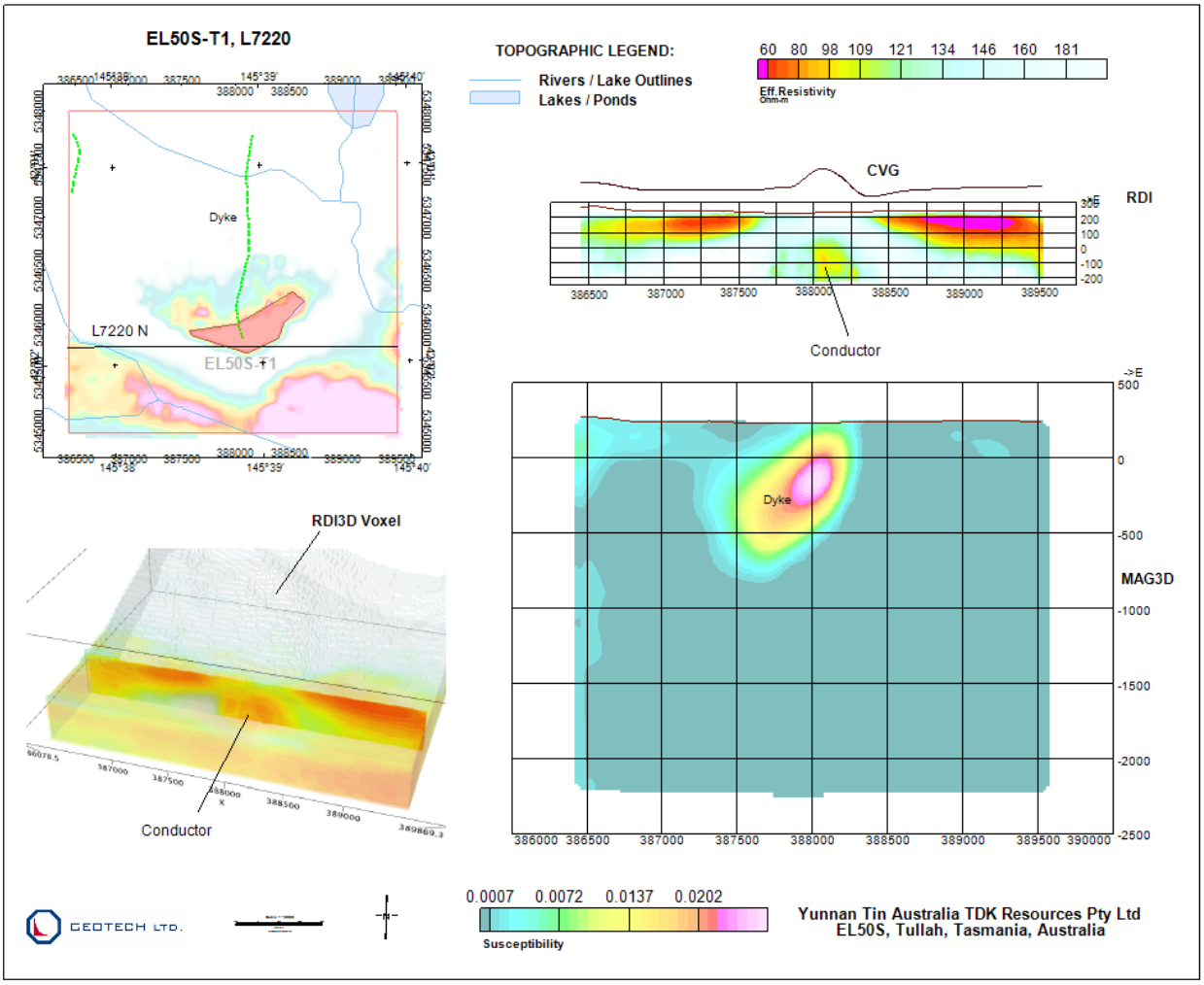

Figure 52: Detailed 2D/3D views of target EL50S-T1, L7220, EL50S.

EL50S-T2, L7290

It appears that the most conductive region of EL50S-T2 is located in the east of the target zone, Figure 53. The conductor is sub-horizontal, about 200m below ground. There is no obvious geological structure associated with target EL50S-T2. Therefore, it could be related to conductive clays in a paleo-channel. There is a stream flowing along WNW-ESE direction, located just to the south.

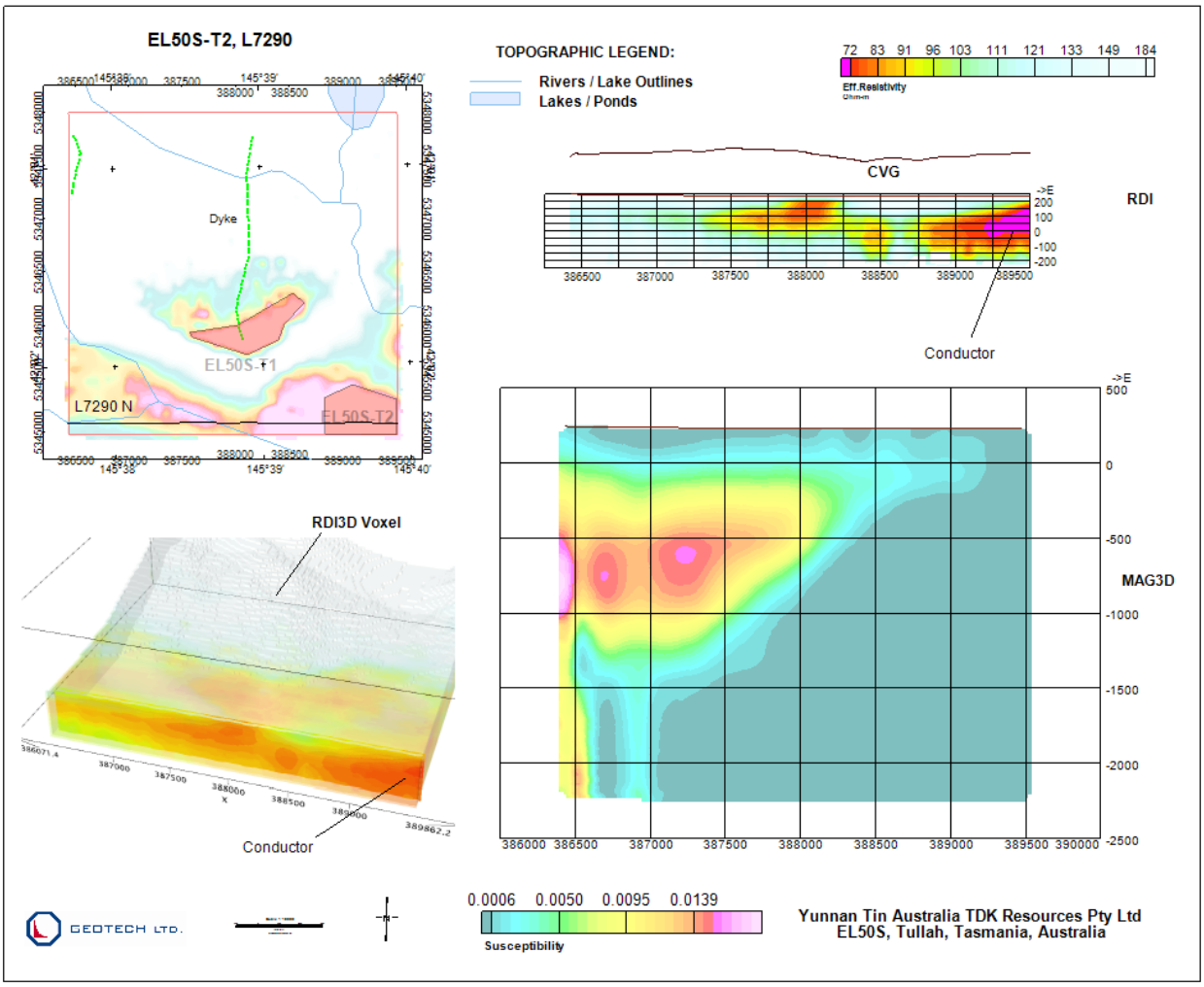

Figure 53: Detailed 2D/3D views of target EL50S-T2, L7290, EL50S.

5. CONCLUSIONS AND RECOMMENDATIONS

The geophysical interpretation of the magnetic and electromagnetic (EM) data from license blocks EL22/2010 (EL22), EL46/2010 (EL46), EL50N/2008 (EL50N) and EL50S/2008 (EL50S), in plans and sections, on behalf of Yunnan Tin Australia TDK Resources Pty Ltd (Yunnan Tin Australia), have been carried out. Advanced magnetic products have been produced in preparation for the interpretations, including MAG3D inversions, depth slices and 2D sections. EM anomaly picks and Resistivity Depth Imaging (RDI) data are generated. RDI depth slices and 2D sections are created also.

These advanced geophysical products have been interpreted using established geophysical interpretation principles. Lithological units, such as volcanic and undifferentiated sedimentary rocks, dykes and intrusives, have been delineated from the RTP, Analytic Signal, and MAG3D depth slices. Faults and magnetic "ridges" are interpreted from the derivatives of the magnetic data. Conductive zones and trends are inferred from the EM data.

Negative transients in the VTEM data from EL50N are observed and investigated. These sign reversal in TDEM response is attributed to possible Inductive Induced Polarization (IIP) effect, which may be caused by disseminated sulphides or clay minerals.

Five (5) possible VMS and/or mafic or ultramafic-related PGE prospective target zones are identified for EL46, four (4) possible VMS targets in EL22 block, one (1) possible VTEM target and two (2) strong possible Airborne Induced Polarization target in EL50N block, and one (1) strong possible VMS targets in EL50S block. Some of the conductors are modeled by Maxwell 2.5D plates.

All the targets are recommended for further ground follow-ups, including test drilling. Recommended drilling parameters for conductive targets (non-AIP) are provided for all Maxwell plate models.

In the following, the recommended test drilling parameters for those targets that are analyzed in detail in Section 4.5, or targets located on the line next to the analysed target, will be provided in summary tables and the target locations illustrated in figures.

EL46 block

The locations of the targets analyzed in detail, or targets located on the line next to the analyzed target, for EL46 block are shown in Figure 54, and the recommended test drilling parameters for those targets are listed in Table 8.

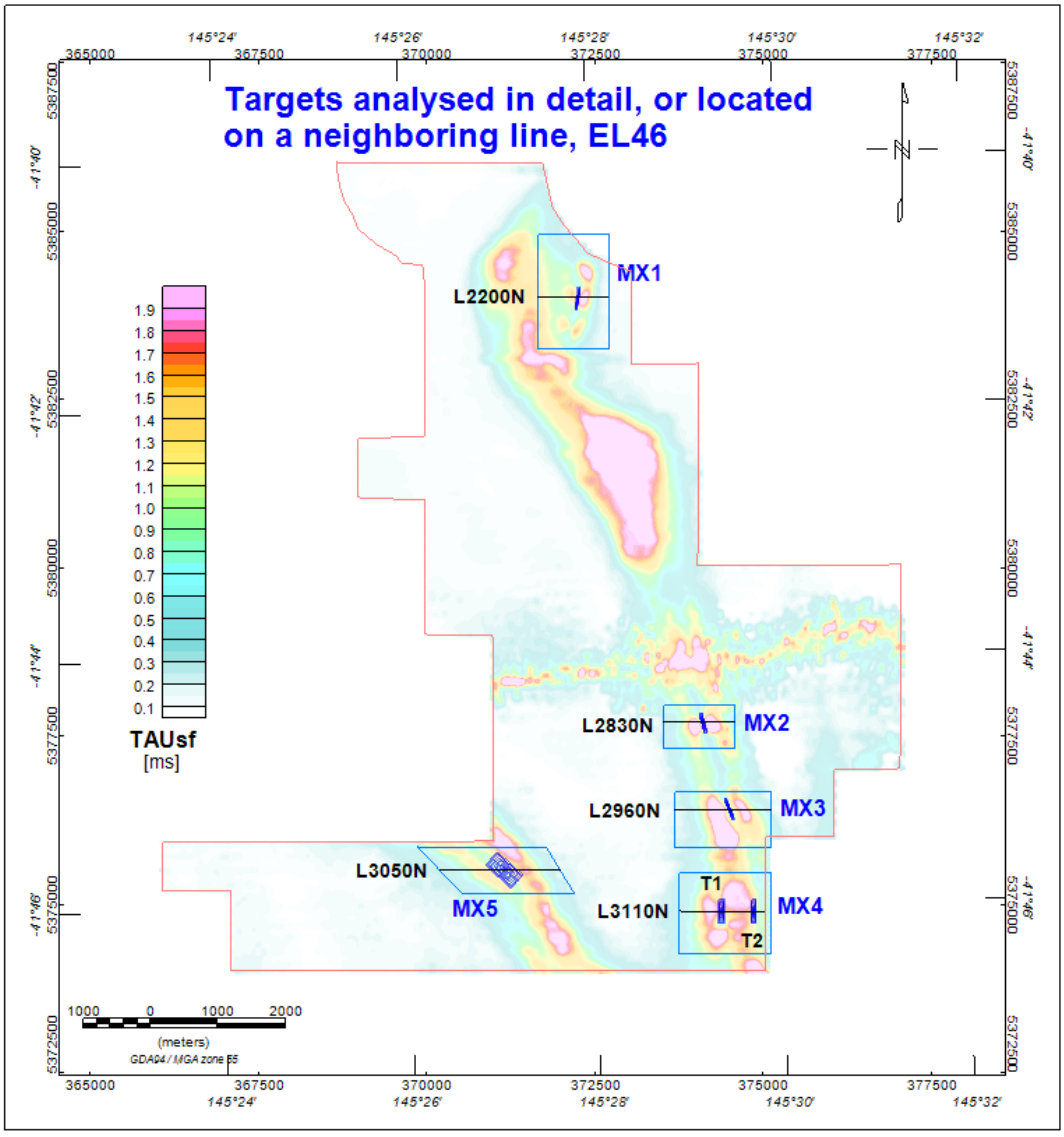

Figure 54: Locations of targets analyzed in detail, or located on a neighboring line, EL46.

Table 8: Recommended test drilling parameters for those targets analyzed in detail, EL46.

Recommended test drilling parameters						
Target_Line	X (m)	Y (m)	Z (m)	Dip (degree)	Azimuth (degree)	Length (m)
	GDA94/MGA Zone 55					
MX1_L2200	372298	5383990	192	45	280	220
MX2_L2830	374178	5377718	176	45	255	260
MX3_L2960	374600	5376450	256	45	247.5	300
MX4_L3110_T1	374300	5374900	182	45	90	300
MX4_L3110_T2	374728	5374900	168	45	90	300
MX5_L3050_T1	371198	5375600	119	45	222.5	300

EL22 block

The locations of the targets analyzed in detail, for EL22 block are shown in Figure 55, and the recommended test drilling parameters for those targets are listed in Table 9.

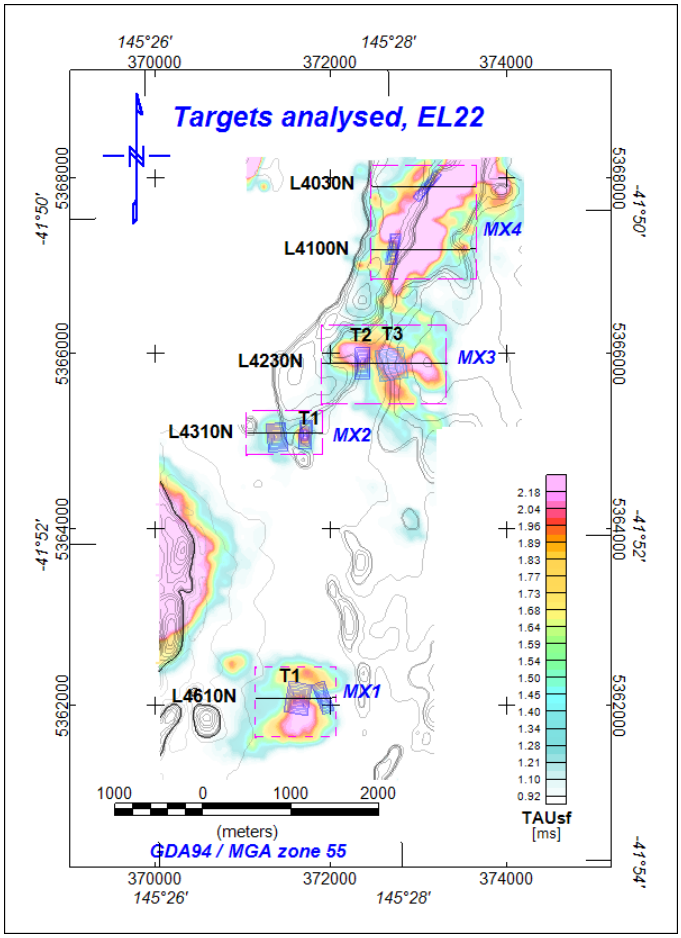

Figure 55: Locations of targets analyzed in detail, EL22.

Table 9: Recommended test drilling parameters for those targets analyzed in detail, EL22.

Recommended test drilling parameters						
Line_Target	X (m)	Y (m)	Z (m)	Dip (degree)	Azimuth (degree)	Length (m)
	GDA94/MGA Zone 55					
L4610_MX1_T1	371608	5362062	478	85	280	260
L4310_MX2_T1	371668	5365080	643	70	96	220
L4230_MX3_T2	372328	5365882	611	60	90	280
L4230_MX3_T3	372588	5365868	652	70	80	300
L4030_MX4	373170	5367850	263	45	310	300
L4100_MX4_T1	372780	5367180	365	60	280	300

EL50N block

The locations of the conductive as well as the AIP targets analyzed in detail, for EL50N block are shown in Figure 56. The full drilling parameters for the conductive targets and drillhole collar locations for those AIP targets are provided in Table 10. Even though the dips, azimuths and lengths of the drillholes for AIP targets are not explicitly recommended, due to the uncertainties about the exact geometries of the targets, the most likely numbers of the dips, azimuths and lengths are 90°, 0° and 200m.

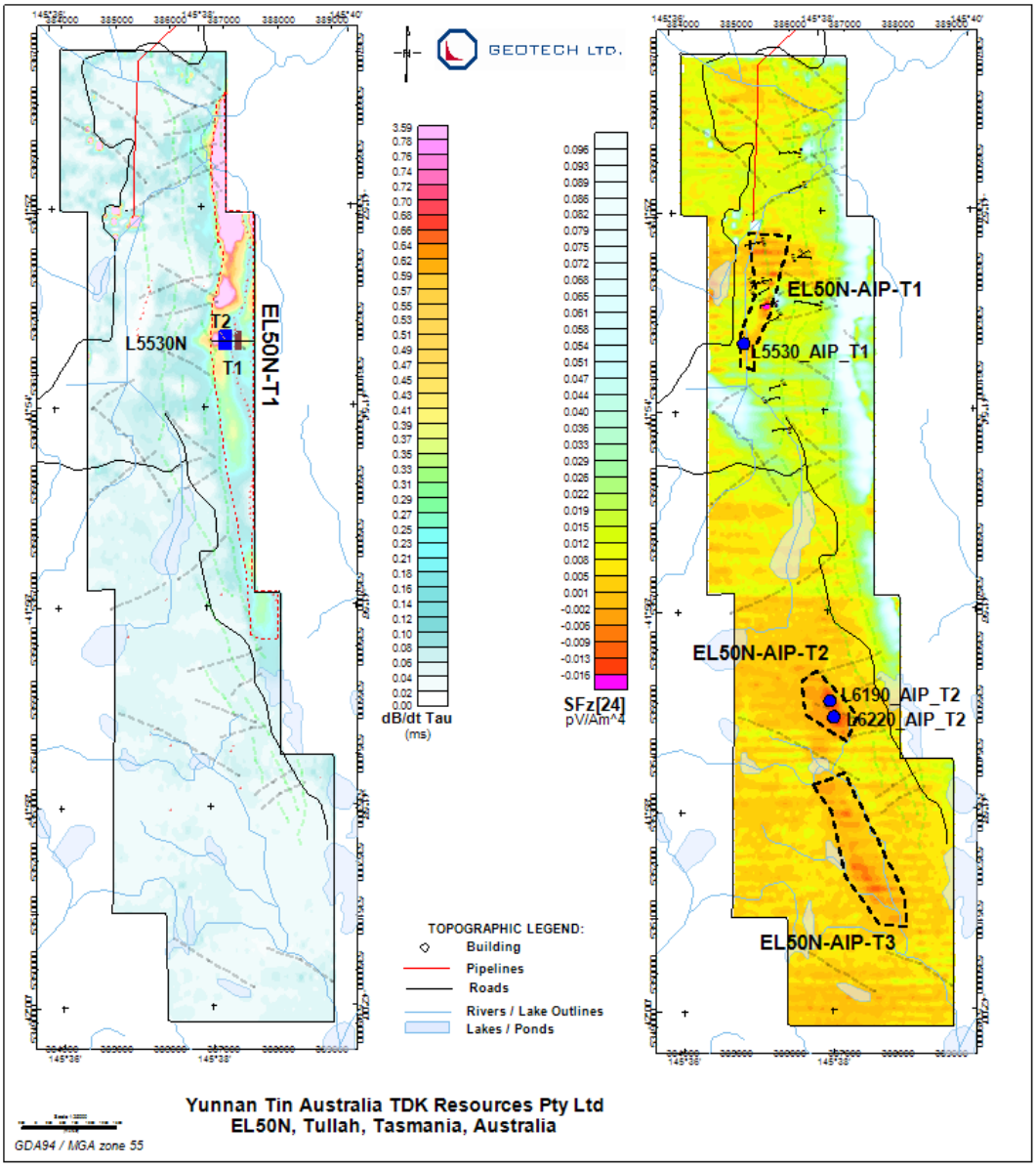

Figure 56: Targets analyzed in detail and recommended AIP target test drilling locations, EL50N.

Table 10: Recommended test drilling parameters for those targets analyzed in detail, EL50N.

Recommended test drilling parameters

Line_Target	X (m)	Y (m)	Z (m)	Dip (degree)	Azimuth (degree)	Length (m)
	GDA94/MGA Zone 55					
L5330_T1	387338	5361649	778	60	270	300
L5530_T2	386932.7	5361650	632	60	90	360
L5530_AIP_T1	385147	5361660	510	*	*	*
L6190_AIP_T2	372588	5365868	652	*	*	*
L6220_AIP_T2	372588	5365868	652	*	*	*

EL50S block

The location of the target analyzed in detail, EL50S-T1, for EL50S block are shown in Figure 57, and the recommended test drilling parameters for the targets are listed in Table 11Table 9.

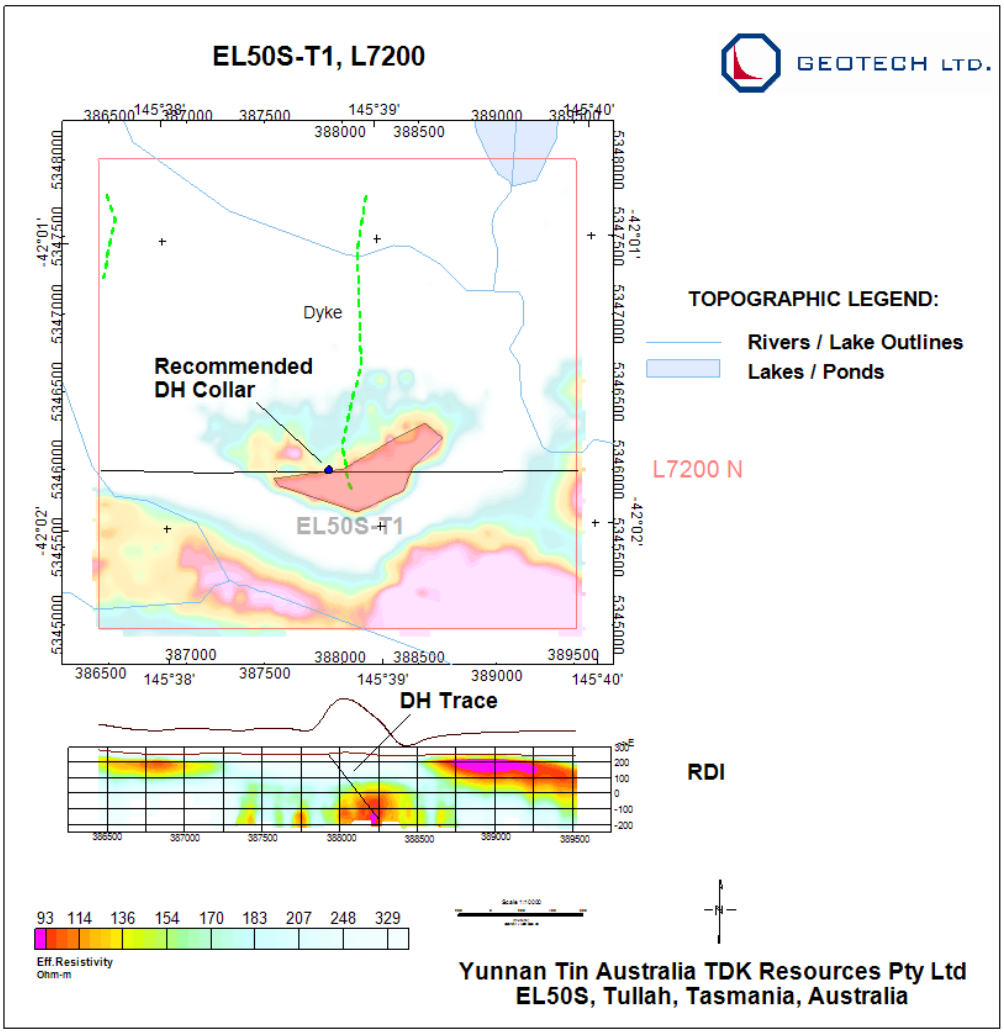

Figure 57: Recommended EL50S-T1 target test drilling location for L7200N, EL50S.

Table 11: Recommended test drilling parameters for target EL50S-T1, L7200N, EL50S.

Recommended test drilling parameters						
Line_Target	X (m)	Y (m)	Z (m)	Dip (degree)	Azimuth (degree)	Length (m)
	GDA94/MGA Zone 55					
L7200_T1	387917	5346000	255	50	90	550

Respectfully submitted[6],

Zihao Han, Ph.D
Geotech Ltd.

Karl Kwan, M.Sc.
Geotech Ltd.

Alexander Prikhodko, Ph.D, P.Geo
Manager of Data Interpretation
Geotech Ltd.

March, 2014

[6] Geophysical Interpretations were carried out by Zihao Han and Karl Kwan, from the office of Geotech Ltd. in Aurora, Ontario, under the supervision of Alexander Prikhodko, P.Geo., PhD, Senior Geophysicist and Manager of Data Interpretation.

REFERENCES

Berry, Ron F. and Bull, Stuart W., 2012: The pre-Carboniferous geology of Tasmania, Episodes Vol.35, no. 1, p.195-204.

Boyko, W., Paterson, N.R. and Kwan, K., 2001: AeroTEM characteristics and field results, The Leading Edge, p.1130-39.

Callaghan, Tim, 2001: Geology and host-rock alteration of the Henty and Mount Julia gold deposits, Western Tasmania, Economic Geology, 98, 1073-1088.

Clark, D.A., and Emerson, D.W., 1991. Notes on rock magnetization characteristics in applied geophysical studies, Exploration Geophysics 22(3) 547-555.

Cole, K., and R. Cole, 1941, Dispersion and absorption in dielectrics, Part I. Alternating current characteristics: Journal of Chemical Physics, 9, 341–351, doi: 10.1063/1.1750906.

Corbett, K.D., 2002: Updating the geology of the Mount Read Volcanics belt, Western Tasmanian Regional Minerals Program Mount Read Volcanics Compilation, Tasmanian Geological Survey Record 2002/19, Mineral Resources Tasmania, Department of Infrastructure, Energy and Resources, Tasmania.

Eckstrand, O.R., and Hulbert, L.J., 2007, Magmatic nickel-copper-platinum group element deposits, *in* Goodfellow, W.D., ed., Mineral Deposits of Canada: A Synthesis of Major Deposit Types, District Metallogeny, the Evolution of Geological Provinces, and Exploration Methods: Geological Association of Canada, Mineral Deposits Division, Special Publication No. 5, p. 205-222.

Ford, K., Keating, P., and Thomas, M.D., 2007, Overview of geophysical signatures associated with Canadian ore deposits, *in* Goodfellow, W.D., ed., Mineral deposits of Canada—A synthesis of major deposit-types, district metallogeny, the evolution of geological provinces, and exploration methods: Geological Association of Canada, Mineral Deposits Division, Special Publication 5, p. 939–970.

Galley, A.G., Hannington, M.D., and Jonasson, I.R., 2007, Volcanogenic massive sulphide deposits, *in* Goodfellow, W.D., ed., Mineral Deposits of Canada: A Synthesis of Major Deposit-Types, District Metallogeny, the Evolution of Geological Provinces, and Exploration Methods: Geological Association of Canada, Mineral Deposits Division, Special Publication No. 5, p. 141-161.

Gemmell, J. Bruce, Large, Ross R. and Zaw, Khin, 1998, Paleozoic volcanic-hosted massive sulphide deposits, AGSO Journal of Australian Geology & Geophysics, 17(4) 129-137.

Green, Geoffrey R., 2012: Ore deposits and Metallogenesis of Tasmania, Episodes Vol.35, no. 1, p.204-215.

Gunn, P.J. and Dentith, M.C., 1997, Magnetic responses associated with mineral deposits, AGSO Journal of Australian Geology and Geophysics, 17(2), p.145-158.

Kratzer, Terence and Macnae, James C., 2012, Induced polarization in airborne EM, Geophysics, vol.77, no. 5, p.E315-E327.

Li, Y. and Oldenburg, D.W., 1996, 3D inversion of magnetic data, Geophysics, Vol. 61, No. 2, P. 394-408.

McNeill, J.D., 1980, Application of transient electromagnetic techniques, Technical Note TN-7, Geonics Limited.

Nabighian, M. N., 1972: The analytic signal of two-dimensional magnetic bodies with polygonal cross-section — its properties and use for automated anomaly interpretation: Geophysics, **37**, 507–517.

Nabighian, M. N., 1984: Toward a three-dimensional automatic interpretation of potential field data via generalized Hilbert transforms—Fundamental relations: Geophysics, **49**, 780–786.

Oldenburg, Douglas, Marchant, David, Haber Eldad and Kang Seogi, 2013: On recovering IP information from EM data, 13th SAGA Biennial Conference and Exhibition.

Salem, Ahmed*, et al.*, 2008: Interpretation of magnetic data using tilt-angle derivatives, Geophysics, vol.73, no.1, p.L1-L10.

Seymour, D.B., Green, G.R. and Calver, C.R., 2007: The Geology and Mineral Deposits of Tasmania: a summary, Geological Survey Bulletin, 72.

Smith, R.S. and West, G.F., 1988: Inductive interaction between polarizable conductors: An explanation of a negative coincident-loop transient electromagnetic response, Geophysics, v.53, no. 5, p. 677-690.

Walker, S., Rudd, J. and Beran, L., 2007, IP Effects in TEM Data, Past, Present and Future, presented at SEG, San Antonio.

Weidelt, P., 2012: Response characteristics of coincident loop transient electromagnetic systems, Geophysics, Vol. 47, No. 9, P.1325-1330.

APPENDIX A

MAG3D SYNTHETIC MODELING RESULTS

Introduction

In order to help the interpretation of magnetic data using UBC's MAG3D inversions, a number of forward and inverse modeling tests were conducted. The results of the tests are presented here to help the interpreters to better understand and interpret the magnetic data.

The models presented here simulated commonly encountered magnetic bodies.

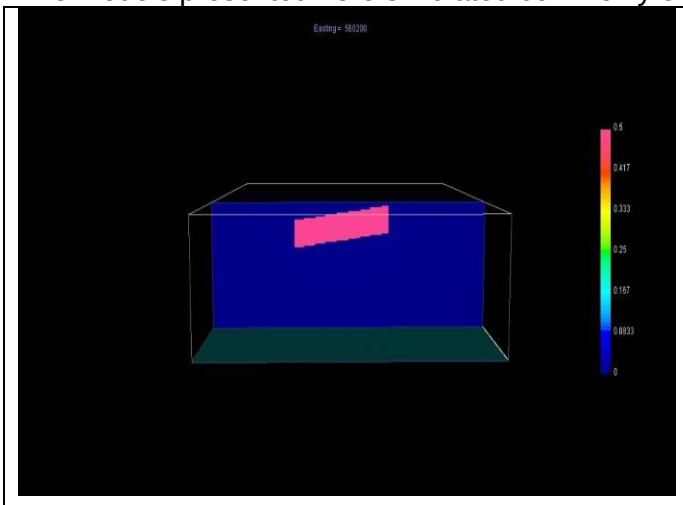

Figure A-1a: Forward model, a near-horizontal rectangular shaped sill-like magnetic body.

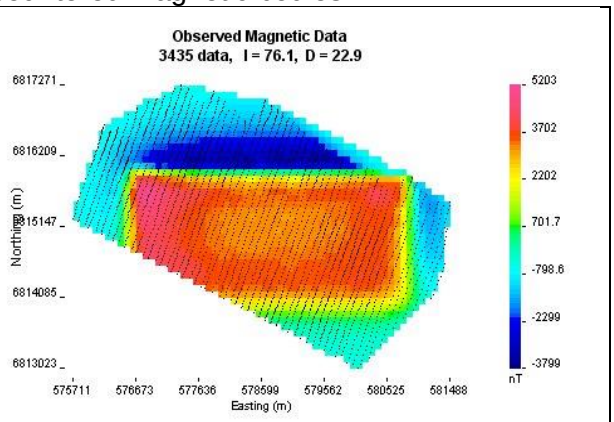

Figure A-1b: Observed magnetic data from the forward model in Figure A-1a.

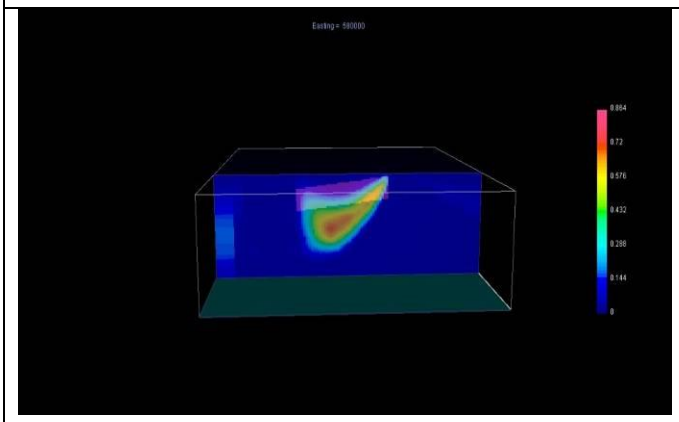

Figure A-2a: Inverted model and the original model displayed together. The inverted model matches the top of the magnetic body fairly well. However, the inverted model tends to exaggerate the depth of the bottom of the magnetic body.

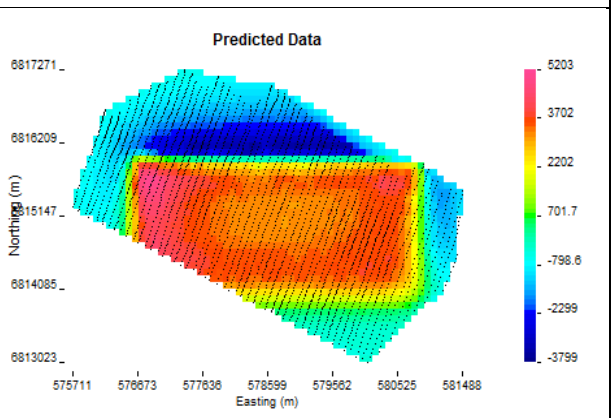

Figure A-2b: Calculated magnetic data from the inverted model shown in Figure A-2a.

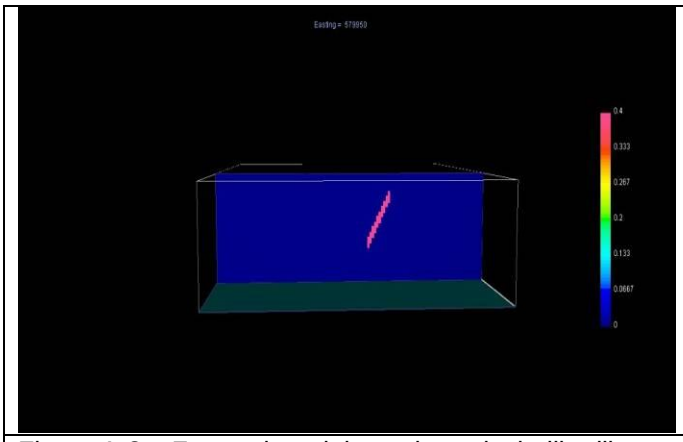

Figure A-3a: Forward model, a sub-vertical, dike-like magnetic body.

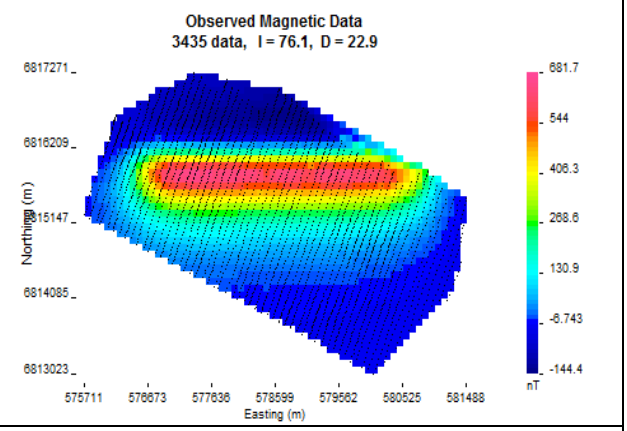

Figure A-3b: Observed magnetic data from the forward model in Figure A-3a.

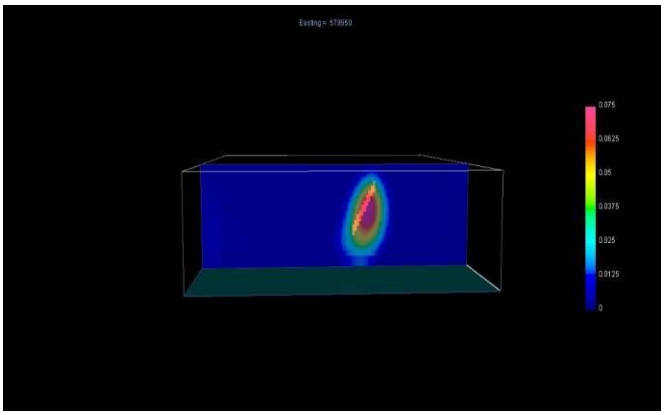

Figure A-4a: Inverted model and the original model displayed together. The inverted model matches the original model reasonably well, in terms of dip, depth to the top and even the vertical length of the magnetic body.

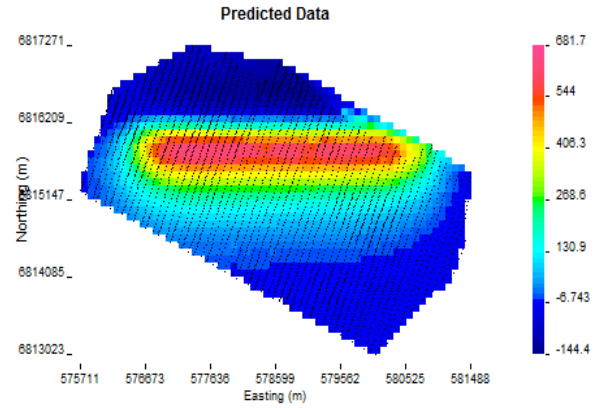

Figure A-4b: Calculated magnetic data from the inverted model shown in Figure A-4a.

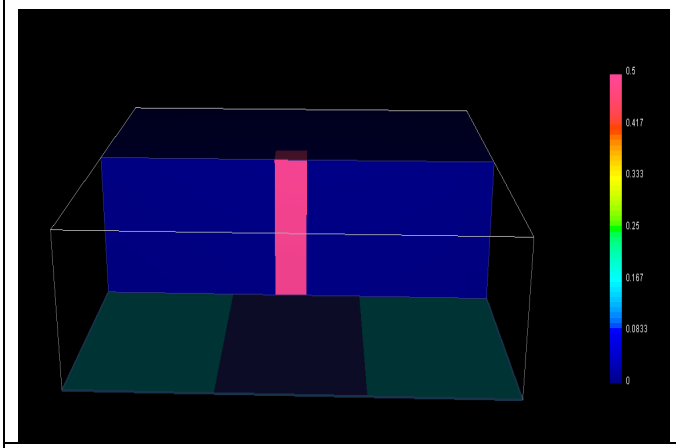

Figure A-5a: Forward model, simulating a magmatic intrusive of high magnetic susceptibility.

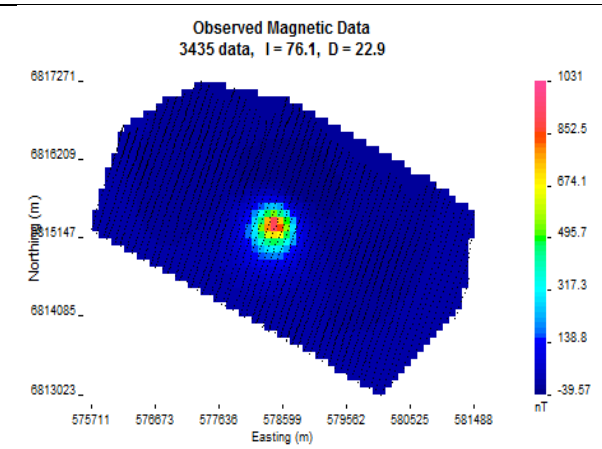

Figure A-5b: Observed magnetic data from the model shown in Figure A-5a.

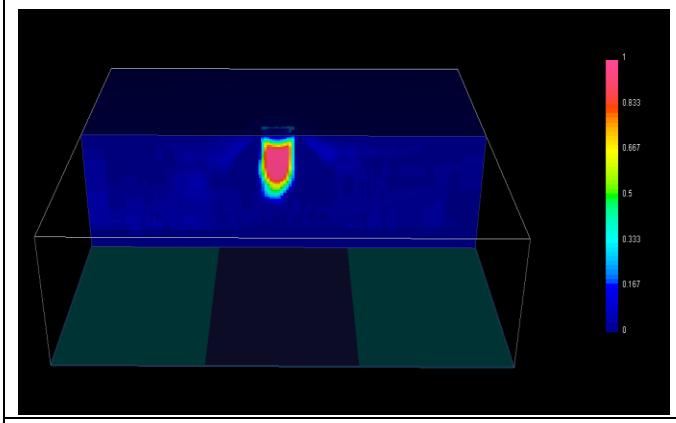

Figure A-6a: Inverted model using the observed data shown in Figure A-5b. The inverted model matches the original model really well at the top, including the sharp planar edges. The depths of the inverted model don't go as deep as the original model though.

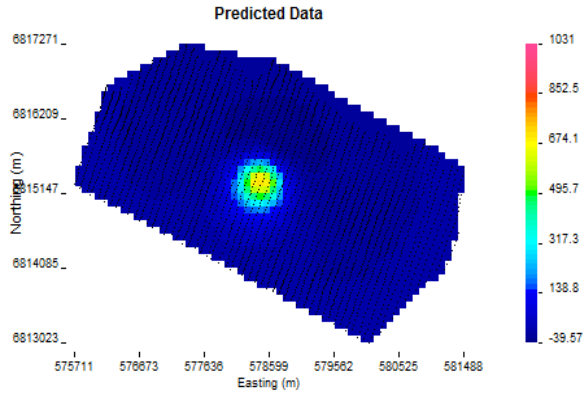

Figure A-6b: Calculated magnetic data from the inverted model shown in Figure A-6a.

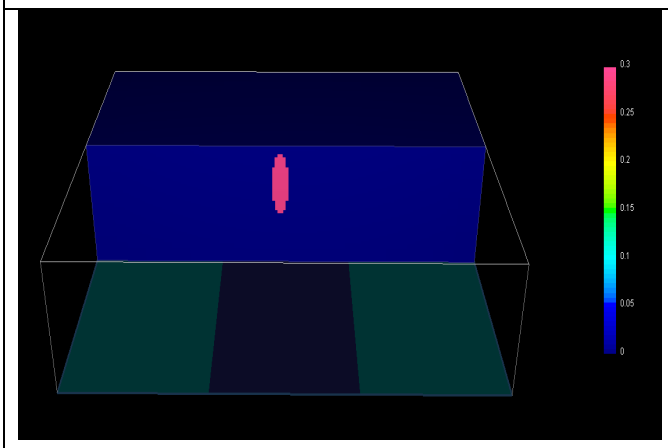

Figure A-7a: Forward model, simulating a kimberlite pipe.

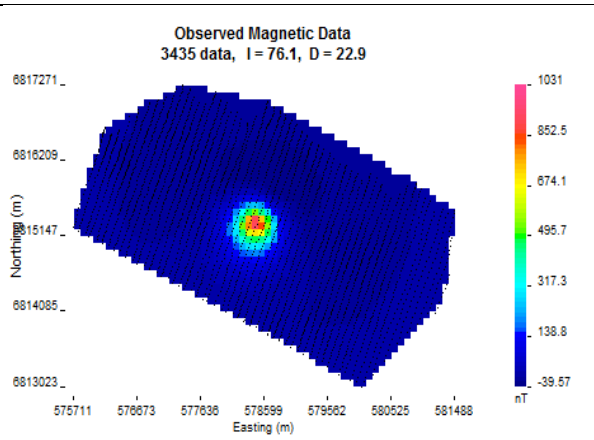

Figure A-7b: Observed magnetic data from the model in Figure A-7a.

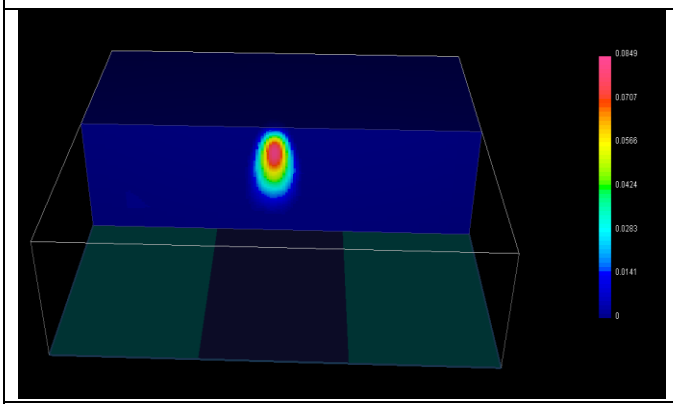

Figure A-8a: Inverted model, using data shown in A-7b.

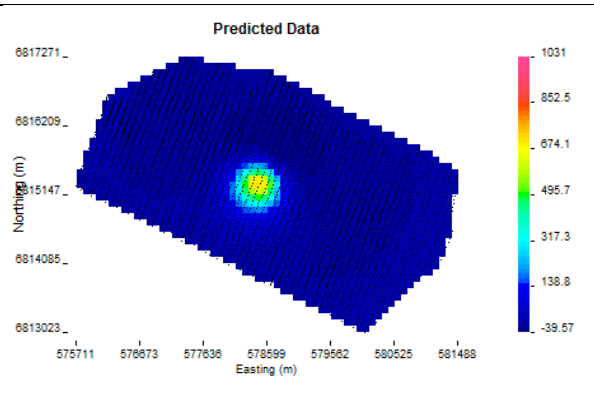

Figure A-8b: Predicated data from the model in A-8a

APPENDIX B

TEM RESISTIVITY DEPTH IMAGING (RDI)

Resistivity depth imaging (RDI) is technique used to rapidly convert EM profile decay data into an equivalent resistivity versus depth cross-section, by deconvolving the measured TEM data. The used RDI algorithm of Resistivity-Depth transformation is based on scheme of the apparent resistivity transform of Maxwell A.Meju (1998)[1] and TEM response from conductive half-space. The program is developed by Alexander Prikhodko and depth calibrated based on forward plate modeling for VTEM system configuration (Figures 1 to 8).

RDIs provide reasonable indications of conductor relative depth and vertical extent, as well as accurate 1D layered-earth apparent conductivity/resistivity structure across VTEM flight lines. Approximate depth of investigation of a TEM system, image of secondary field distribution in half space, effective resistivity, geometry and position of conductive targets are the main parameters which can be inferred from the RDIs.

Maxwell forward modeling with RDI sections from the synthetic responses (VTEM system)

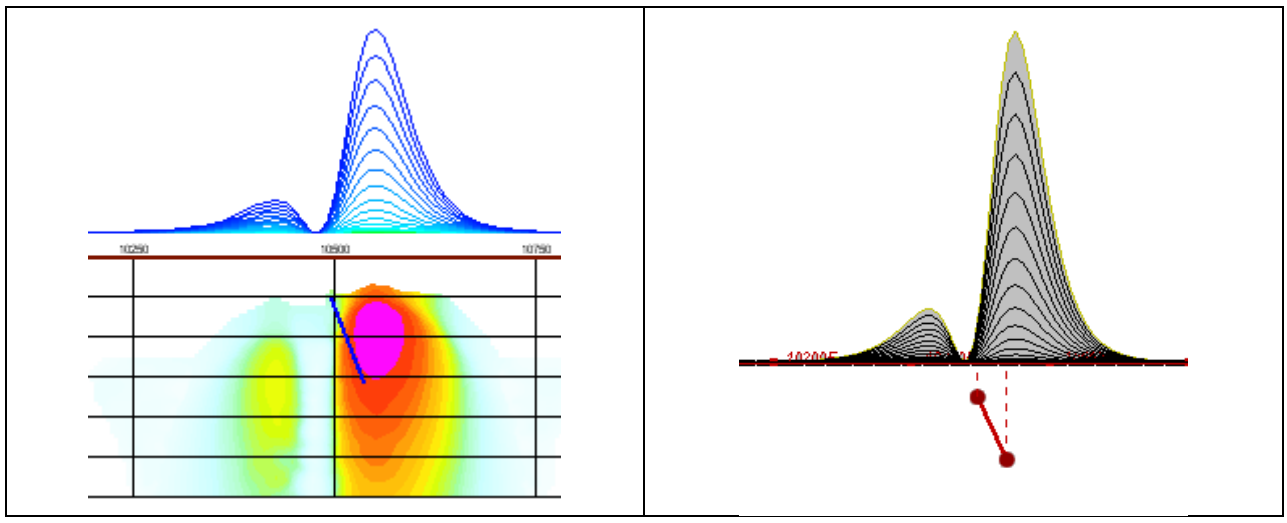

Figure 1: Maxwell plate model and RDI from the calculated response for conductive “thin” plate (depth 50 m, dip 65 degree, depth extend 100 m).

[1] Maxwell A.Meju, 1998, Short Note: A simple method of transient electromagnetic data analysis, Geophysics, **63**, 405–410.

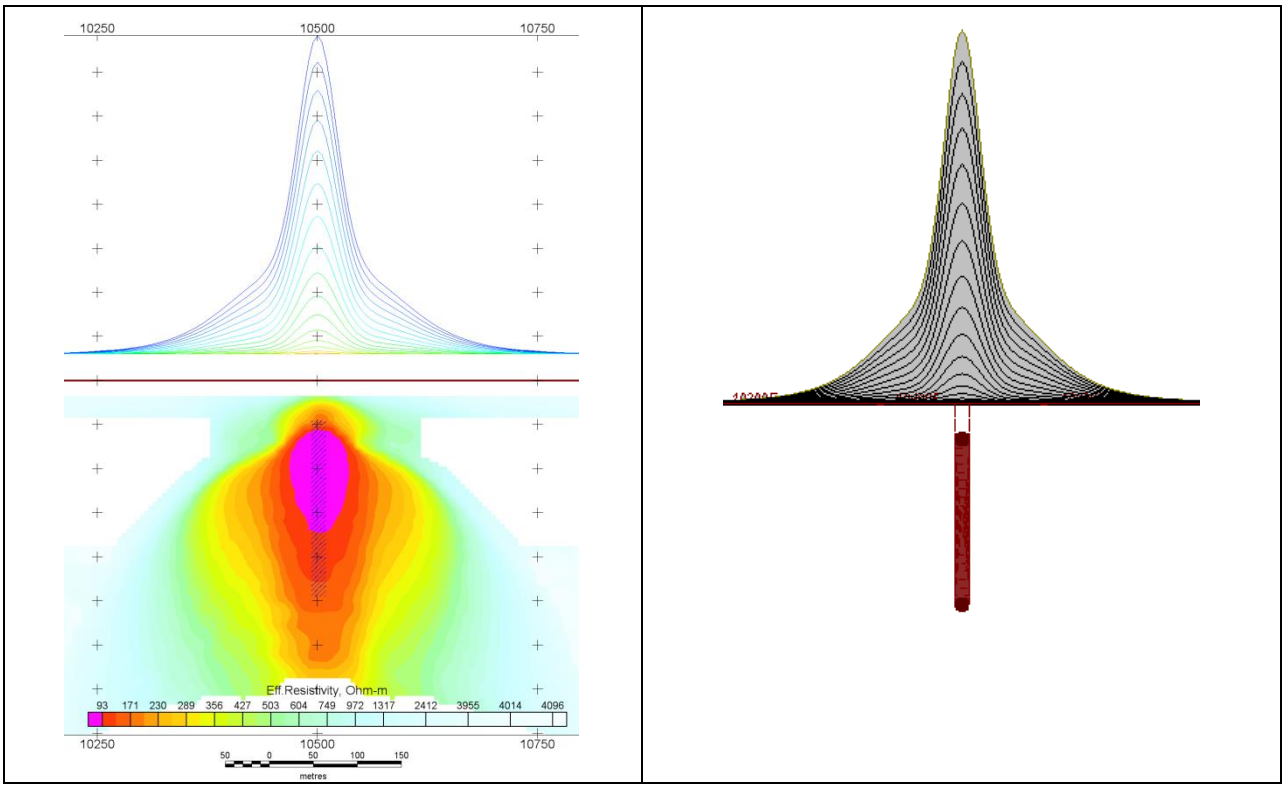

Figure 2: Maxwell plate model and RDI from the calculated response for "thick" plate 18 m thickness, depth 50 m, depth extend 200 m).

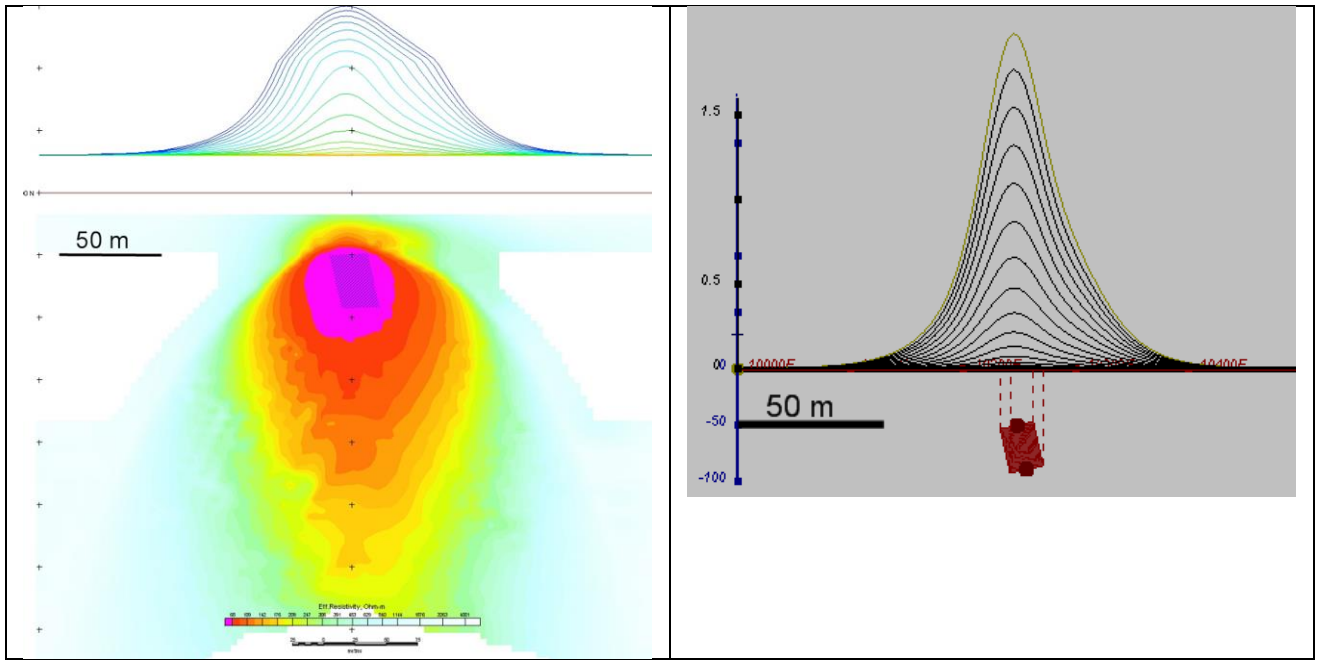

Figure 3: Maxwell plate model and RDI from the calculated response for bulk ("thick") 100 m length, 40 m depth extend, 30 m thickness

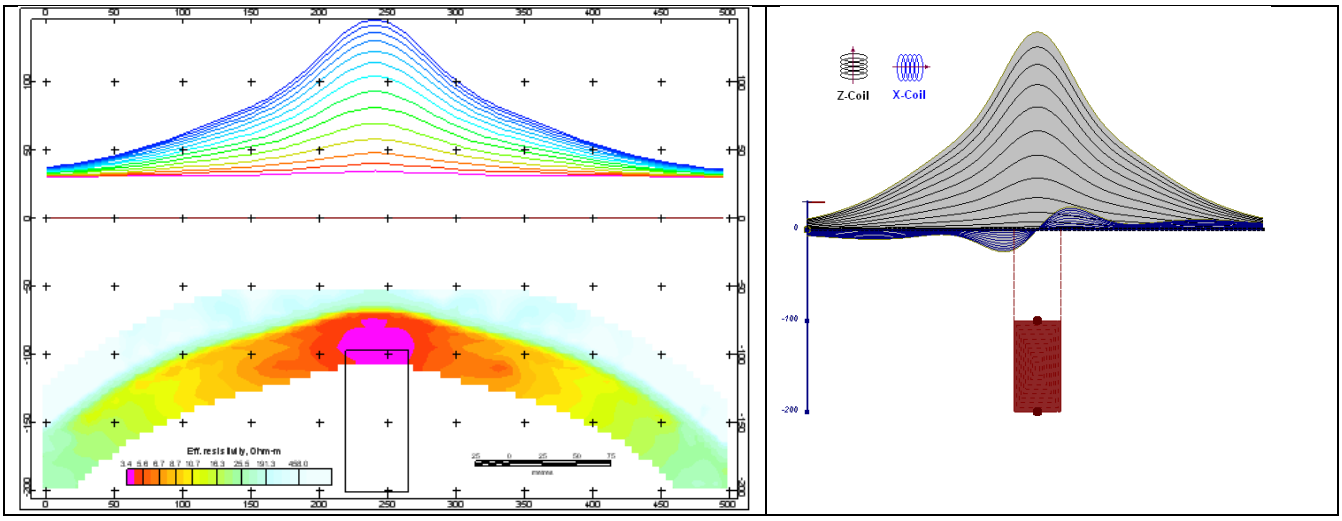

Figure 4: Maxwell plate model and RDI from the calculated response for "thick" vertical target (100 m depth and 100 m extent) using channels 19-44.

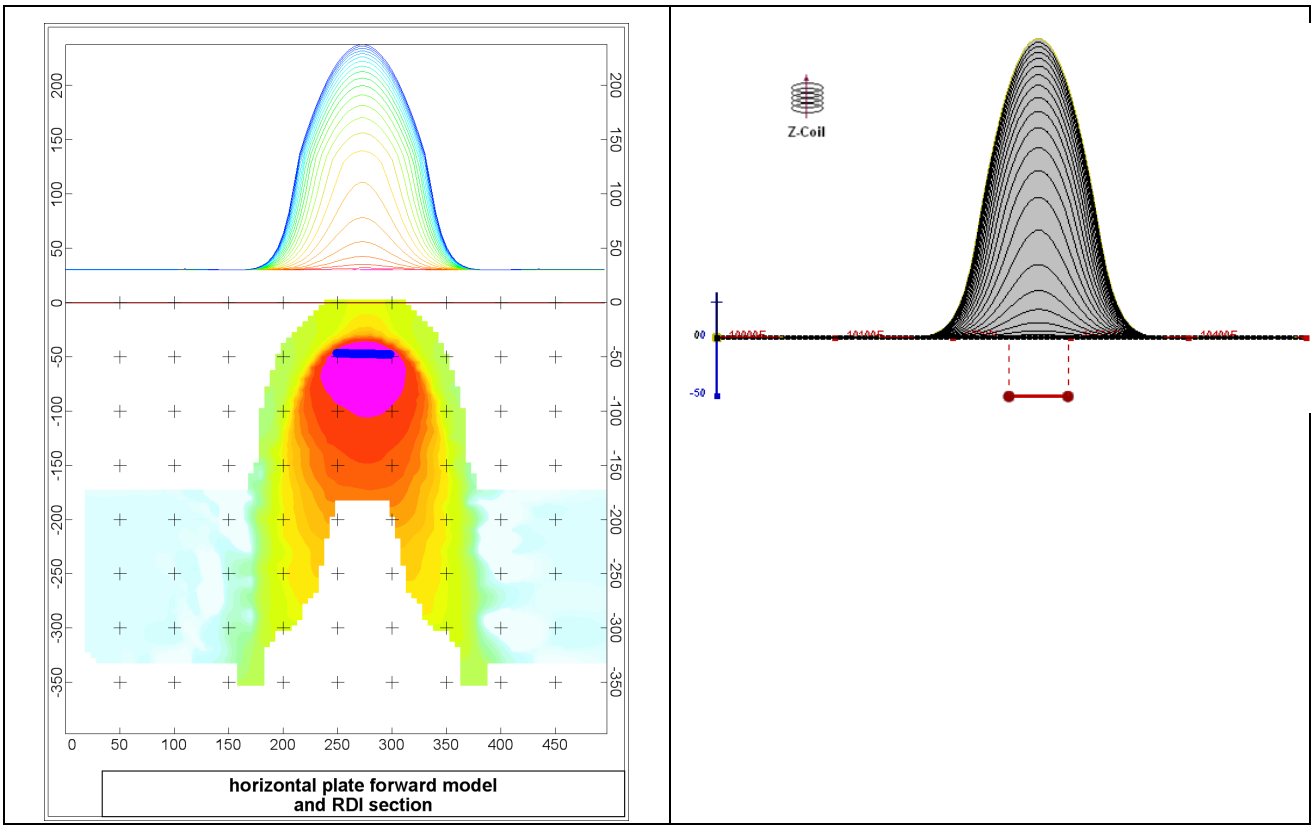

Figure 5: Maxwell plate model and RDI from the calculated response for horizontal thin plate (depth 50 m, dim 50x100 m). 15-44 chan.

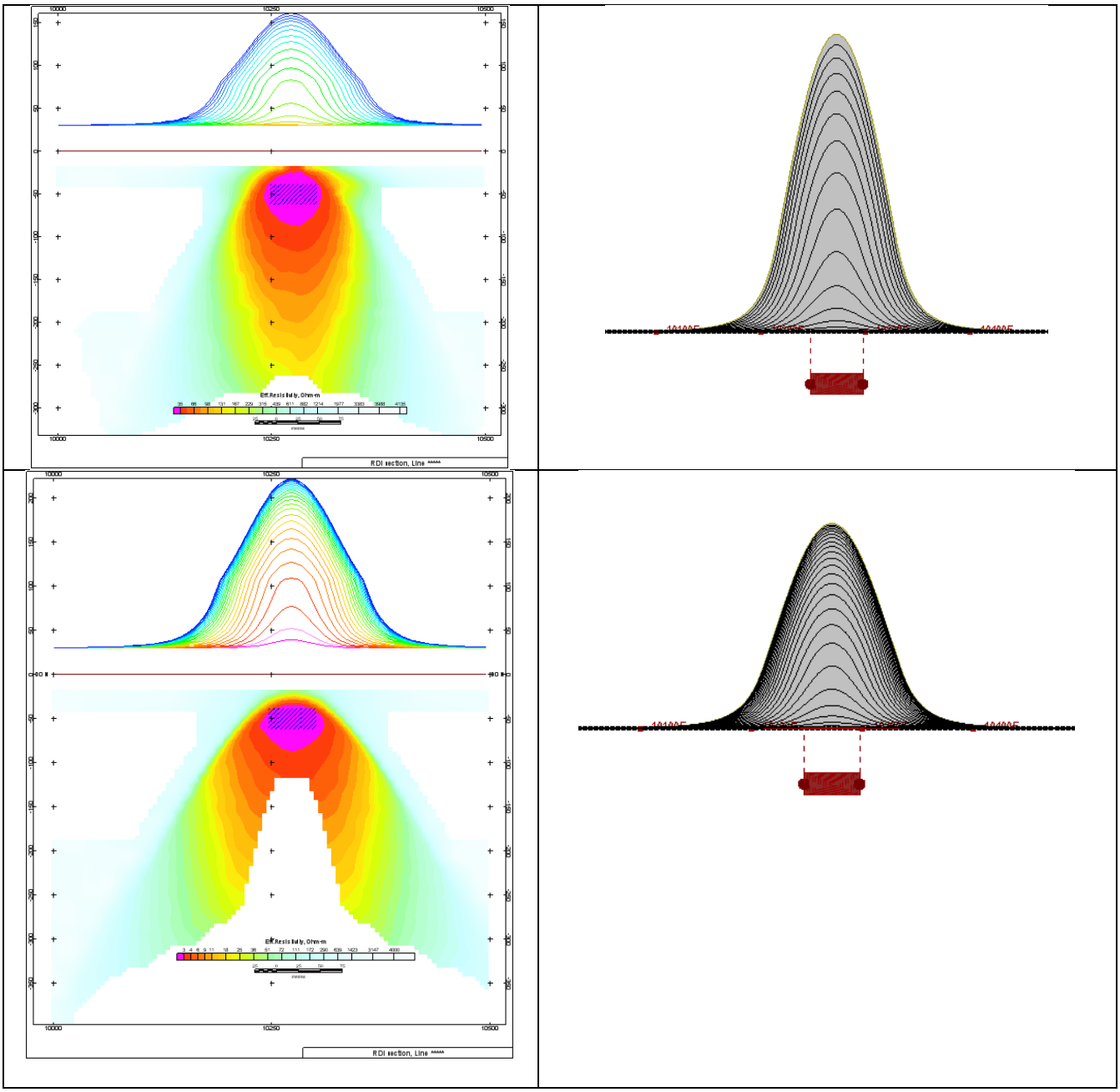

Figure 6: Maxwell plate model and RDI from the calculated response for horizontal thick (20m) plate – less conductive (on the top), more conductive (below)

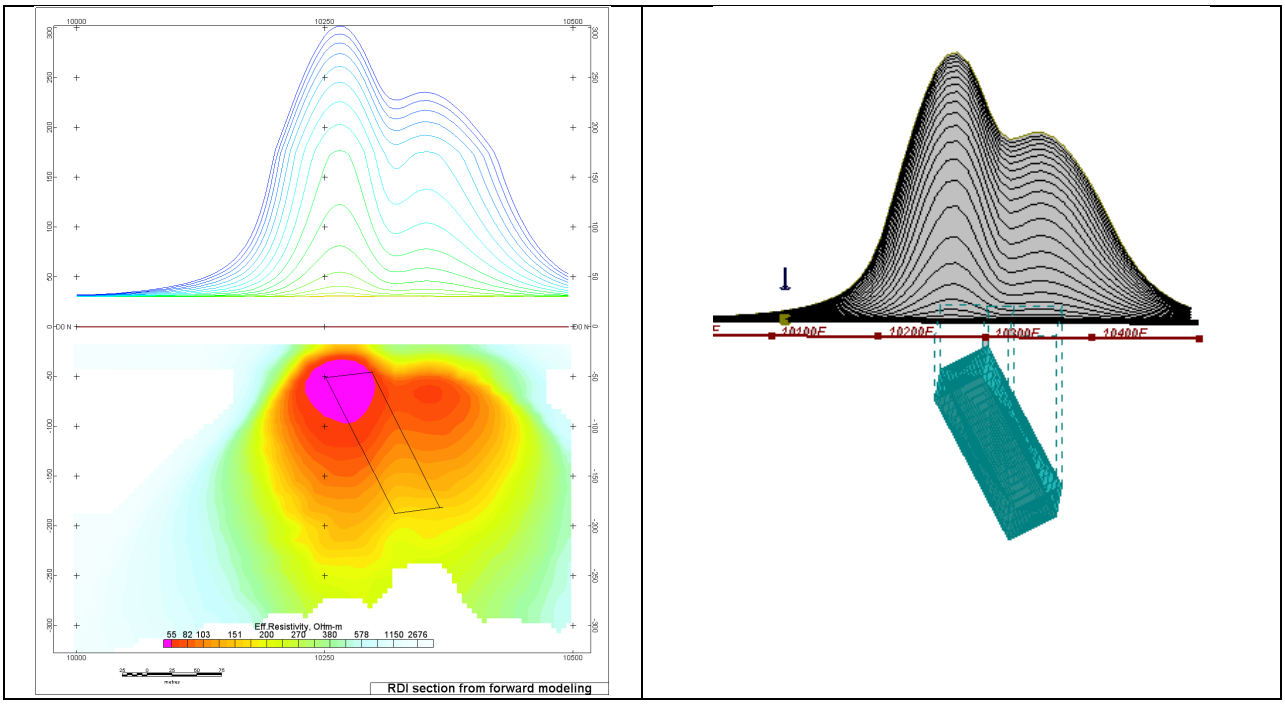

Figure 7: Maxwell plate model and RDI from the calculated response for inclined thick (50m) plate. Depth extends 150 m, depth to the target 50 m.

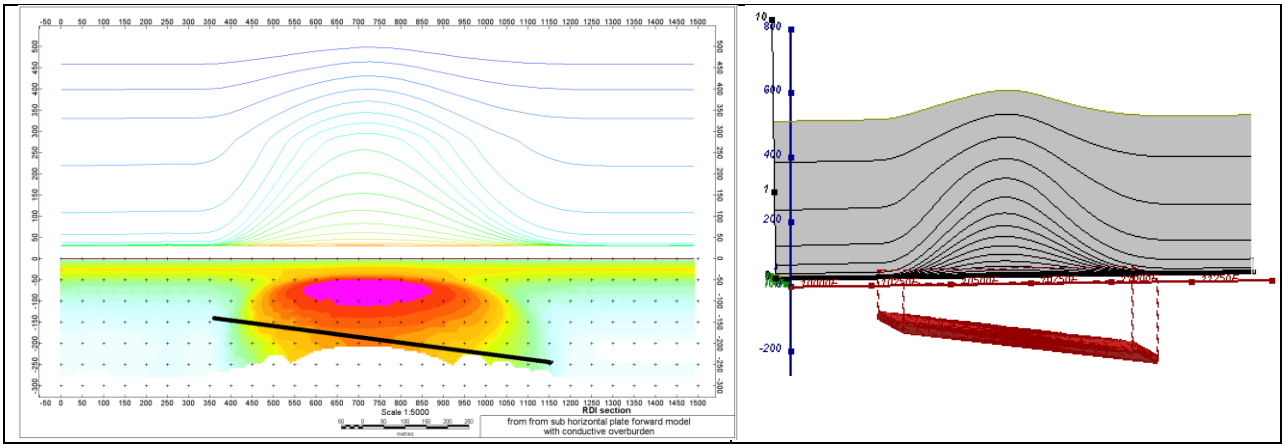

Figure 8: Maxwell plate model and RDI from the calculated response for the long, wide and deep sub-horizontal plate (depth 140 m, dim 25x500x800 m) with conductive overburden.

APPENDIX C

MAXWELL 2.5D PLATE MODELS FOR THE VTEM SYSTEM

Introduction

The VTEM system is based on a concentric or central loop design, whereby, the receiver is positioned at the centre of a transmitter loop that produces a primary field. The waveform is a bi-polar, modified square wave with a turn-on and turn-off at each end.

During turn-on and turn-off, a time varying field is produced (dB/dt) and an electro-motive force (emf) is created as a finite impulse response. A current ring around the transmitter loop moves outward and downward as time progresses. When conductive rocks and mineralization are encountered, a secondary field is created by mutual induction and measured by the receiver at the centre of the transmitter loop.

Efficient modeling of the results can be carried out on regularly shaped geometries, thus yielding close approximations to the parameters of the measured targets. The following is a description of a series of common models made for the purpose of promoting a general understanding of the measured results.

A set of models has been produced for the Geotech VTEM® system dB/dT Z and X components (see Figures 1 to 15). The Maxwell ™ modeling program (EMIT Technology Pty., Midland, WA, Australia) is used to generate the following responses assuming a resistive half-space. The reader is encouraged to review these models, so as to get a general understanding of the survey results. While these models do not cover all possibilities, they give a general perspective of the simple and commonly encountered VTEM anomalies.

For example, as the thin plate dips away from the vertical position, the peaks become asymmetrical. As the dip increases, the aspect ratio (Min/Max) decreases and this aspect ratio can be used as an empirical guide to determine the dip angles from near 90º to about 30º. The method is not sensitive enough where dips are less than 30º.

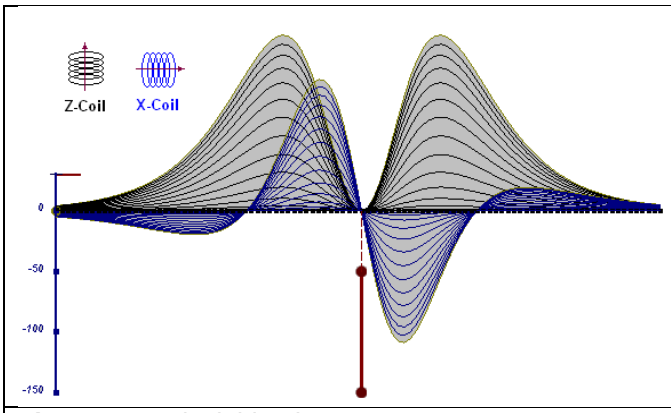

Figure 1: vertical thin plate

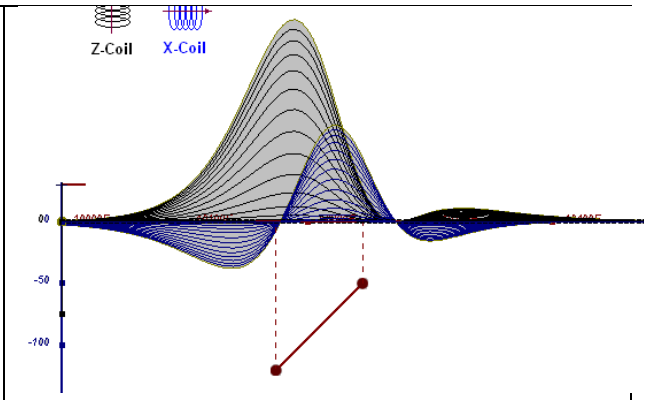

Figure 2: inclined thin plate

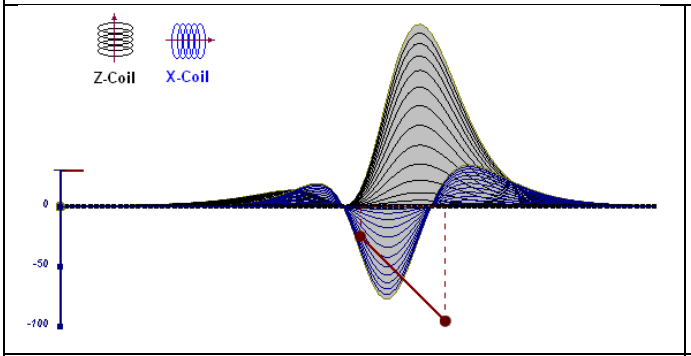

Figure 3: inclined thin plate

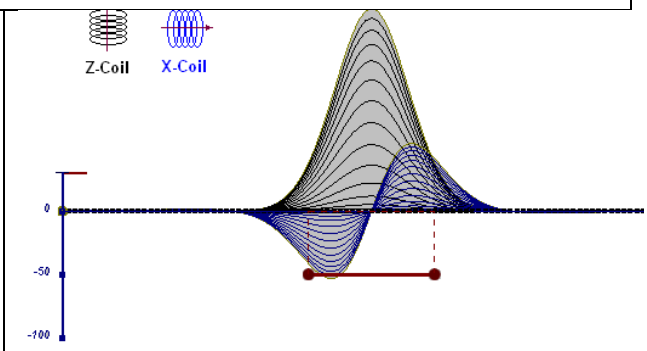

Figure 4: horizontal thin plate

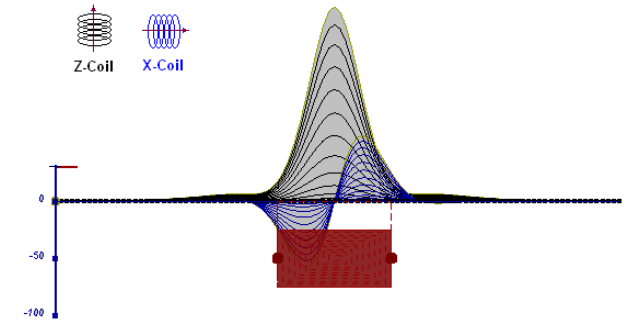

Figure 5: horizontal thick plate (linear scale of the response)

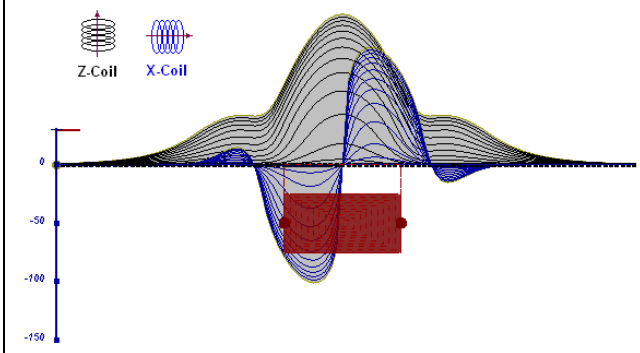

Figure 6: horizontal thick plate (log scale of the response)

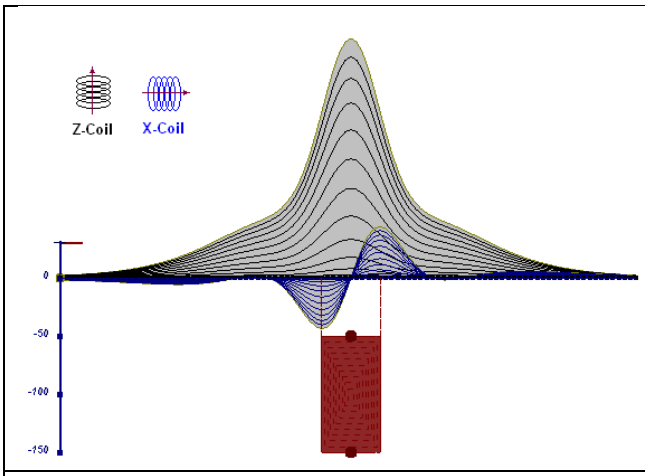

Figure 7: vertical thick plate (linear scale of the response). 50 m depth

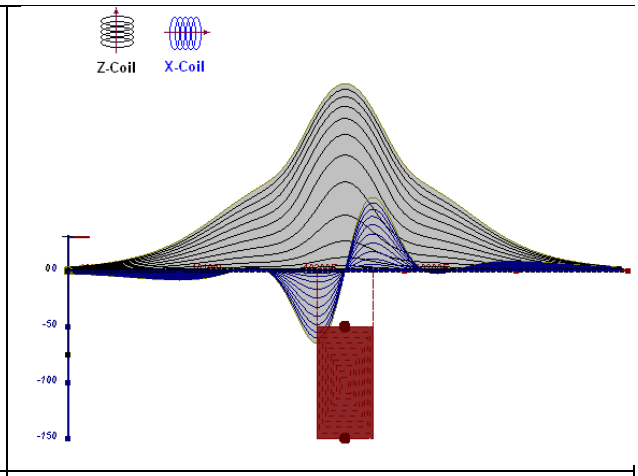

Figure 8: vertical thick plate (log scale of the response). 50 m depth

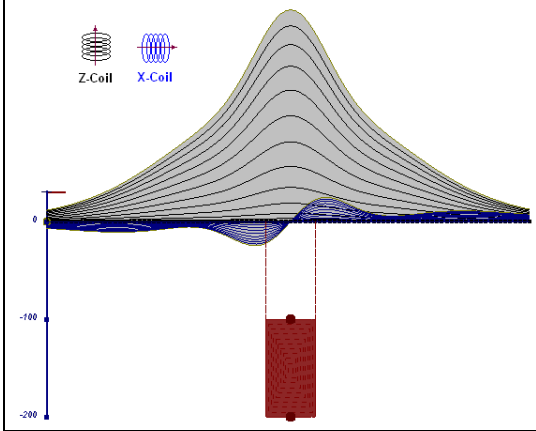

Figure 9: vertical thick plate (linear scale of the response). 100 m depth

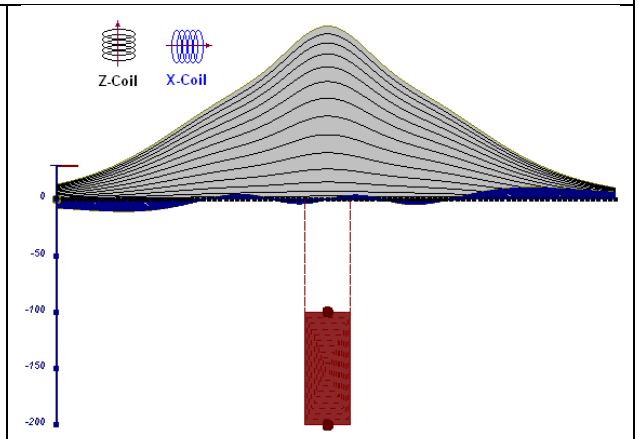

Figure 10: vertical thick plate (linear scale of the response). Depth/hor.thickness=2.5

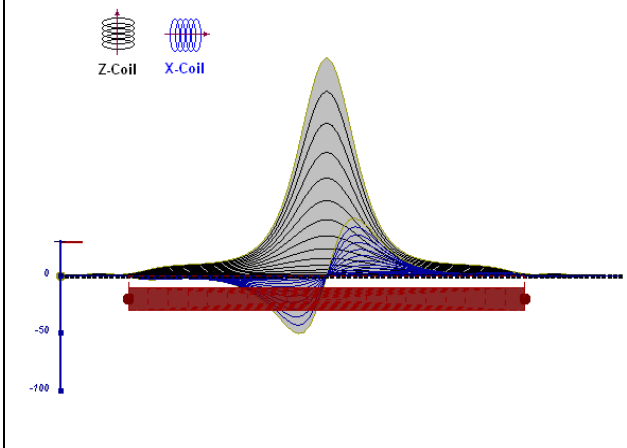

Figure 11: horizontal thick plate (linear scale of the response)

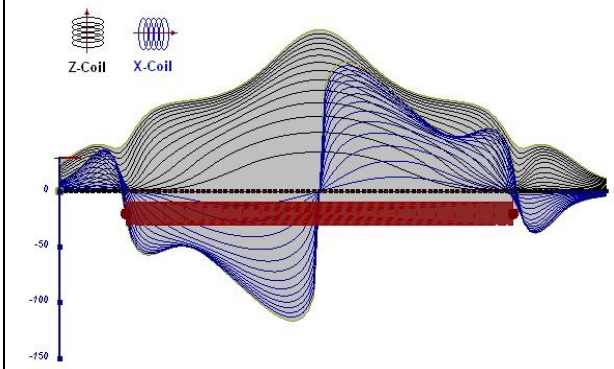

Figure 12: horizontal thick plate (log scale of the response)

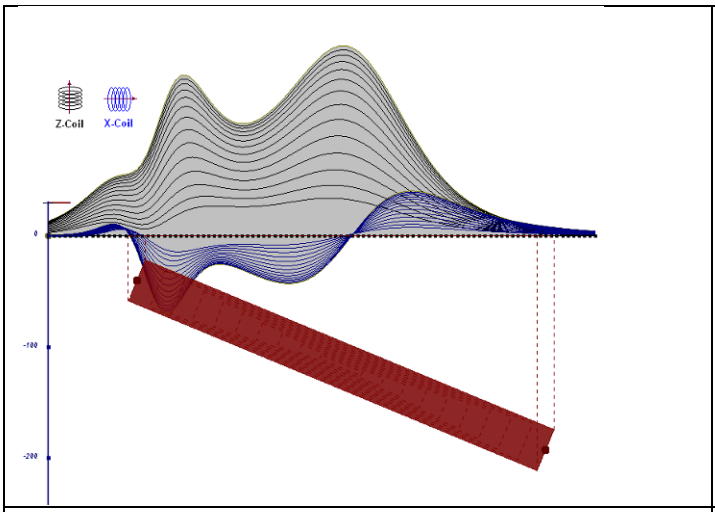

Figure 13: inclined long thick plate

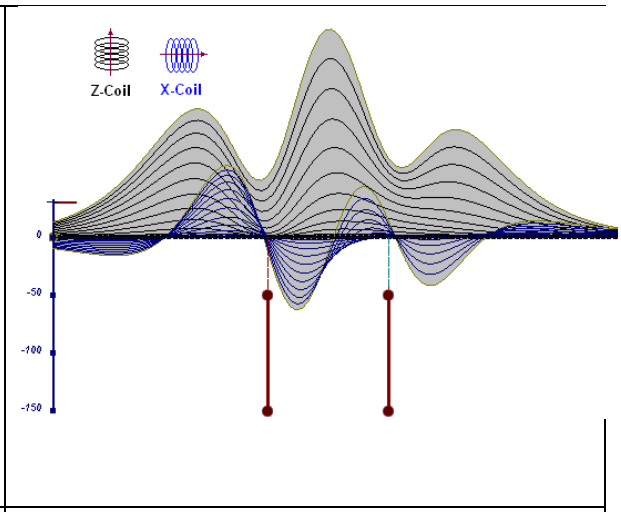

Figure 14: two vertical thin plates

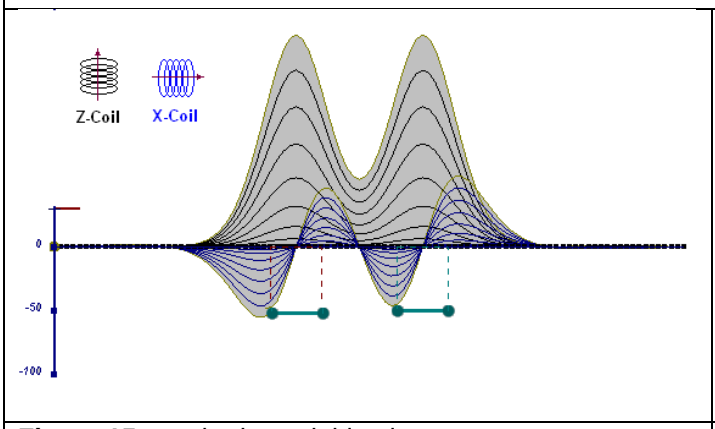

Figure 15: two horizontal thin plates

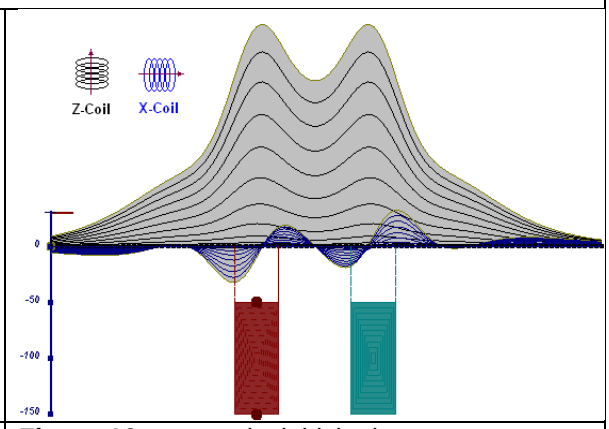

Figure 16: two vertical thick plates

Another set of examples are shown in Figure 17. VTEM responses of a vertical thin plate with variable thickness are calculated. The VTEM responses transition from a double-peak for thin plates to a single-peak for thick plates.

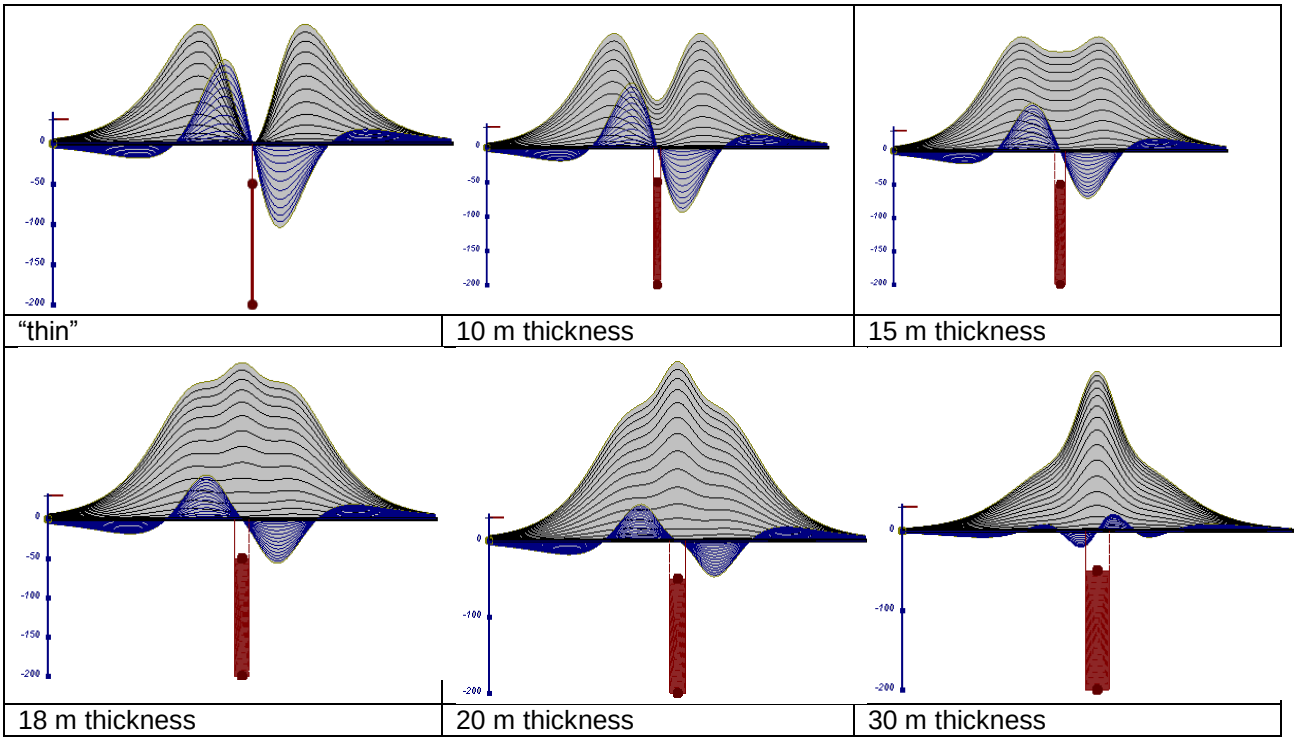

Figure 17: Conductive vertical plate, depth 50 m, strike length 200 m, depth extent 150 m.

The results of Maxwell 2.5D plate modeling of selected conductors are presented in separate documents for the blocks where Maxwell 2.5D plate modeling has been performed. The documents, provided on the final DVD, are:

EL22, AA1362_EL22_Maxwell_Modeling_R.pdf;
EL46, AA1362_EL46_Maxwell_Modeling.pdf.

APPENDIX D

Advanced RDI Products

Digital Geosoft grids of the RDI depth slices are provided on the final DVD.

RDI 2D sections for all traverse lines in Geosoft map format for EL22, EL46, EL50N and EL50S are provided;

RDI2D sections for all traverse lines in PDF format for EL46 are provided and it is named as vtem_AA1362_EL46_2010.pdf.

APPENDIX E

Advanced MAG3D Products

Digital MAG3D 3D voxels (xyz and xydepth), Geosoft grids of magnetic susceptibility depth slices and 2D sections for all regular lines for EL46 are provided on the final DVD.

Digital MAG3D 3D voxels (xyz and xydepth), Geosoft grids of magnetic susceptibility depth slices and 2D sections of selected lines for EL22, EL50N and EL50S are provided on the final DVD.